

# Hydrological Modelling of the West Coast of India

Suprit Kumar

Thesis

submitted to Goa University

for the Degree of

Doctor of Philosophy

in

Physics

551.48

KUM / Hyd.

Goa University

September 2010

*Examined. All corrections have been incorporated*

*[Signature]*  
(24.9.11)

K. Srinivasan

24/09/2011.

(External Examiner)

T-534

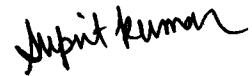
to *papa, mummy* and

*Madhurima*

# Statement

As required under the University ordinance OB-9.9.(iv), I state that this thesis entitled *Hydrological modelling of the west coast of India* is my original contribution and it has not been submitted on any previous occasion.

The literature related to the problem investigated has been cited. Due acknowledgements have been made wherever facilities and suggestions have been availed of.



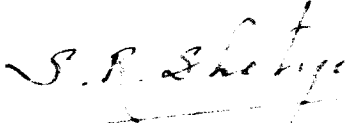
SUPRIT KUMAR

*National Institute of Oceanography, Goa*

*27 September 2010*

## Certificate

This is to certify that the thesis entitled *Hydrological modelling of the west coast of India*, submitted by Suprit Kumar to Goa University for the degree of Doctor of Philosophy, is based on his original studies carried out under my supervision. The thesis or any part thereof has not been previously submitted for any other degree or diploma in any university or institution.



SATISH R. SHETYE

*National Institute of Oceanography, Goa*

*27 September 2010*

# Vita

**Name** Suprit Kumar

**Born** 10 February 1979, Ara, Bihar

**Education**

M.Sc. Cochin University of Science and Technology, Kochi  
May 2003

B.Sc. (Hons.) Veer Kunwar Singh University, Ara, Bihar  
March 2000

**Work**

Research Fellow National Institute of Oceanography, Goa  
December 2003 to December 2008

Project Assistant National Institute of Oceanography, Goa  
January 2009 to date

**Address for communication**

By post Physical Oceanography Division,  
National Institute of Oceanography,  
Dona Paula, Goa 403 004,  
India.

By e-mail [suprit.kumar@gmail.com](mailto:suprit.kumar@gmail.com)

---

## List of Publications

- **K. Suprit.** *Radiative parameterisation: A study of radiative transfer over Bay of Bengal.* M.Sc. Dissertation, Cochin University of Science and Technology, Kochi. 2003.
- **K. Suprit** and D. Shankar. Simulating the Discharge of the Mandovi River, Goa. In: *Prediction in ungauged basins for Sustainable water resources planning and management.* (Ed.) K. S. Raju. Jain Brothers, New Delhi. 2006.
- S. R. Shetye, D. Shankar, **K. Suprit**, G. S. Michael, and P. Chandramohan. The environment that conditions the Mandovi and Zuari estuaries. In: *The Mandovi and Zuari Estuaries.* (Eds.) S. R. Shetye, M. Dileep Kumar, and D. Shankar. National Institute of Oceanography, Goa. 2007.
- **K. Suprit** and D. Shankar. Resolving orographic rainfall on the Indian west coast. *International Journal of Climatology*, 28:643–657, 2008.
- **K. Suprit**, Aravind Kalla, V. Vijith. A GRASS-GIS-based methodology for flash flood risk assessment in Goa. National Institute of Oceanography, Goa. 2010.
- P. M. Kessarkar, K. Srinivas, **K. Suprit**, and A. K. Chaubey. Proposed landslide mapping method for Canacona region. National Institute of Oceanography, Goa. 2011.
- **K. Suprit**, D. Shankar, V. Venugopal, and N. V. Bhatkar. Simulating daily discharge of the Mandovi river, west coast of India. (Manuscript accepted for publication in *Hydrological Sciences Journal*, 2011.)

# Acknowledgements

I am greatly indebted to Dr. S. R. Shetye for providing me an opportunity to pursue my doctoral study with him. He was the inspiration behind this work. I am very grateful to him for his continuous support, encouragement, and invaluable guidance throughout my research work.

I would like to express my deep sense of gratitude to Dr. D. Shankar for his keen interest, constant inspiration, unending support and invaluable guidance. He introduced me to this challenging subject and has given me the freedom to think and work. Learning with him was an experience that will be cherished forever. His scientific temperament, innovative approach, dedication towards research, and modest yet straightforward nature has inspired me the most. He has shown immense patience and understanding, instilling a sense of discipline which helped me sail through the difficult times and see things in proper perspective. Without his help, it would have been practically impossible to complete this thesis. I consider myself fortunate to have had the opportunity to work with him.

The insightful comments, suggestions, and advice offered by Dr. D. Nagesh Kumar and Dr. V. Venugopal during the frequent visits to the Indian Institute of Science, Bangalore proved crucial for the completion of my thesis. They were always available for solving doubts and queries, despite their busy schedules. I have learnt a lot from them and I gratefully acknowledge their magnanimous help, encouragement and guidance.

I am grateful to Dr. S. S. C. Shenoi, Project Leader and a member of my FRC committee, and Dr. A. S. Unnikrishnan, Project Leader, for their keen interest in my work and constant encour-

agement and support.

I would like to express my sincere gratitude to Prof. P. R. Sarode, Dr. R. V. Pai, Prof. J. A. E. Desa, Prof. G. M. Naik and Prof. K. S. Rane, Goa University, for their constant help and kind advice. I would like to especially thank Dr. R. V. Pai for his constant support and encouragement; he was always available for guidance during my visits to the department. The help rendered by Shri Ramchandra P. Naik from the office of the Department of Physics is highly appreciated.

Ms. Vidya Kotamraju was the local GRASS-GIS guru when I joined NIO. I am thankful to her for her help during my initial learning days. I had the privilege of working with Mr. Nagesh V. Bhatkar, who extended the work started by Vidya. Working with him was a great experience and I gratefully acknowledge his help.

Prof. Ramola Antao went through the draft of the thesis and corrected English grammar and usage. Her kind and timely help is gratefully appreciated. Madhurima also went through the draft and helped in correcting the language and style.

Dr. Michael Coe was kind enough to offer his invaluable comments and suggestions during the entire course of this investigation. His encouraging remarks were very helpful in the improvement of our work. I thank him profusely for the same.

I would also like to acknowledge the role of the entire GRASS GIS team, especially Prof. H. Mitasova and Dr. M. Neteler. Prof. H. Mitasova kindly answered my queries on the RST method and I am indebted to her.

I thank India Meteorological Department and Central Water Commission, Government of India for providing the Rainfall and Discharge data for my work. In particular, I am extremely grateful to Dr. M. Rajeevan and Mr. Sreejith for their help with the IMD data.

Apart from GRASS-GIS, several other open source and free softwares have been used extensively in this thesis, e. g., FERRET, GMT, Openoffice suite. I am grateful to the developers of each one of these softwares.



This thesis has been typed using L<sup>A</sup>T<sub>E</sub>X 2<sub>ε</sub>. I have made use of the Goa University thesis style file, `guthesis.sty`, shared kindly by Dr. D. Shankar. I am also grateful to Shri A. Y. Mahale for helping with the cover page design.

I am thankful to Dr. M. R. Ramesh Kumar, Dr. V. Gopalakrishna, Mr. D. Sundar, Mr. G. S Michael and Mr. Anslem Almeida for their help and encouragement during my PhD.

Soumava Ghosh and Mandeep Singh of BITS-Pilani helped in integrating the RST interpolation code with THMB. Sandeep Agrawal of C-DAC, Pune helped in the parallelisation of the RST code. I am highly grateful to them.

I have benefited a lot from the many discussions with my lab seniors Rabindra Nayak, Mohammad Alsafani, Manoj, Aparna, and Suresh. I am thankful to them for their help and guidance.

Working with colleagues Pramila, Pallavi, Mahalingam and Aravind was always a pleasure.

I am thankful to our system administrators Dattaram, Kaushik, Krupesh, Ashok and Sarvesh for providing hassle-free computer and peripheral support.

After passing M. Sc., I was looking for a research position and NIO was not on my radar. Roxy, my senior from CUSAT and later on at NIO, was the one who informed me about NIO and the interesting research being pursued there.

A gang of senior CUSATIANS at NIO - Krishnan, Nuncio, Sreekumar, and Ramesh created a friendly and comfortable atmosphere during my initial days at NIO.

My colleagues in the division deserve a special word of thanks for creating a pleasant and conducive working atmosphere. I especially thank Syam, Grinson, Nisha, Aboobacker, Ricky Fernandes, Sindhumol, Murali, Deepthi, Balu, Vivek, Rashmi Vinayak, Abishek, Amol Prakash, Vijith, Arnab, Nanddeep and many others.

I would like to thank my senior friends Rajeev, Bhaskar, Vinod, Pranab, Pramod, Sameer, Satyaranjan and also Anand, Ravi, Vishwas, Mandar, Ankush, Shashikumar, Rajdeep, Sanjay Singh and Rana, Sumit, Rajesh, Suthirtha, Nagraj, Sabyasachi, Rubel, Kishen, Swaraj, and Girish for providing great company, friendly support and help during my stay in NIO. The times spent

with them will always be cherished.

My deepest sense of gratitude go to my parents for their patience, goodwill and blessings. I am indebted to them. My younger brothers Dr. Sukrit and Sumit have always been very supportive and I thank them for their belief in me.

No words can express my gratitude to my best friend, my wife, Madhurima. She has been a constant source of motivation and encouragement. The task of completion of the thesis seemed unsurmountable with each passing day, but her crucial support and help allowed me to wade through.

I would like to thank National Institute of Oceanography (NIO). As a student, working here has been a very pleasant and hassle-free experience, because of the continuous help and support of various sections or units such as HRM, NICMAS, ITG and others. I will be always grateful. I also duly acknowledge the financial assistance in the form of research fellowships from the Council of Scientific and Industrial Research (CSIR) and the SIP project of NIO that allowed me to continue my work uninterruptedly.

SUPRIT KUMAR

*National Institute of Oceanography, Goa*

*September 2010*

# Synopsis

Freshwater is one of the most essential requirements for human civilization and rivers are the most important and easily available source of freshwater. They provide water for various purposes such as agriculture, industry, domestic and recreational use. Water availability depends upon the vagaries of weather and climate, and issues related to it arouse considerable interest.

Rivers are a vital component of terrestrial hydrology, which also includes other surface water bodies such as lakes and wetlands. They also form a crucial link between the land-ocean-atmosphere interaction processes as they transport freshwater from land to ocean. The role of river discharge in the hydrological cycle makes it an important climatic variable.

There are two important issues associated with the large spatio-temporal variability observed in hydrological variables: first, quantitative estimation of the hydrological variables, and second, understanding the climatic feedback processes causing this variability. For example, in the vicinity of the Indian subcontinent, heavy rainfall over northern Bay of Bengal is related to its ability to remain warm even after the onset of the monsoon: the Arabian Sea cools, but the bay does not. This difference has been attributed to the stable stratification in the bay, in which water with low salinity (low density) sits on top of water with high salinity (high density). The source of this low-salinity water is the copious discharge from rivers like the Ganga and the Brahmaputra and the rainfall over the bay.

Although rainfall over India is estimated fairly accurately, very little quantitative information is available on river discharge on the relevant scales. This is primarily due to two reasons: first,

the dearth of information related to the variables of interest, and second, the lack of a quantitative framework that can put these variables in perspective. A quantitative framework is needed to address both these issues. The framework should be simple, freely distributable, scalable and the demand it makes on the database should be consistent with the availability of data in India and the other countries in the region.

This study begins with the above premises. An existing hydrological modelling framework has been modified to simulate the river discharge on the west coast of India. The west coast is also a region of heavy rainfall; it is one of the two rainfall maxima in the region, the other being the northeastern Bay of Bengal. The heavy rainfall and the small geographical area of the coast ensure that a large number of small rivers drain into the eastern Arabian Sea. Therefore, the freshwater influx into the eastern Arabian Sea is expected to be large, making the region similar to the bay. Are the feedback processes also the same? We do not know, as there are no quantitative estimates of river discharge available (except on the global scales, which invariably suffer from poor data coverage and coarse resolution). A large percentage of west-coast rivers is ungauged or poorly gauged, making hydrological modelling the only viable tool.

The motivation for this thesis is presented in Chapter 1. The aim of the thesis is to modify an existing hydrological modelling framework to simulate daily river discharge. We apply the framework to the Mandovi, a typical west-coast rain-fed river. It has two discharge gauges (one on the main river and another one on a tributary). Most of the west-coast rainfall (~ 90%) occurs during the summer monsoon (June–September). As a consequence, most of the discharge also occurs during this season, with a peak during July–August.

In Chapter 2, we describe the components of the modelling framework. At the heart of the framework is a hydrological routing algorithm called THMB (Terrestrial Hydrological Model with Biogeochemistry; THMB was earlier known as HYDRA), which, given the local rainfall and evapotranspiration, routes the runoff through the land surface to its destination—the sea or an inland lake. THMB has been used to model water budget of basins ranging in sizes from a few

square kilometers to continents. The framework derives the basin geometry, including river-flow directions and basin area, from a DEM (Digital Elevation Model). The DEM used in this study is called GLOBE (Global Land One-kilometer Base Elevation), and it has a resolution of  $\sim 1$  km. The framework includes a free and open-source geographical information system called GRASS GIS.

The modelling framework was applied to the Mandovi river to simulate the annual discharge and simulations were compared with the observations. THMB, when forced with monthly maps of available spatial rainfall datasets, gave large errors and heavily underestimated the annual discharge. This underestimate implied that the available rainfall datasets underestimate the rainfall in the region. Hence, we had to obtain rainfall maps by interpolating available rain-gauge data. The rainfall mapping algorithm has been discussed in Chapter 3. Mapping rainfall on the west coast is made difficult by the complex mountainous terrain, the large spatial gradients of rainfall, and the sparsity of rain gauges. Part of the Mandovi basin lies in the Sahyadri mountain ranges and the basin has only five rain gauges. A multivariate interpolation method (Regularised Spline with Tension (RST)), using elevation as the third variable, was used for interpolating rainfall. The method requires locations and heights of the rain gauges, along with a DEM, to obtain the rainfall maps, and depends upon two interpolation parameters called tension ( $T$ ) and smoothing ( $S$ ). The optimal values of  $T$  and  $S$  were determined by a cross-validation procedure. The interpolation was done separately for the leeward and windward sides by specifying the ridge line *a priori*. The resulting spatial fields were merged together to get the rainfall forcing; the simulated annual discharge compared well with the observations. Specifying the ridge was the key to reducing underestimation of rainfall.

In THMB, the runoff was calculated as a fixed fraction of rainfall minus evapotranspiration. This simple partitioning worked well for the annual simulations as discharge does not have any memory from year to year: it starts from a near-zero value to reach its peak in July–August, and then slowly recedes to a near-zero level at the end of the calendar year. This approach, however,

is not adequate for simulations at higher temporal resolutions. The highest temporal resolution of rainfall data available to us was a day; the daily rainfall was available for the rain gauges. Hence, our next step was to simulate the daily discharge. On the daily time scale, rainfall, and hence runoff, shows large variability. To capture this variability, a rainfall-runoff model is required. To address this issue, a conceptual rainfall-runoff model based on the Soil Conservation Service Curve-Number (SCS-CN) method was incorporated into THMB. The SCS-CN method, one of the most popular rainfall-runoff models, was derived empirically from studies done on small catchments. For each day in a grid cell, given the rainfall and two parameters ( $CN$  and initial abstraction coefficient ( $\lambda$ )) based on the physical characteristics of the basin, this method converts rainfall into surface runoff and sub-surface runoff. The SCS-CN method provides a reference value of  $\lambda$  and  $CN$  for the basin. For the same rainfall, wet conditions produce more runoff than dry conditions. This temporal variability in moisture conditions is accounted for in the SCS-CN method through the antecedent moisture condition (AMC) classes based on the rainfall over the preceding five days. In Chapter 4, we discuss the incorporation of the SCS-CN method into THMB and present the daily discharge simulations.

$CN$  and  $\lambda$  depend on the physical characteristics, such as soil type and cover, vegetation cover and land use, of the basin, and these characteristics are seldom homogeneous over the whole basin. Apart from the spatial variations encountered in the basin, the soil moisture condition (or AMC) varies with season. For example, a wet spell in the peak-monsoon season is different from that in the post-monsoon season. In the first case, almost all the rainfall appears in the river (higher runoff) as the soil is already saturated with moisture, and in the second case, a part of the rainfall has to wet the drying soil (lower runoff). Thus, the model parameters have to be a function of both space and long-term variations or seasons. To resolve the spatio-temporal variability, exhaustive data sets are required, but were not available. Spatial parameterisation was incorporated using the limited information available on the physical properties of the basin, and the DEM was used to divide the basin into four homogeneous regions. An objective method to distinguish the long-term

moisture regimes was also developed. This method uses rainfall and cumulative rainfall at each grid cell and defines different states of prevailing moisture conditions, which affect the runoff generation in the SCS-CN method. The strength of the parametrisation lies in the limited demand it makes on the input data: apart from some information on the average soil type in the basin, the parameterisation is built solely on the basis of the rainfall that is used to force the model. In Chapter 5, we discuss these spatio-temporal parameterisations incorporated into the SCS-CN method. After introducing these parameterisations, simulated daily discharge compares well with the observations.

A detailed discussion on the implications of the modelling framework is discussed in Chapter 6. This Chapter also discusses the strengths and caveats of the framework. The biggest strength of the framework is its low demand on input data, which makes it viable for simulating the discharge of other ungauged basins on the Indian west coast. On the west coast, the inter-river variations are much less than the intra-annual and interannual discharge variations for a river, implying that the framework will also work for the other west-coast rivers.

In summary, we develop a modelling framework to simulate river discharge over a range of scales. The modelling framework is highly scalable, it simulates river discharge, its demand on input data is minimal. The conclusions of the thesis are summarized in Chapter 7, and the salient points are presented below.

1. The modelling framework is applied and tested for the Mandovi river. The discharge simulations compare well with the observations on annual to daily timescales.
2. Rainfall is the most important variable in the modelling framework owing to its availability and relative accuracy. The complex mountainous terrain of the west coast, the large gradients of rainfall and small geographical area of the west-coast basins lead to a large underestimation of rainfall in existing global and regional rainfall datasets. To resolve this orographic rainfall on the west coast and obtain the rainfall forcing field, a rainfall mapping

algorithm was incorporated into THMB.

3. Resolving spatial and temporal variability in the runoff-generation process, which is parameterised by the SCS-CN method, requires exhaustive data on the physical, geographical, and biological characteristics, which are not available easily. The strength of our method is that these processes, specially long-term seasonal variation, are parameterised using only the input rainfall data. For most of the west-coast river basins, the only available data is the rainfall from the sparse distribution of rain gauges. That the model does not need to be calibrated separately for each river is important because most of these basins are ungauged. Hence, though the model has been validated only for the Mandovi, its potential region of application is considerable for prediction in the several ungauged basins on the Indian west coast.



# Contents

<b>Statement</b>	<b>iii</b>
<b>Certificate</b>	<b>iv</b>
<b>Vita</b>	<b>v</b>
<b>Acknowledgements</b>	<b>vii</b>
<b>Synopsis</b>	<b>xi</b>
<b>List of Tables</b>	<b>xxi</b>
<b>List of Figures</b>	<b>xxii</b>
<b>1 Introduction</b>	<b>1</b>
1.1 Motivation . . . . .	1
1.1.1 River discharge . . . . .	2
1.2 Setting of the problem . . . . .	3
1.2.1 Geography of the region . . . . .	3
1.2.2 Climate of the region . . . . .	6
1.3 Problem . . . . .	10
1.3.1 Mandovi river system . . . . .	14

---

1.4	Objective of the thesis . . . . .	16
<b>2</b>	<b>Hydrological Modelling framework</b>	<b>17</b>
2.1	Hydrological modelling process . . . . .	17
2.1.1	Runoff production and flow processes . . . . .	17
2.1.2	Hydrological reservoir routing model . . . . .	20
2.1.3	Linear reservoir model . . . . .	21
2.2	Background and approach . . . . .	22
2.3	THMB model . . . . .	23
2.3.1	Basin geometry and DEM . . . . .	25
2.3.2	Flow directions . . . . .	25
2.4	Viability of the model: Mandovi river basin . . . . .	26
2.4.1	Editing of DEM . . . . .	26
2.4.2	Inadequacy of existing rainfall data sets . . . . .	27
2.4.3	Need to build the rainfall forcing . . . . .	31
<b>3</b>	<b>Rainfall mapping</b>	<b>33</b>
3.1	Introduction . . . . .	33
3.1.1	Spatial interpolation of rainfall . . . . .	34
3.1.2	Regularised spline with tension . . . . .	35
3.2	Application to the Mandovi basin . . . . .	39
3.2.1	Separate interpolation for windward and leeward sides . . . . .	39
3.3	Simulation results and discussions . . . . .	45
3.3.1	Rainfall mapping on higher temporal scale . . . . .	48
3.3.2	Discussion . . . . .	49
<b>4</b>	<b>Rainfall-runoff modelling</b>	<b>51</b>

---

4.1	Introduction . . . . .	51
4.1.1	Limitations of the framework: Model parameterisation . . . . .	59
4.1.2	Rainfall-runoff model . . . . .	59
4.2	Soil Conservation Service (SCS) method . . . . .	60
4.2.1	Parameters of the SCS method . . . . .	63
4.3	Application to the Mandovi basin . . . . .	70
4.3.1	Sensitivity to $CN$ . . . . .	70
4.4	Results and discussion . . . . .	74
<b>5</b>	<b>Spatio-temporal variability in rainfall-runoff model</b>	<b>77</b>
5.1	Introduction . . . . .	77
5.2	Spatial variations . . . . .	78
5.2.1	Regionalisation . . . . .	78
5.2.2	Estimation of parameters . . . . .	79
5.2.3	Simulation $S2$ . . . . .	80
5.3	Temporal variations . . . . .	81
5.3.1	The seasonal change in abstraction . . . . .	84
5.3.2	Seasonal variation of SCS parameters . . . . .	86
5.3.3	The temporal regimes . . . . .	86
5.3.4	Objective criteria for transition . . . . .	88
5.3.5	Estimation of the SCS parameters . . . . .	93
5.4	Results and discussion . . . . .	97
5.4.1	Simulation $S3$ . . . . .	97
5.4.2	Evapotranspiration and abstraction . . . . .	97
5.4.3	Discussion . . . . .	103

---

<b>6</b>	<b>Implications of the modelling framework</b>	<b>112</b>
6.1	Introduction . . . . .	112
6.2	Generality of framework: West-coast rivers . . . . .	113
6.2.1	Annual variability and spatial variability . . . . .	114
6.3	Assessment of the framework and future directions . . . . .	118
6.3.1	Caveats of the modelling framework . . . . .	118
6.3.2	Strengths of the modelling framework . . . . .	119
6.3.3	Future directions . . . . .	122
<b>7</b>	<b>Summary</b>	<b>128</b>
<b>A</b>	<b>Basic hydrological variables</b>	<b>132</b>
A.1	Precipitation . . . . .	132
A.2	Evapotranspiration . . . . .	133
A.3	Subsurface water . . . . .	133
A.3.1	Infiltration . . . . .	134
A.3.2	Soil water . . . . .	134
A.3.3	Groundwater . . . . .	135
A.4	Surface water . . . . .	135
A.4.1	River discharge measurements . . . . .	136
A.5	Basin geometry . . . . .	136
<b>B</b>	<b>Rainfall-mapping algorithm</b>	<b>138</b>
B.1	General problem of mapping . . . . .	138
B.2	Multivariate interpolation by regularised spline with tension (RST) . . . . .	139
B.2.1	Implementation of RST in modelling framework . . . . .	141
	<b>Bibliography</b>	<b>143</b>

# List of Tables

2.1	Gridded rainfall datasets . . . . .	28
2.2	Discharge comparison . . . . .	29
3.1	Rain-gauge stations . . . . .	40
3.2	Discharge comparison using interpolated rainfall . . . . .	43
4.1	Abstraction coefficient used in literature . . . . .	68
4.2	SCS <i>CN</i> table . . . . .	69
5.1	SCS parameters for Simulation <i>S2</i> . . . . .	80
5.2	Seasonal regimes . . . . .	87
5.3	Objective criteria of transition . . . . .	90
5.4	SCS parameters for Simulation <i>S3</i> . . . . .	98
5.5	Simulations detail . . . . .	101

# List of Figures

1.1	Geographical setting of the Indian subcontinent . . . . .	4
1.2	Rivers of the Indian subcontinent . . . . .	5
1.3	Climatological rainfall over India. . . . .	7
1.4	Monthly discharge for some rivers of west coast of India . . . . .	8
1.5	Monthly discharge for some rivers draining into the Bay of Bengal . . . . .	9
1.6	Rivers of west coast of India . . . . .	11
1.7	Mandovi river system . . . . .	13
1.8	Rainfall and discharge climatology for Mandovi river basin . . . . .	14
1.9	Daily rainfall and discharge for Mandovi river basin . . . . .	15
2.1	Hydrological processes. . . . .	18
2.2	THMB schematic. . . . .	24
2.3	Rainfall for CRU, IMD, and TRMM data sets. . . . .	31
2.4	Rainfall and orography . . . . .	32
3.1	Model domain and interpolation domain for Mandovi river system . . . . .	38
3.2	RMSE for interpolation . . . . .	41
3.3	Interpolated rainfall maps . . . . .	42
3.4	Interpolated and observed rainfall at stations . . . . .	44

---

3.5	Simulated annual discharge . . . . .	47
4.1	Catchment integrated rainfall and discharge . . . . .	53
4.1	(continued) . . . . .	54
4.1	(continued) . . . . .	55
4.1	(continued) . . . . .	56
4.1	(continued) . . . . .	57
4.2	Daily discharge simulation ( <i>S0</i> ) with THMB . . . . .	58
4.3	Schematic of THMB-SCS . . . . .	64
4.4	Inter-annual variability of discharge and rainfall . . . . .	66
4.5	Kolmogorov-Smirnov diagram for inter-annual variability of discharge . . . . .	67
4.6	Sensitivity tests for the SCS parameters . . . . .	72
4.7	Determination of AMC . . . . .	73
4.8	Simulation <i>S1</i> results . . . . .	75
5.1	Spatial regions in the Mandovi basin . . . . .	79
5.2	AMC thresholds . . . . .	81
5.3	Simulation <i>S2</i> results . . . . .	82
5.4	The Temporal regimes . . . . .	89
5.5	Spatial variation of <i>CN</i> . . . . .	95
5.6	Temporal variation of <i>CN</i> . . . . .	96
5.7	Simulation <i>S3</i> results . . . . .	99
5.8	Comparison of Simulation <i>S3</i> with <i>S0</i> , <i>S1</i> and <i>S2</i> . . . . .	100
5.9	Error histograms for three calibration years . . . . .	102
5.10	Abstraction in Simulation <i>S3</i> . . . . .	105
5.11	Error histograms for fifteen validation years . . . . .	106
5.12	Simulation <i>S3</i> results for validation years . . . . .	107

---

5.12 Simulation results (continued) . . . . .	108
5.12 Simulation results (continued) . . . . .	109
5.12 Simulation results (continued) . . . . .	110
5.13 Correspondence plot . . . . .	111
6.1 Location of three west-coast rivers . . . . .	115
6.2 Normalised discharge for three west-coast rivers . . . . .	116
6.3 Cumulative distribution plot for three west-coast rivers . . . . .	117
6.4 Spatial variation of runoff . . . . .	119
6.5 Simulated discharge at Panaji . . . . .	121
6.6 Bar chart of spatial variation of discharge . . . . .	122
6.7 Unedited GLOBE DEM . . . . .	124
6.8 Comparison of GLOBE and SRTM DEM . . . . .	125
6.9 River basins of Goa derived from SRTM DEM . . . . .	126



# Chapter 1

## Introduction

### 1.1 Motivation

From time immemorial rivers are the most important and easily available source of freshwater to us. All the great civilizations of the past were based on the banks of rivers. In this modern era the demand for freshwater for agriculture, industries and domestic usage has increased many fold, making economy and development of a region closely dependent on water. Issues related to water resources attract considerable interest. Water resource planning, alternative and renewable sources of energy (hydroelectric projects), waste-effluent strategy and flood forecasting are some of the many facets in which rivers play an important role. Rivers are also crucial for maintaining some of the most delicate environments like wetlands and coastal-estuarine ecosystems.

Rivers carry freshwater to their destination which is usually a sea or a lake. In this way rivers play a crucial role in the movement of water on the land surface, thus making it a very important component of the global hydrological cycle [Dai and Trenberth, 2002; Coe, 1998; Döll et al., 2003]. The water evaporated from the oceans is returned through the rivers along with direct precipitation over the ocean. Rivers carry the water precipitated over land to oceans, and thus help maintain the freshwater balance in the oceans. The freshwater influx forces changes in the salinity

of the sea water. Variability in the freshwater forcing to the oceans has been shown to affect the global climate [Dickson et al., 1988; Aagaard and Carmack, 1989; Andrews, 2009; Peterson et al., 2002; Hatun et al., 2005; Alley et al., 2003; Kingston et al., 2006; Lenton et al., 2008].

The weather and climate models incorporate a representation of the physics of moisture, energy and momentum balances between land, ocean and atmosphere. In these models, representation of land surface hydrology plays a crucial part to validate or close the moisture and energy budget.

As rivers flow through land surface, they modify it through erosion, chemical weathering and deposition. These processes cause the river discharge to carry particulate and dissolved minerals and nutrients to the oceans, affecting the global biogeochemical cycles. These processes change the surface characteristics of land (albedo, heat capacity and exchange of energy, moisture and momentum), affecting the climate.

### 1.1.1 River discharge

One of the most important aspects of river discharge is that it can be measured directly, giving a unified account of the complex hydrological variables in the catchment. In fact among all the hydrological variables, river discharge is one of the most accurately measured quantities [Hagemann and Dumenil, 1998; Fekete and Vörösmarty, 2007]. Unfortunately, the importance of river discharge in climate studies was not realized early enough; the river discharge data were collected by hydrological agencies through out the world for the sole purpose of managing or designing hydrological projects and utilisation of water resources. Since the data were primarily collected with the view to solve the problem of water resources, only water developed areas were preferred. These reasons also limited the scientific community's access to the data. Thus, although river discharge is very useful and is one of the most accurately measured hydrometeorological variables, its monitoring and sharing is limited to the catchment or regional scales only.

The importance of river discharge was duly recognized in the 1970s, and efforts to make the

discharge information available were made. One of the earliest estimates were global maps of river discharge prepared by Baumgartner and Reichel [1975]. The United Nations declared 1980s as the hydrological decade and the first compilation of river discharge data sets were released in the form of printed books [UNESCO IHP, 1984]. These data sets formed the basis of World Meteorological Organisation's (WMO) Global Runoff Data Centre (GRDC) data archive under the World Climate Program. GRDC was established in 1987 with a mandate to collect, archive and disseminate data pertaining to river flows and surface runoffs on a continuous long-term basis for the member countries and scientific community. The access to the actual discharge time series is by request, but the metadata information of GRDC data catalogue is available freely on the web.

There are other sources, which by synthesis of observations (GRDC and other sources) and various analytical tools, provide river discharge datasets [Graham et al., 1999; Cogley, 1989; Dai and Trenberth, 2002; Fekete et al., 2002; Peel and McMahon, 2006; Perry et al., 1996; Vörösmarty et al., 1996]. In addition, there exists a whole range of numerical models to simulate river discharge on global scales [Coe, 1998, 2000; Döll et al., 2003; Miller et al., 1994; Yates, 1997; Sausen et al., 1994].

## 1.2 Setting of the problem

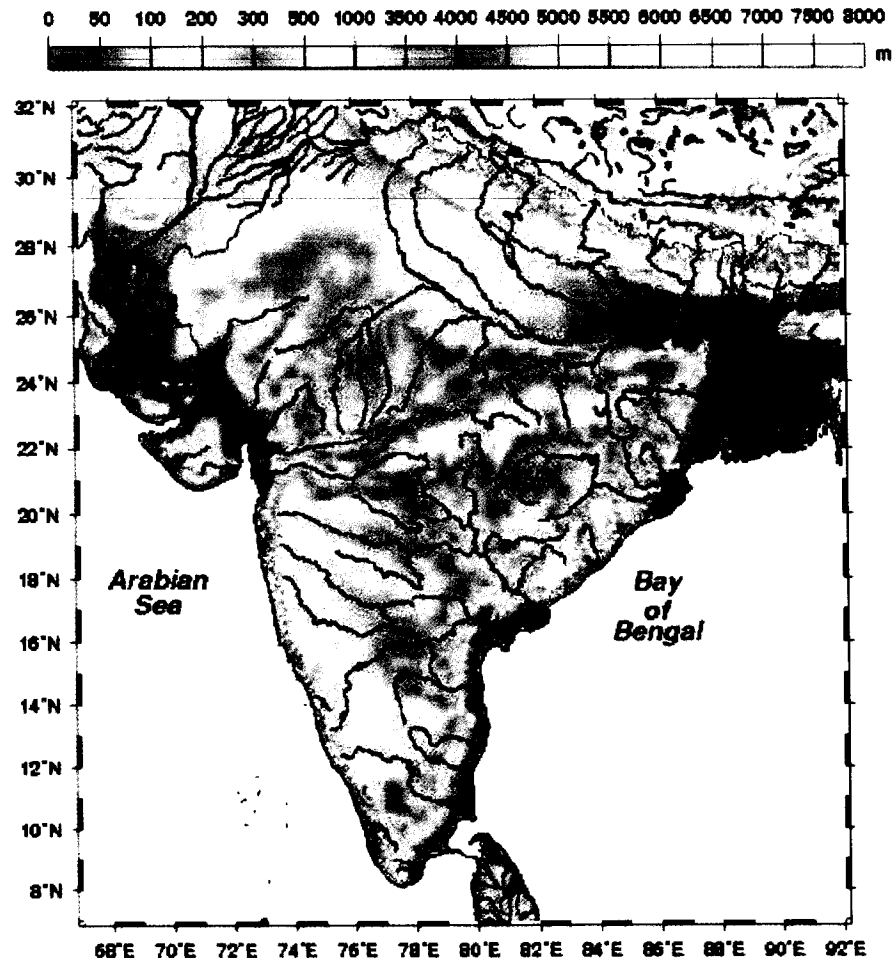
### 1.2.1 Geography of the region

Its unique position makes the Indian subcontinent a land of diverse geographical and climatic conditions. It is bounded along the north by the Himalayas range and by the Arabian Sea to the southwest, Bay of Bengal to the southeast, and Indian Ocean to the south<sup>1</sup> (see Figure 1.1). This makes the Indian subcontinent a unique geographical and climatic entity.

---

<sup>1</sup>Together these seas are called North Indian Ocean (NIO).

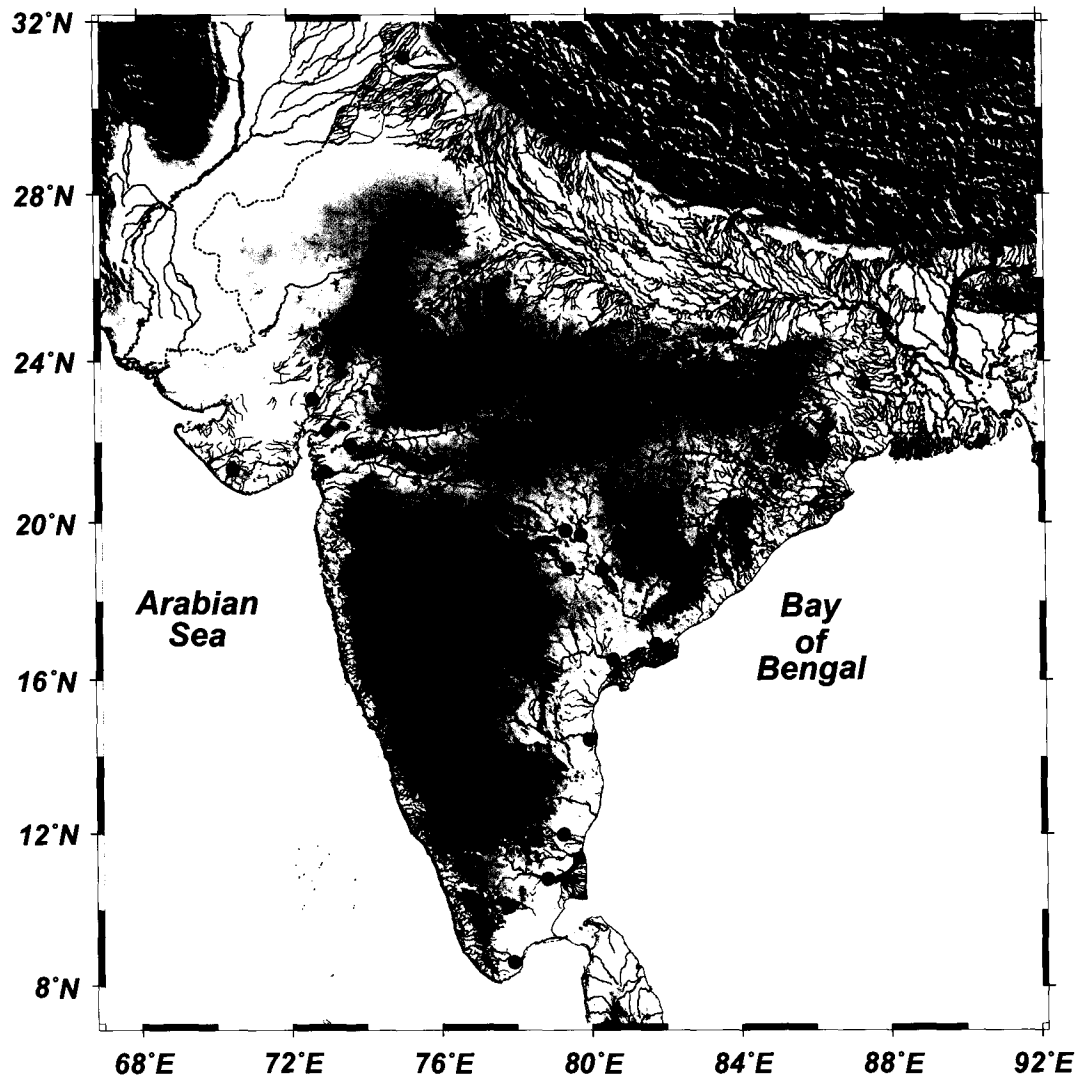
**Figure 1.1** Topography of the Indian subcontinent (in metres above mean sea level) based on the 2' (~ 4 km) ETOPO data [ETOPO, 2006]. Major rivers are also shown.



The Indian subcontinent is well fed by numerous rivers, all of them draining into either the Bay of Bengal or Arabian Sea (Figure 1.2). These rivers can be classified into different categories by considering their final destination, size or by the place of origin. In the subcontinent the rivers can be categorised broadly into three types by their place of origin:

1. The Himalayan rivers;

**Figure 1.2** Rivers (in blue) of Indian subcontinent on the shaded relief map. Almost all the rivers drain into either the Arabian Sea or Bay of Bengal. The data (drainage network) is extracted from the *Digital Chart of the World Server* (available from <http://www.maproom.psu.edu/dcw/>). The black circles represent the discharge gauges included in GRDC, showing the sparsity of observations available from India in global data sets.



2. The central Indian rivers;
3. The western ghat rivers.

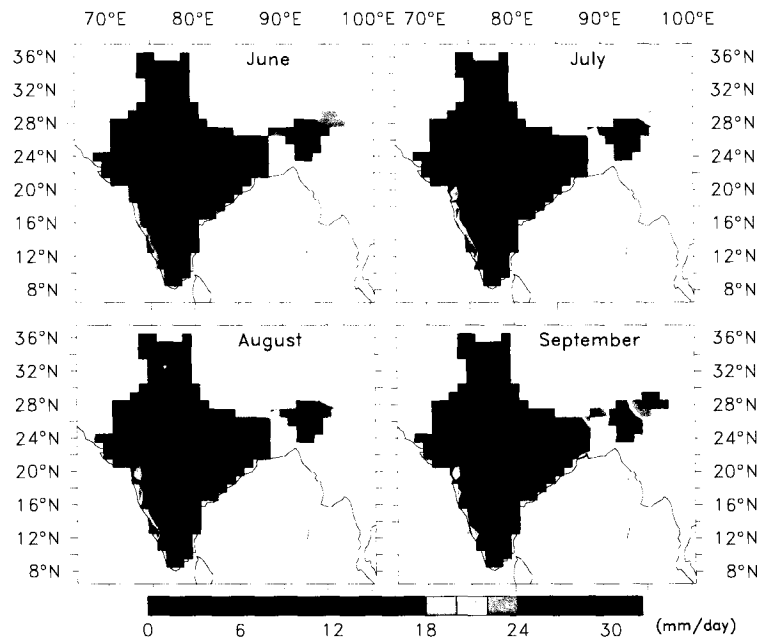
### 1.2.2 Climate of the region

The major feature of the Indian climate is the intra-annual variation of the atmospheric and oceanic circulation. A feature of the intra-annual variation of atmospheric circulation is the complete reversal of winds and precipitation pattern, which is known as the *monsoons*. The whole subcontinent depends upon the vagaries of the monsoon. Hence, concentrated efforts have been made to improve our understanding of the climate. A major step in this regard is to understand the variability of the monsoon and oceans over a range of scales. For most of the country (except east coast of India), a major share of rainfall ( $\sim 70\%$ ) occurs in four months, June to September, known as the summer monsoon season. There are clearly two regions of rainfall maxima, the west coast and the northeastern part of India (Figure 1.3).

Rainfall during the monsoon season is the source of water in the rivers of the Indian subcontinent. Almost 75% of rainfall occurs in monsoon. As rainfall is the main source of water in rivers, they also swell up during the monsoon season (Figures 1.4 and 1.5).

This unique geographical setting makes the climate of the subcontinent dependent on the atmosphere-land-ocean interaction processes. The air-sea interaction processes and differential heating of land and sea are some of the well-known processes affecting the monsoon. The freshwater discharge influences oceanic circulation on various time scales. This freshwater discharge reduces the salinity of the sea water it mixes with. This fresher water, of low salinity, is lighter and sits on the top of the denser saline oceanic waters. It changes the stability and salinity of the surface water layer in the ocean, making it more stable. This stable stratification has implications for the climate as the upper layer of the ocean is always in contact with the atmosphere. The role of freshwater in the physics of surface mixed layer is relatively well known for the Bay of Bengal

**Figure 1.3** Climatological rainfall ( $\text{mm day}^{-1}$ ) over India for June to September. The rainfall is from India Meteorological Department (IMD) gridded rainfall data [Rajeevan et al., 2006b].



region. Rivers like Ganga (Figure 1.4) and Brahmaputra bring huge amounts of freshwater into the bay. The ability of the Bay of Bengal to support the tropical convection has been attributed to the high freshwater influx into the bay through high river discharge and rainfall over the bay. There are global data sets which resolve the rainfall over the sea. But again, there is a lack of quantitative information on the river discharge; whatever little is available is from global-scale, coarse-resolution studies or estimates based on gross generalization. The situation is worse for the western coast of India, where there is practically no information on the river discharge.

The most striking feature of the Indian west coast is the presence of the Sahyadri range (Western Ghats), which runs parallel to the coast. The coast itself is narrow, no more than a few tens of kilometres wide and extending up to the foothills of the Sahyadris. From the foothills, the slopes of the Sahyadris rise abruptly in the form of an escarpment to an average elevation of  $\sim 700$  meters. At several places, the escarpment is broken by river valleys. The axis of the range lies per-

**Figure 1.4** Monthly discharge (in  $\text{m}^3 \text{s}^{-1}$ ) for three west coast rivers. The rivers are Narmada (northern part of the coast), Mandovi (central) and Periyar (southern). The discharge data are taken from GRDC.

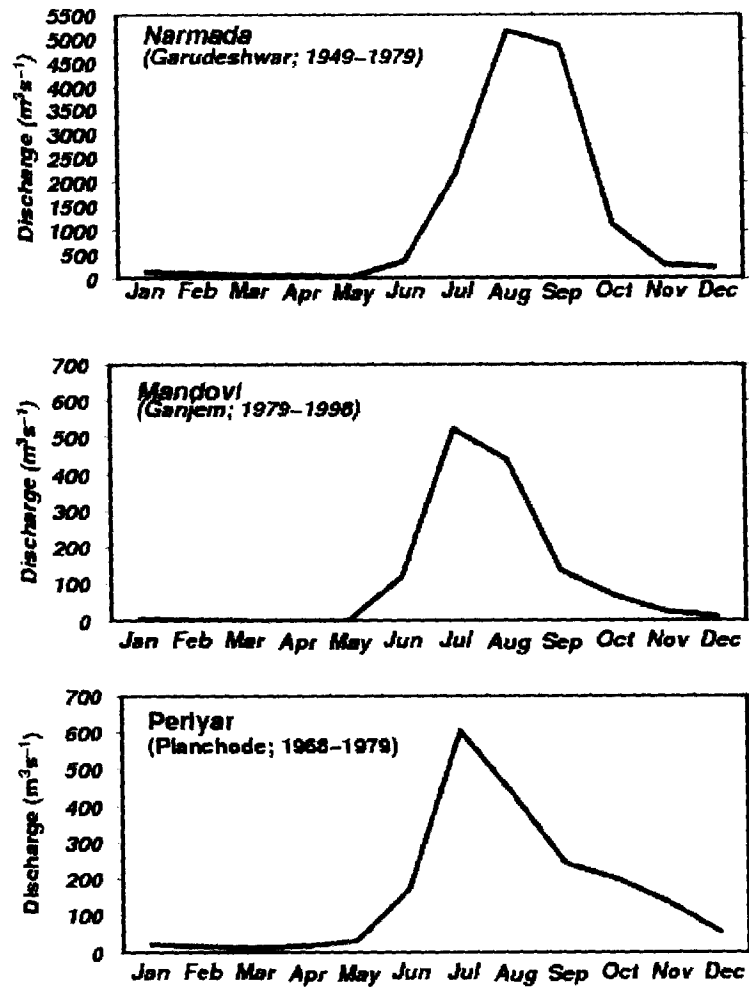
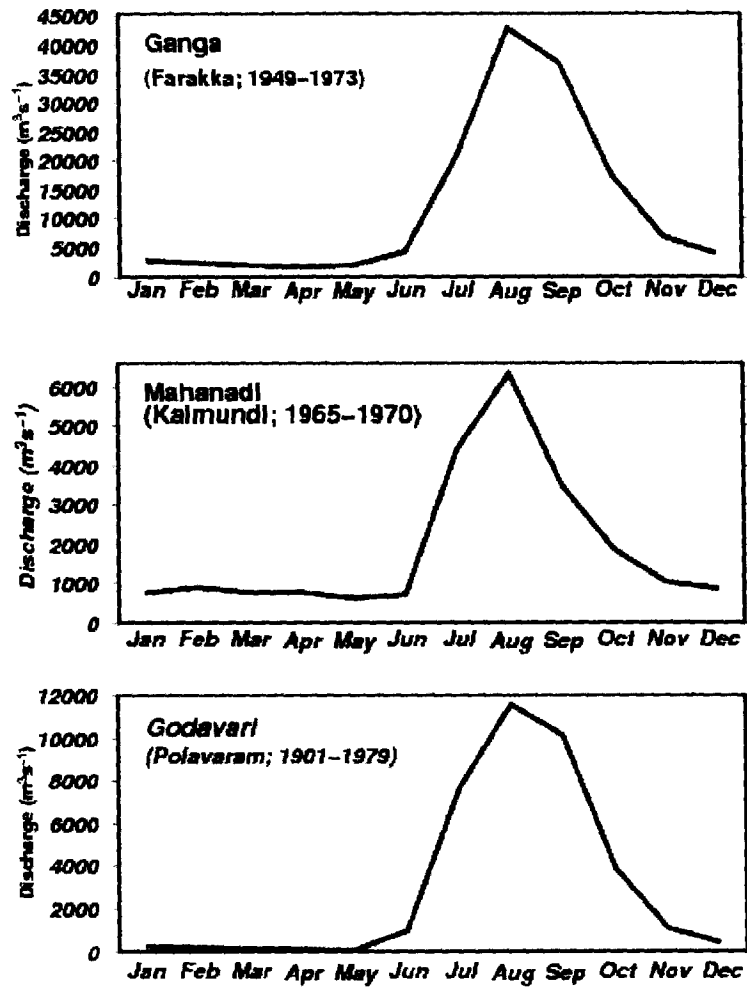




**Figure 1.5** Monthly discharge (in  $\text{m}^3 \text{s}^{-1}$ ) for Ganga, Mahanadi, and Godavari rivers. The discharge data are taken from GRDC.

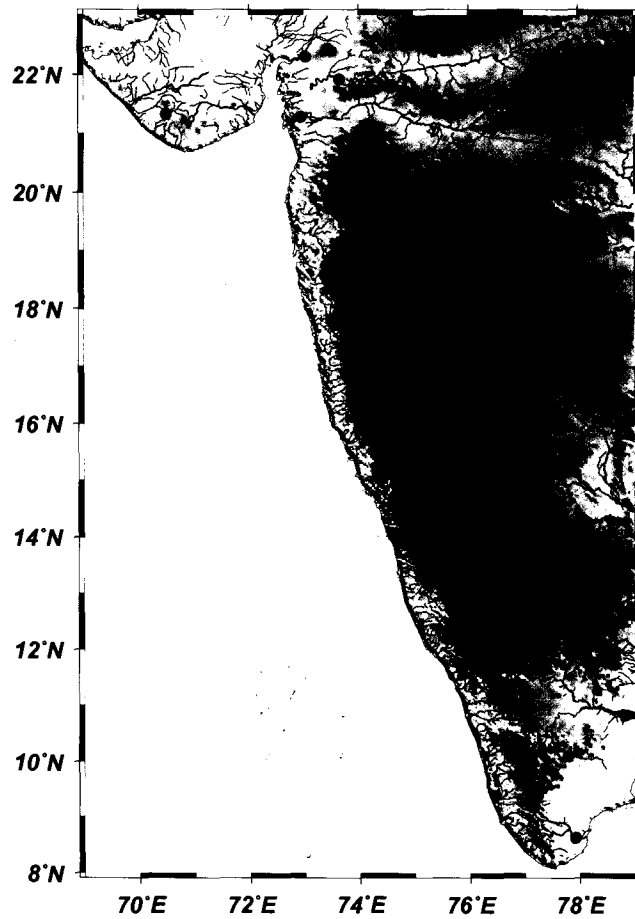


pendicular to the prevailing summer-monsoon winds. The moisture-laden monsoon winds cause heavy rainfall on the windward side of the range, distinguishing it from the much drier leeward side. Most of the west-coast rainfall ( $\sim 90\%$ ) occurs during June–September (summer monsoon), there being negligible rainfall during December–April. The heavy rainfall and small coastal plain bounded by hills of Sahyadris ensure that a huge number of rivers ( $\sim 600$  by an estimate of Central Water Commission (CWC)) flow into the eastern Arabian Sea and most of them do not have river discharge observations (Figure 1.6). Establishing gauges on each river is practically not possible. Furthermore, for most rivers with available discharge data, there is only one discharge gauging station, that too maintained away from the coast (see Figures 1.2 and 1.6). For the west coast this distance is of the order of  $\sim 50$  km because discharge measurements from conventional methods are not feasible in tidal streams. The discharge gauge has to be located upstream of the regime influenced by tides.

### 1.3 Problem

As pointed out earlier, on the global scale the role of rivers on climate is studied in detail. For the Indian subcontinent, their role is still not studied in detail because of lack of information on discharge. Global datasets on discharge suffer from estimates from very few discharge gauges (Figure 1.2) often situated hundreds of kilometers from the river mouth, coarse resolution and their ability to provide only annual discharges [Fekete et al., 2000]. Even bigger rivers like the Brahmaputra and Ganga have very limited records in the global discharge datasets [Dai and Trenberth, 2002]. In the north Indian Ocean, the importance of river discharge for the thermodynamics of the upper ocean [Han et al., 2001; Howden and Murtugudde, 2001; Shenoi et al., 2002] and low-frequency variability of sea level along the Indian coast [Shankar and Shetye, 1999, 2001; Shankar, 2000; Han and Webster, 2002] has been highlighted. The dearth of information on discharge forced most of the studies listed earlier to use estimates [Baumgartner and Reichel, 1975;

**Figure 1.6** Same as Figure 1.2, but zoomed to show rivers (blue) of the west coast of India. High rainfall and small geographical terrain of the coast results in a large number of smaller rivers, contributing substantial discharge into the Arabian Sea. The black circles represent the discharge gauges included in GRDC.



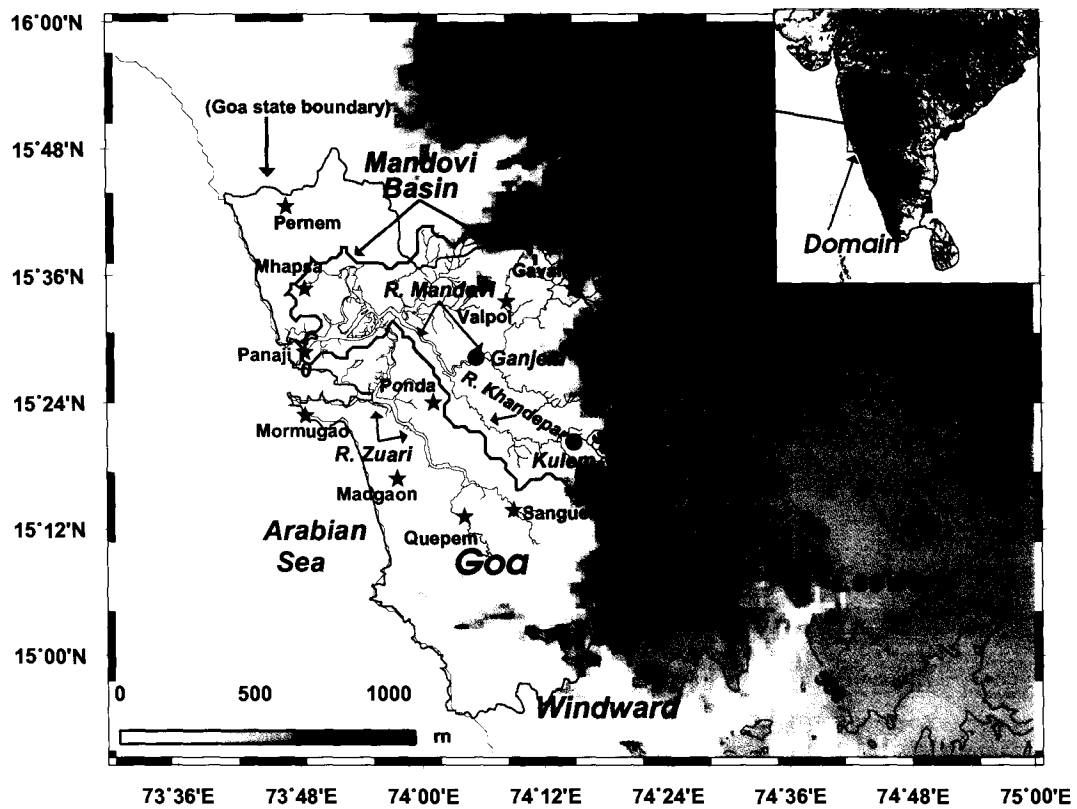
Martin et al., 1981] made decades earlier, leading, at times, to attempts to determine the discharge through inverse modelling [Yaremchuk et al., 2005]. The type of study required to fill this void is non-existent, not only for the west coast of India but for the entire Indian subcontinent [Shankar et al., 2004]. A little more detailed information on river discharge is available through the work of Rao [1975]. Recently, few articles appeared on climate and water resources of the country [Ramesh and Yadava, 2005; Narasimhan, 2005, 2008] and a new book has been also published by Jain et al. [2006]. Although they are very useful for qualitative information and other metadata information like watershed area and other observations, the information about quantitative estimates and methods is not enough as the approach is more of a descriptive kind. This lacuna is due to lack of quantitative studies on the relevant scale [Shankar et al., 2004]. The problem of management and planning of water resources in India is still viewed as a typical engineering problem, which is surprising since the economy of the subcontinent is driven by the vagaries of climate and related water resource issues.

To address this issue along with the issues related to water resources, what is needed is a modelling framework which provides a reliable quantitative estimate of the water resources. Shankar et al. [2004] highlighted the strong need for quantitative estimation of river discharge and other hydrological variables on a resolution fine enough to evolve strategies for an average Indian district, yet large enough to make possible estimates on the scale of the subcontinent. Simulations give us a tool to estimate the discharge at any point on a river. Once the simulations are validated reasonably, they can be used to fill the gaps in observations, or even to extend the record backwards as long as forcing fields are available. They give us a tool to study and carry out numerical experiments for different climatic scenarios. This information can be useful to various sections of society, such as climate scientists, policy makers, industrial managers and agriculture practitioners at the level of the issues and scales relevant to them.

This objective led Shankar et al. [2004] to assemble a framework for estimating river discharge. To demonstrate its viability the framework was applied and tested for the Mandovi (Fig-

ure 1.7), a river system in Goa on the Indian west coast (Figure 1.2). The framework is simple to implement, consists of freely available tools, and requires only the basic data input for any hydrological model: topography, rainfall, and evaporation. The framework is based on Terrestrial Hydrologic Model with Biogeochemistry (THMB)<sup>2</sup>, a numerical model developed by Coe [2000]. THMB model provides a reliable water balance of a river system.

**Figure 1.7** The Mandovi and Zuari (all rivers digitized from Survey of India maps) are the two major rivers of Goa (border overlaid on the map). The Mandovi originates in the Sahyadris and drains into the Arabian Sea near Panaji. The Mandovi basin (black curve), has two discharge gauging stations, at Ganjem on the Mandovi itself and at Kulem on its major tributary, the Khandepar. The region has two distinct topographical and climatic features: to the west lies a coastal plain with heavy rainfall (windward side), and to the east lies a plateau with less rainfall (leeward side). The rainfall stations in and around the basins are marked by black star.

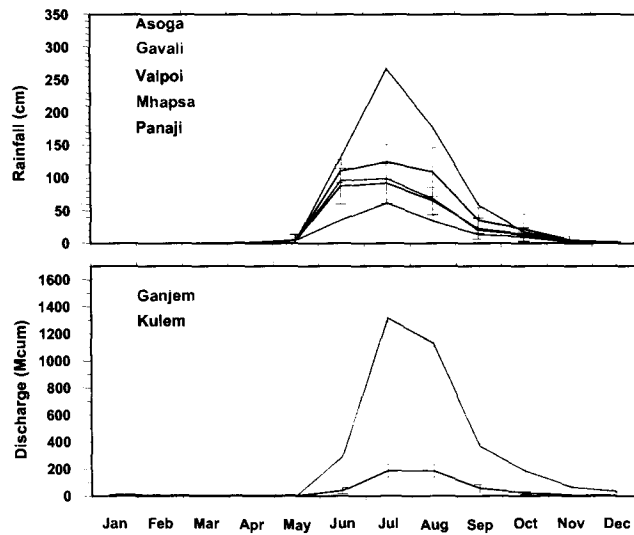


<sup>2</sup>This model was earlier called HYDrological Routing Algorithm (HYDRA).

### 1.3.1 Mandovi river system

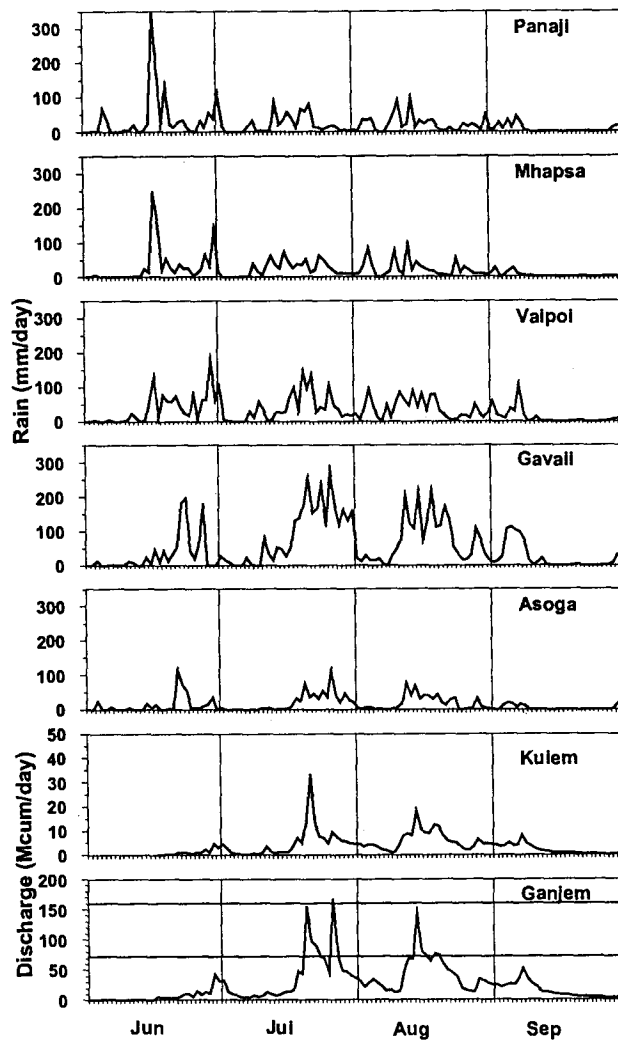
Mandovi river is the major river of Goa, and it has two discharge gauges for which daily estimates of the discharges are available (Figure 1.7). It is typical of the small rivers flowing down from the Western Ghat mountains (Sahyadris) into the eastern Arabian Sea (Figure 1.6). As over the rest of the west coast,  $\sim 90\%$  of the rainfall in the Mandovi basin occurs in the monsoon months (June–September) and consequently  $\sim 90\%$  of discharge too occurs at this time. There is considerably more variability in both the discharge and rainfall in the basin on the seasonal and inter-annual time scales (Figure 1.8). The rainfall variability in space is also prominent; rainfall increases as we go eastwards from the coast (Panaji), on the hills and slopes of Sahyadris (Gavali), and decreasing thereafter in the rain shadow zone on the leeward side (Asoga) (Figures 1.7 and 1.8).

**Figure 1.8** Rainfall climatology (cm; for 1981–1998) at the five rain gauge stations in the Mandovi basin (Panaji, Mhapsa, Valpoi, Gavali, and Asoga) and discharge climatology (Mcum or  $\text{Mm}^3$  ( $10^6 \text{ m}^3$ ); for 1981–1998) at the two runoff gauging stations in the Mandovi basin (Ganjem and Kulem). The vertical bars indicate the standard deviation of the monthly rainfall and runoff; the height of the bars is a measure of the inter-annual variability.



There is also considerably more variability in the discharge and rainfall on the intra-annual time scale (Figure 1.9). On the daily time scale, the correspondence between discharge and rainfall

**Figure 1.9** Daily rainfall (mm; for 1992) at the five rain gauge stations in the Mandovi basin (Panaji, Mhapsa, Valpoi, Gavali, and Asoga) and discharge (Mcum or  $\text{Mm}^3$  ( $10^6 \text{ m}^3$ ); for 1992) at Ganjem and Kulem.



is less obvious, especially during monsoon-onset (June) and late-monsoon (September) seasons.

## 1.4 Objective of the thesis

This thesis presents our attempt to develop a viable quantitative framework to simulate the river discharges on the west-coast of India. Since the Mandovi is typical of the west coast rivers, it is assumed that the modelling framework will also work for the other river basins on the west coast of India. The modelling framework components and tools are described in chapter 2. The framework requires a rainfall forcing field: a method to map the rainfall from rain gauges to the model grid is presented in chapter 3. Monthly rainfall maps were generated to simulate the annual discharge of the Mandovi river; the mapping method and simulation results are described in this chapter. The modelling framework is unable to simulate daily discharge, and the framework has to be extended by incorporating a rainfall-runoff model. This extension of the modelling framework is the subject of Chapter 4. Though the rainfall-runoff model improves the simulations considerably, it is unable to capture the large intra-annual variability accurately. Hence, we introduce spatio-temporal variability into the rainfall-runoff model; this parameterisation is the subject of Chapter 5. The applicability and generality of the framework, along with its strengths and weaknesses, are discussed in chapter 6. Finally, the main findings of the thesis are summarized in Chapter 7.



## Chapter 2

# Hydrological Modelling framework

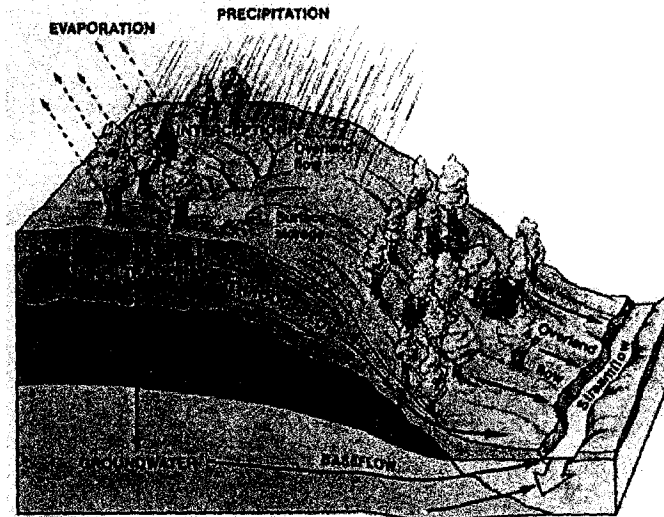
### 2.1 Hydrological modelling process

#### 2.1.1 Runoff production and flow processes

River discharge is a vital component of surface hydrology, integrating various processes occurring at varying temporal and spatial scales (catchment scale). What are these processes? Let us begin by considering what happens when rainfall occurs in the catchment (Figure 2.1).

1. Rainfall varies both in space and time.
2. Some of the rainfall will fall directly (*throughfall*) on the ground and flow according to local topography.
3. Some of the water will be intercepted by the vegetation canopy (*interception*) and evaporated back to the atmosphere.
4. Vegetation can concentrate the flow near itself by collecting and directing the rainfall through branches, leaves and stem (*stemflow*). This channeling results in higher concentration of water, resulting in higher intensity flow near plants.

**Figure 2.1** Different hydrological processes on the catchment scale. Cartoon modified from [http://snobear.colorado.edu/IntroHydro/geog\\_hydro.html](http://snobear.colorado.edu/IntroHydro/geog_hydro.html). (See Appendix A for a brief description of basic hydrological variables.)



5. As the water reaches the ground, it starts infiltrating (*infiltration*) the soil surface to increase the soil moisture and some part of this water even *percolates* (*percolation*) to deeper levels. If the underlying ground consists of an impermeable area of rock or artificial structure, the runoff will start immediately. This near-surface downslope rapid flow is known as *through-flow*. The rate of infiltration depends on the rainfall *intensity* and the infiltration capacity of the soil. When the rate of rainfall exceeds the *infiltration* capacity, excess water flows over land surface as *overland flow*, according to the *local* topographic gradient. Some of this excess water is retained in the surface depressions (*surface storage*) before overland flows occur.
6. The water that percolates the soil column will also *tend* to flow downslope (*baseflow*), especially if the soil column is saturated and sitting over an impregnable layer of rock. The flow due to subsurface processes is called *subsurface runoff* and is important in catchments with

high infiltration capacities and a deep layer of soil.

Thus, a part of rainfall becomes runoff and flows as surface or subsurface flow to appear at the catchment outlet. The rest of the rainfall can be said to be hydrologically abstracted; either it is returned to the atmosphere or percolates deep down in the groundwater. The moment the runoff appears in a river, it is called *streamflow* or *channel runoff* or *river discharge*; it has to be transported on the land surface through the surface hydrological network.

The surface hydrological processes can be understood in terms of a dynamically linked system in which rivers, lakes, and wetlands can be defined as a continuous hydrological network. Through this network the locally derived runoff is transported across the land surface and is eventually transported to the ocean or an inland lake [Coe, 1998, 2000].

Thus, there are three very important aspects of hydrological modelling. The first one is runoff generation: it decides how much water goes into the stream during and after a rainfall event.

The second aspect is how this runoff travels from the source areas to outlet — the routing of the runoff. It is not possible to measure this inflow into stream network directly as it depends upon the velocities of the surface and subsurface flows on the ground as well as upstream components of the flow in the streams.

The third aspect is similar to the earlier one and is concerned with the manner in which the streamflow travels through the land surface in the river channel. This is known as river routing. Thus, essential criteria for modelling the river flows in time and space include at least three components:

1. to determine how much of the rainfall is converted into runoff (runoff generation);
2. how this runoff is routed over the land and translated to the stream network;
3. how the stream network transports this water.

It should be clear, however, that it is very difficult to separate these three components at any given time. In the catchment all the three processes appear simultaneously.

A technique called reservoir routing is utilized here to model these flows. A reservoir is a conceptual tool (similar to a natural or artificial reservoir) that is designed to store the incoming water and release it based upon its intrinsic properties. The function of this reservoir depends on the inflow into the reservoir, initial condition of the reservoir and its reservoir characteristics (like time scales), and a mathematical expression is used to relate these quantities. For example, water flowing on the surface can be represented by a “surface water reservoir”. Similarly, water flowing into subsurface reservoir can be represented by a “subsurface reservoir” which will be different from surface reservoir in the flow time scales: surface flow will be much faster than the subsurface flow.

### 2.1.2 Hydrological reservoir routing model

One of the most widely used techniques for reservoir modelling is to use the concept of conservation of mass. In one-dimensional flow the conservation of mass can be stated by the equation of continuity. As water is an incompressible fluid, the equation of continuity states that in the direction of flow, change in flow per unit length is balanced by the change in flow area per unit time.

$$\frac{\partial Q}{\partial x} + \frac{\partial A}{\partial t} = 0, \quad (2.1)$$

where  $Q$  is the flow rate ( $\text{m}^3 \text{s}^{-1}$ ) and  $A$  is the flow area (in this case width of the flow element multiplied by depth). Equation (2.1) can be written in incremental form for an element of finite length  $\Delta x$  for the time interval  $\Delta t$  as

$$\frac{\Delta Q}{\Delta x} + \frac{\Delta A}{\Delta t} = 0. \quad (2.2)$$

The change in flow rate ( $\Delta Q$ ) is nothing but the inflow minus outflow ( $I - O$ ) of the water in the volume element. The change in the volume can be defined a quantity called ‘Storage’  $\Delta S$

( $\text{m}^3$ ) which is  $(\Delta A \times \Delta x)$ . Then Equation (2.2) can be spatially averaged over the length scales of interest and is written in the form:

$$\frac{\Delta S}{\Delta t} = I - O. \quad (2.3)$$

For  $\Delta t \rightarrow 0$ , Equation (2.3) can be written in the differential form

$$\frac{dS}{dt} = I - O, \quad (2.4)$$

which implies that in the reservoir, the difference between outflow and inflow is balanced by the rate of change in storage volume. The reservoir is physically equivalent to a bucket being filled by water and having a hole at the bottom for escape of the water as outflow.

### 2.1.3 Linear reservoir model

Equation (2.4) can be used to calculate the outflow for a given input (inflow), only when the storage  $S$  is known. For the real flows outflow is a function of both  $S$  and  $I$ , but Equation (2.4) can be simplified using an assumption that for an ideal reservoir, storage is a function of outflow. For a linear reservoir model this relationship is assumed to be linear: outflow is directly proportional to the storage.

$$O = KS, \quad (2.5)$$

where  $K = 1/T$  is a constant of proportionality. Physically this parameter is equivalent to the inverse of residence time of water in the reservoir. Based on Equation (2.5), the equation of a linear reservoir model can be written as

$$\frac{dS}{dt} = I - \frac{S}{T}. \quad (2.6)$$

Although in reality the relationship between rainfall and runoff is never linear, this approximation makes the mathematics of hydrology much simpler to handle. Many authors have used this relation

to successfully model catchment hydrology [Beven, 2001].

## 2.2 Background and approach

This simpler approach avoids the use of more complex 'hydraulic' routing methods in which both momentum and mass conservation are used to obtain the discharge. Conservation of momentum and mass leads to the shallow water equations (in hydrology, better known as Saint Venant equations), which are parameterised differently to obtain the various routing schemes (for more information, see standard hydrological textbooks such as Beven [2001] and Chow et al. [1988]). In hydrological literature, the two most used parameterizations for the flow velocities are kinematic wave [Hagemann and Dumenil, 1998; Vörösmarty et al., 1996; Miller et al., 1994] and diffusion wave [Julien et al., 1995; Downer et al., 2002] method.

In this thesis we use a linear reservoir hydrological routing model called THMB (previously called HYDRA) of Coe [2000, 1998]. It uses the concept of linear reservoirs to route the runoff through the grid cells defining the region. The flow velocities are constant over time and are parameterised as a function of the topographic gradient and the grid size. As one moves downstream through the river, the flow generated by the model increases as more cells contribute to the flow. The rate at which water moves to a downstream grid depends mainly on the mass of the water that is above the sill depth (depth over which water can flow to the next grid), the mean distance between the grid cell and its immediate neighbour and the downstream topographic gradient. The flow rates are parametrized in the model by using reference velocities. The modelling approach is similar to that of Hagemann and Dumenil [1998], Costa and Foley [1997], and Sausen et al. [1994].

### 2.3 THMB model

The THMB modelling framework was already tested by Shankar et al. [2004] for the Indian west coast. Given the distribution of local rainfall and evapotranspiration, THMB can route the surface runoff and subsurface runoff to its destination, the sea or an inland lake. It uses a linear reservoir model to simulate water transport in terms of local flow directions derived from the local topography, residence times within a grid cell, and effective flow velocities.

The water transport is represented by the time-dependent change of three linear reservoirs (Figure 2.2). The first is the river water reservoir ( $W_R$ ), which contains the sum of upstream and local water in excess of that which is required to fill a local surface water depression; the second reservoir is the surface runoff pool ( $W_S$ ), which contains water that has run off the surface locally and is flowing towards a river; the third reservoir is the subsurface runoff pool ( $W_D$ ), which contains water that has drained through the local soil column and is flowing towards a river. The water entering the hydrological network is the sum of the land surface runoff ( $R_S$ ), subsurface runoff (drainage) ( $R_D$ ), and the flux of water from upstream grid cells ( $\sum F_{in}$ ). THMB also contains the terms including rainfall and evaporation over the water surface [Coe, 2000] which were neglected by Shankar et al. [2004] because there is no significant water body in the Mandovi basin.

The flow is governed by three differential equations similar to Equation (2.6) and given by Coe [2000]:

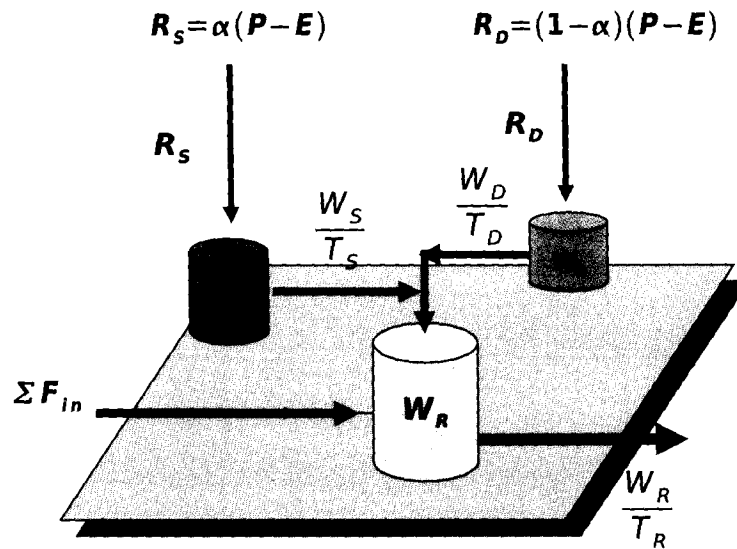
$$\frac{dW_S}{dt} = R_S - \frac{W_S}{T_S}; \quad (2.7)$$

$$\frac{dW_D}{dt} = R_D - \frac{W_D}{T_D}; \quad (2.8)$$

$$\frac{dW_R}{dt} = \left( \frac{W_S}{T_S} + \frac{W_D}{T_D} \right) - \frac{W_R}{T_R} + \sum F_{in}. \quad (2.9)$$

Here,  $T_S$ ,  $T_D$ , and  $T_R$  denote the residence times of water in their respective reservoirs. (The

**Figure 2.2** Schematic representation of THMB. The figure shows a THMB grid cell and the fluxes into and out of the three reservoirs (surface runoff, subsurface runoff, and river water) associated with each cell.  $(P - E)$  denotes the runoff, the difference between rainfall and evapotranspiration; determines the fraction of runoff (surface runoff  $R_S$ ) that goes into the surface water reservoir ( $W_S$ ),  $T_S$  being the time scale over which water flows out of the reservoir;  $R_D$  is the subsurface runoff;  $W_D$  denotes the subsurface water reservoir,  $T_D$  being the time scale over which water flows out of this reservoir. Water flows from both surface and subsurface reservoirs into the river-water reservoir ( $W_R$ ), from which water flows out of the cell to a downstream cell over a timescale  $T_R$ .  $\Sigma F_{in}$  is the total inflow from all upstream cells into the river water reservoir.



reservoirs are expressed in  $m^3$ , the residence times in seconds, and the surface and subsurface runoffs and  $\Sigma F_{in}$  in  $m^3 s^{-1}$ ). Following Coe [2000] and Shankar et al. [2004] the first two residence times were considered constant for simplicity. The stream flow residence time,  $T_R$ , is defined as the ratio of the distance between the centres of the local and downstream grid cells (a function of the DEM resolution) and the effective velocity of water; the effective velocity is parameterized differently for grid cells with and without wetlands or standing water (see Coe [2000] for more details). The model equations are integrated forward in time using an explicit differencing scheme. THMB requires the following inputs: a DEM (Digital Elevation Model) to map the topography, and surface runoff and subsurface runoff for each grid cell. THMB then derives



the hydrological network from the DEM representations of the land surface topography. This hydrological network is linked to a linear reservoir model and forced with estimates of runoff over land.

### 2.3.1 Basin geometry and DEM

Rivers flow on the surface of the earth and follow the terrain. In the numerical modelling framework the topography of the terrain needs to be specified digitally. A DEM represents an estimate of the average elevation for a given grid cell. There exist a number of freely available DEMs with varying degrees of resolution (from 3-arc second to coarser resolutions). The choice of DEM depends upon the computing resources and nature and scale of the basin.

### 2.3.2 Flow directions

The runoff generated in the river basin has to be transported to the mouth of the river through the flow paths. There must be directed paths connected to the grid-cells from the headwaters of the river to the grid cells which are successively closer to the mouth of the river. Then there must be a way to specify how fast the water moves from a grid cell to its immediate downstream neighborhood. The flow paths are denoted by the river direction values at each of the grid cells. The river direction values are calculated by an algorithm based on a 8-cell algorithm. As a first estimate, river direction of a grid is the direction to the neighbouring grid (out of the possible 8 grid cells) with lowest elevation. Further, if a grid is identified as lying in a pit or depression, an additional step is performed. Then all depressions are filled using a filling algorithm and the land surface is sloped towards the outlet of the depression. Using the filled surface, flow directions are again calculated. This is done iteratively until all the grid cells have unique river direction [Coe, 1998, 2000].

The river direction values are not dependent upon a season, but are determined by topography. And whether a flow is observed or not in the dry season, each cell has its own unique river direction

value. Apart from the flow directions, the algorithm also takes into account the lakes or depressions that may be present in the region.

## 2.4 Viability of the model: Mandovi river basin

The discharge simulations can be compared with observations to assess the viability of the framework. As stated earlier in chapter 1, Mandovi river has two discharge gauges. Apart from these, there exist five rain gauges in the basin to map the rainfall. This, combined with the fact that Mandovi is a typical west-coast river, makes it suitable for testing the modelling framework.

A freely available DEM called GLOBE (Global Land One-Kilometre Base Elevation) [GLOBE, 2004], with a resolution of 30-arc seconds ( $\sim 1$  km), was used in this study (same as Shankar et al. [2004] and Suprit and Shankar [2008]).

### 2.4.1 Editing of DEM

Over a large fraction of its length, the Mandovi is much less than a kilometre wide. A DEM cannot represent the surface topographic features smaller than its resolution; hence, the GLOBE DEM failed to resolve the narrow river valleys in the Mandovi basin, and local flow directions derived from it were inaccurate. Therefore, Shankar et al. [2004] developed a set of tools based on a Geographic Information System (GIS) called Geographical Resources Analysis Support System (GRASS) GIS [Neteler and Mitasova, 2002] to edit the DEM manually [Kotamraju and Shankar, 2004] so that the river could be represented accurately in the model. The modified DEM was able to resolve the river basin accurately: the area of the basin was estimated to be  $1896 \text{ km}^2$ , within 10% of previously published estimate of  $2032 \text{ km}^2$  [Rao, 1975]. The catchment area at Ganjem was estimated at  $872 \text{ km}^2$ , just 1% less than the estimate of the Central Water Commission (CWC) river discharge data. (High-resolution DEMs like Shuttle Radar Topography Mission ((SRTM) with resolution 3 arc seconds) [USGS, 2004] also show similar routing problems (and therefore

require editing) at least when they are averaged to a 30 arc-seconds grid.)

#### 2.4.2 Inadequacy of existing rainfall data sets

Shankar et al. [2004] used rainfall and evapotranspiration data from the National Center for Environmental Prediction (NCEP)/National Center for Atmospheric Research (NCAR) Reanalysis [Kalnay et al., 1996] and also rain-gauge data from Panaji and Valpoi in the Mandovi basin to demonstrate the viability of the framework. Following Coe [2000], they partitioned the difference between rainfall and evapotranspiration (both of which, they assumed to be uniform over the basin in the absence of a method to map the spatial variability) between surface runoff (30%) and subsurface runoff (70%). Shankar et al. [2004] showed that global models like the one used for creating the NCEP/NCAR Reanalysis are incapable of resolving the orography of the Sahyadris (owing to a coarse resolution) and therefore considerably underestimate the rainfall in the Mandovi basin. In the NCEP/NCAR reanalysis, rainfall is a Class C variable (minimum impact of data assimilation) [Kalnay et al., 1996] and has been shown to be unsuitable for climatic studies owing to large errors associated with the data (e. g., Janowiak et al. [1998]). Better results were obtained by Shankar et al. [2004] by using rain-gauge data, but the in situ data had to be mapped to the uniform model grid. They showed that mapping the spatial variation of rainfall was critical for simulating the discharge at Ganjem.

There exist a few other rainfall data sets for the Indian subcontinent and we first checked if they yielded discharge estimates comparable to those observed at Ganjem.

#### Testing existing gridded data sets

Gridded rainfall data sets based on observations are now available at various spatial and temporal scales. Some of these data sets are based on rain-gauge measurements and some on satellite estimates; some of them use model-derived reanalysis data. We tested three available rainfall data sets to see if these rainfall data produced discharge estimates consistent with the observations.

**Table 2.1** Description of the gridded rainfall data sets tested for discharge simulations.

Dataset	Resolution	Type	Remarks
NCEP/NCAR	2.5°, Monthly, Global	Model Reanalysis	Shankar et al. [2004]
CRU TS 2.0	0.5°, Monthly, Global	Gridded observed data set	Available from CRU
IMD	1.0°, Daily, Regional	Gridded observed data set	Available from IMD
TRMM	0.25°, Monthly, Tropics	Merged TRMM	Algorithm 3B43

In all cases, the evapotranspiration was the same and was based on the NCEP/NCAR Reanalysis [Kalnay et al., 1996]; evapotranspiration was assumed to be uniform over the basin. The discharge data at Ganjem and Kulem were obtained from CWC.

#### CRU data set

The Climate Research Unit's (CRU, University of East Anglia) CRU TS 2.0 is a widely used long-term data set for climatic variables. This data product consists of nine monthly climate variables gridded on a 0.5° grid; the product is based on surface meteorological observations [New et al., 1999, 2000]. The data are available online (Table 2.1) for 1901–2000. The grids were constructed by interpolating various available observational data sets using a thin-plate spline interpolation scheme. We forced THMB with the monthly rainfall field from CRU. As with NCEP/NCAR, the rainfall forcing was assumed to be constant over the catchment. As there are four CRU grid cells that contain a part of the Mandovi basin, the highest of the four rainfall values was used to force THMB (the grid cell is marked by a solid dot in Figure 2.3). The simulated discharge was considerably less than the observed, the average error over 1981–1998 being 53% (Table 2.2). The problem is the grid size, the area of a single CRU cell being larger than the Mandovi basin; hence, it was unable to resolve the rainfall variability in the basin.

**Table 2.2** Comparison of simulated and observed discharges at Ganjem; all the discharges are in Mm<sup>3</sup>. Column 2 (C2): Observed discharge at Ganjem (OG); C3: simulated discharge at Ganjem for CRU forcing; C4: as in C3, but for IMD forcing. In columns 1 and 2, the numbers in parenthesis denote percentage error (simulated minus observed discharge). The last two rows of table show the mean (percentage error in parentheses) and standard deviation (SD) of the respective variables

Year	OG	CRU	IMD
1981	3895	2188 (-43.8)	2338 (-40.0)
1982	4214	1456 (-65.4)	1943 (-53.9)
1983	3787	2413 (-36.3)	2561 (-32.4)
1984	3540	1329 (62.5)	1523 (-57.0)
1985	3171	1005 (-68.3)	2003 (-36.8)
1986	2543	1214 (-52.3)	1068 (-58.0)
1987	2275	866 (-61.9)	1700 (-25.3)
1988	4187	2092 (-50.0)	1943 (-53.6)
1989	2762	1302 (-52.9)	1633 (-40.9)
1990	4018	1230 (-69.4)	1748 (-56.5)
1991	3305	1582 (-52.1)	1442 (-56.4)
1992	3326	1849 (-44.4)	1661 (-50.1)
1993	3333	1466 (-56.0)	1456 (-56.3)
1994	4718	2545 (-46.1)	1734 (-63.2)
1995	2940	1036 (-64.8)	2298 (-21.8)
1996	2557	1448 (-43.4)	2098 (-17.9)
1997	3721	2214 (-40.5)	2170 (-41.7)
1998	2906	1658 (-42.9)	1870 (-35.7)
<b>Mean</b>	3400	1605 (-53)	1844 (-44)
<b>SD</b>	648	489	359

### IMD data set

IMD released a 1° gridded daily rainfall data set, covering whole of the country for 1951–2003, based on their network of rain gauges (Table 2.1) [Rajeevan et al., 2006b].

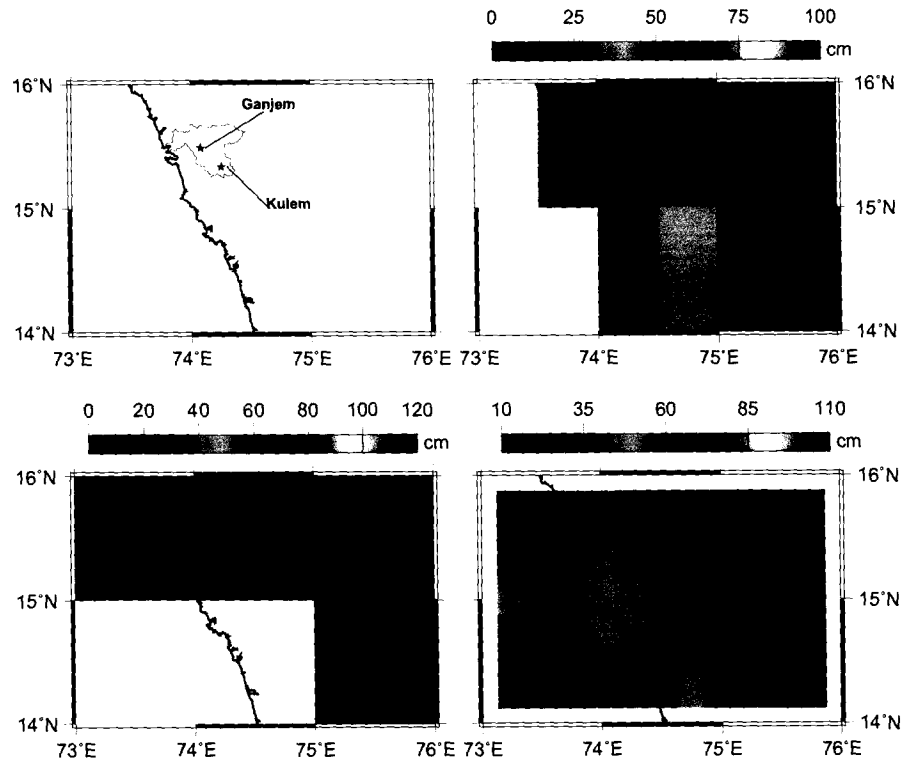
This data set was constructed by interpolating station data using Shepard's interpolation scheme, which is essentially an inverse-distance weighting scheme. We tested it by forcing THMB with the IMD rainfall product. The Mandovi basin spread across two IMD cells, with each cell accounting for a part of the basin (Figure 2.3). The catchment upstream of Ganjem fell in the eastern cell

('E'), but the rainfall over this cell was much less than the rainfall over the western cell ('W'), in which fell the basin area downstream of Ganjem. We took this to be an artefact of the grid, with the eastern (western) cell with low (high) rainfall representing the leeward (windward) side of the Sahyadris. Hence, the rainfall data used to force THMB were taken from the western cell ('W'). The daily rainfall data were averaged to obtain monthly values for THMB. The estimated discharge (Table 2.2) was better than the discharge simulated using the CRU data, but the errors were still unacceptably high: average error was 44% over 1981–1998. The discharge was underestimated by the IMD rainfall, the error being larger in years with high discharge (and therefore high rainfall). Thus, the IMD data were unable to capture the large interannual variability inherent in the west-coast monsoon rainfall and the simulated discharge had a much lower variance than observed.

#### **TRMM data set**

The third rainfall data set we tested was Tropical Rainfall Measuring Mission (TRMM) [TRMM, 2006]. We used TRMM data product 3B43 (Combined TRMM and other data sources), which combines calibrated satellite data (from TRMM and other satellite precipitation sensors) and ground-based global rain-gauge data sets to produce the 'single, best-estimate data' [TRMM, 2006]. The 3B43 rainfall data are available on-line on a 0.25° grid from January 1998 onwards. Since discharge measurements were available only till 1999, the TRMM data set was tested only for 2 years, 1998 and 1999. The error in simulated discharge, and therefore in the TRMM rainfall estimate, was 75% for 1998 and 69% for 1999. As with the CRU and IMD data, TRMM also considerably underestimates rainfall over the basin. Thus, of the three data sets tested, the best discharge estimates were obtained with the IMD data (though it had the lowest resolution) because it used in situ rain-gauge data. The problem with the IMD data set is that its objective was to map the rainfall over India, not just over its west coast. This led to the interpolation algorithm ignoring the effect of elevation and the need to ensure continuity led to the use of fewer rain gauges

**Figure 2.3** Rainfall distribution in July for the CRU, IMD, and TRMM data sets. The upper left panel shows the two discharge gauging stations. Note the different spatial resolutions of these gridded data sets. See the text for an explanation for the 'W' and 'E' marked on the panel for the IMD data set and the solid dot marked on the panel for the CRU data set.



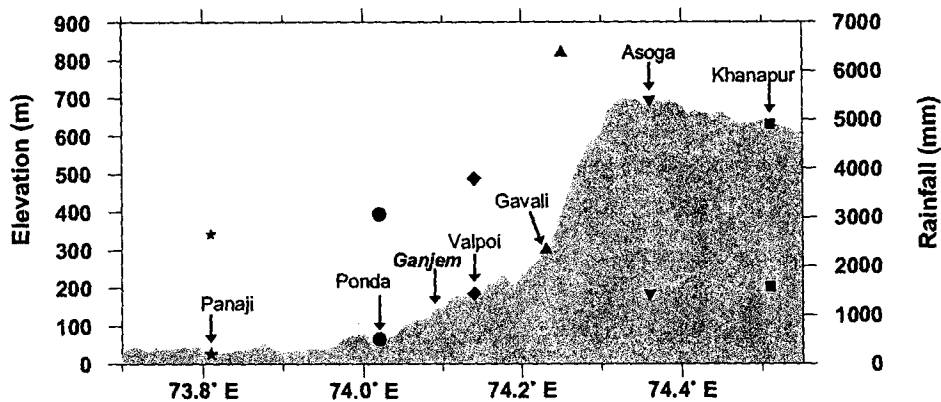
than were actually available for (say) the Mandovi basin.

### 2.4.3 Need to build the rainfall forcing

It is clear from the above section that the available rainfall forcing data sets are not suitable for simulating river discharge on the Indian west coast. They produce huge errors, simulated discharge underestimating the observed discharge (Table 2.2). The reason for this is the strong influence of orography on the rainfall on the Indian west coast (Figure 2.4). This strong dependence, when combined with the complex terrain of Sahyadris and data sparsity, makes it very difficult to map the rainfall on the west coast. Global and regional data sets like CRU and IMD suffer primarily due

to their coarser resolution and stricter data length requirement for inclusion of more representative stations. Satellite data sets like TRMM are known to produce large errors in mountainous terrain.

**Figure 2.4** Influence of topography on rainfall. The topography (meridionally averaged over the interpolated domain) of region is shown shaded along with the mean monsoonal precipitation (for June–September) along an approximate east-west transect passing through Panaji and Khanapur (see Figure 1.7). The symbol at the top of the shaded topography marks the station location. The same symbol is used to denote the rainfall at that station. For example, the lower (upper) asterisk (inverted triangle) for Panaji (Asoga) marks the location and the upper (lower) asterisk (inverted triangle) the rainfall at Panaji (Asoga). Note that the heights shown are not the station heights but the meridional average of the elevation at a given distance from the coast. All the stations shown, except Ponda and Khanapur, lie in the Mandovi basin.



Using data for years for 22 stations from the area around the Mandovi basin, Suprit and Shankar [2006] showed that it is possible to generate a rainfall data set that results in more accurate discharge estimates. Their study was limited, however, by the short length of the time series and their rain-gauge data had not passed through the same levels of quality checks that are mandatory in IMD. In the next chapter, a method to generate a rainfall forcing dataset is discussed.



## Chapter 3

# Rainfall mapping

### 3.1 Introduction

At any given time, rainfall is measured at a place (point) using a rain gauge. Rainfall, however, is not a point quantity; it varies in space along with its variation in time. It is defined as a continuous spatial variable. Generally, this variation is more pronounced in a complex terrain than in a flat region. In hydrology, estimating the spatial and temporal variability of rainfall is of utmost importance. Temporal variability of rainfall is relatively easier to resolve as long records of daily rainfall are available from rain-gauge measurements. In some cases rainfall data for resolution even as fine as hourly are available. Spatial variability, however, is not easy to resolve; it cannot be measured directly. In land surface hydrology, estimating spatial rainfall over a region (areal rainfall and its variability) is important. It is estimated by available rain gauges in a region and there always are limitations regarding the placement of rain gauges. One has to transform available rain-gauge measurements into a spatial field of rainfall, called the rainfall map. Creating rainfall maps from rain-gauge data is known as spatial interpolation.

Spatial variability of rainfall can also be estimated by remote sensing techniques using satellites and radars. These are recent advances: satellite and radar records are available only for recent

decades. As technology evolves, the accuracy of these estimates is fast improving, but they are still indirect measurements. They require rain-gauge data for validation and their use and reliability in hydrology is still under investigation. They are useful for identifying coarse scale patterns of rainfall, but quantitative estimates are still a long way from the desired accuracy. A more practical problem is availability of data; rain-gauge data and discharge data are available for a much longer period.

Hydrological models require rainfall as a forcing field. THMB requires rainfall maps on the model grid (Figure 2.2). As discussed earlier Chapter 2, THMB, when forced with the existing rainfall maps, heavily underestimated the discharge. Thus, the existing rainfall maps were unable to resolve the rainfall in the Mandovi basin and they underestimate the rainfall. Of all the tested data sets, the IMD dataset, which is based on rain gauges, performed better (see Tables 2.1 and 2.2). Hence, to produce the rainfall forcing field for THMB, existing rain-gauge measurements, in and around the Mandovi basin, had to be interpolated to the model grid. The spatial interpolation problem becomes acute in a complex terrain like the west coast of India, where rainfall is strongly related to the topography, owing to the sparse distribution of rain gauges (Figure 2.4).

### 3.1.1 Spatial interpolation of rainfall

The importance of spatial variability of rainfall (rainfall maps) in hydrology was realised long ago. Initially, hydrologists, equipped with the knowledge of rainfall in the region, used subjective method of contouring (rainfall contours are called isohyets) to obtain rainfall maps. Later, interpolation techniques such as inverse-distance weighted (IDW), Thiessen polygons, splines (whole variety of splines, including membrane, minimum curvature, thin plate, regular splines, splines with tension, etc.), kriging, and many others including downscaling and assimilation techniques came into use. These interpolation methods were both quantitative and, for the most part, objective (see Appendix B for more detailed discussion).

In essence, there are a large number of methods available, and one has to choose a method based on the specific requirement of the problem. This is crucial in a data-sparse region like the west coast of India, where large gradients of rainfall, combined with complex terrain, make mapping quite difficult (Figures 2.4 and 1.7). Thus, a good interpolation technique should not only be objective, but also be subjective enough to use the already known facets of spatial distribution of rainfall in the complex terrain so as to complement the sparsity of data. In general, a good rainfall map should fulfil the following criteria: It should be able to reproduce known spatial characteristics of rainfall (as it is known to a local observer), it should compare favourably with station rainfall, and it should be validated with independent criteria like water budget calculations.

### 3.1.2 Regularised spline with tension

Suprit and Shankar [2006]<sup>1</sup> and Suprit and Shankar [2008] adopted a spline method for interpolating rainfall on the west coast. Spline method was chosen because it is based on variational technique, hence it is physically more meaningful than statistical techniques [Mitas and Mitasova, 1999]. Geostatistical methods like kriging were not chosen because of the need for subjective decisions [Journel, 1996]: data in a data-sparse region like the Mandovi basin may not contain enough information about the important features to enable such subjectivity to succeed. The two methods, however, have been shown to be formally equivalent [Cressie, 1993].

Splines have been used extensively in the interpolation of various climate variables [Hutchinson, 1995, 1998a,b; New et al., 1999; Hofierka et al., 2002; Jeffrey et al., 2001]. An implementation of the multivariate spline interpolation method called *Regularized Spline with Tension (RST)* has been developed and incorporated within GRASS GIS [Neteler and Mitasova, 2002]. The method has been applied successfully to regions having complex topography. A detailed discussion of the mathematical formulation of the *RST* method is presented by Mitasova and Mitas [1993] and Hofierka et al. [2002]. The spline interpolation technique is based on the premise that the interpo-

---

<sup>1</sup>Rain-gauge data available to Suprit and Shankar [2006] was from a non-standard source (not from IMD, hence, not passed through mandatory quality check) and of short duration.

lation function should pass through or close to the data points while trying to remain as smooth as possible [Mitas and Mitasova, 1999].

The method is able to capture a more complex, spatially variable relation between rainfall and elevation than the traditional methods based on statistical correlation [Hofierka et al., 2002]. The explicit form of *RST* function and solutions for undetermined coefficients are given in Mitasova and Mitas [1993] and Hofierka et al. [2002]. To interpolate rainfall with elevation as the third dimension, an approach similar to that of Hutchinson [1995] is used in the *RST* module in GRASS; the interpolated function is therefore a function of horizontal co-ordinate as well as elevation, which can be interpreted as the intersection of the *RST* volume model of rainfall with the terrain surface [Neteler and Mitasova, 2002]. The introduction of elevation as a co-variate serves as an important proxy for rainfall in complex data-sparse regions. Incorporating elevation in the interpolation tends to improve the results of interpolation [Goovaerts, 2000; Hofierka et al., 2002].

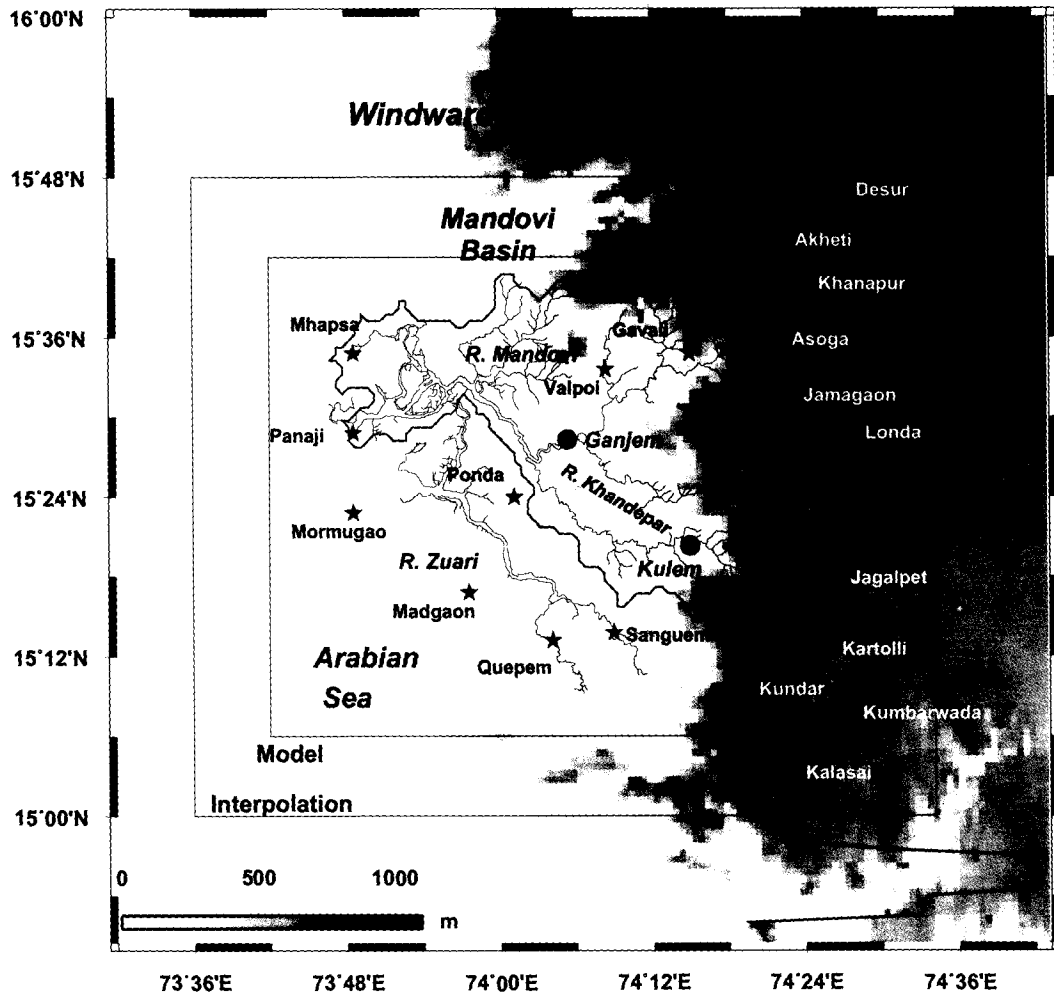
This trivariate (3D, with elevation as the third dimension) form of *RST* method is implemented in the GRASS GIS as the module `v.vol.rst` [Neteler and Mitasova, 2002; GRASS Development Team, 2008]. It requires the location and height of the rain gauges as inputs to interpolate rainfall to a 3D grid. The resulting 2D rainfall field is obtained by intersecting the interpolated volume by the terrain surface represented by a DEM. An important feature of the implementation is a set of tuning parameters, which provide the flexibility needed in the interpolation procedure to represent the modelled phenomena. The most important parameters are tension ( $T$ ) and smoothing ( $S$ ) [Neteler and Mitasova, 2002].  $T$  controls the range over which a given point influences the resulting surface. For high  $T$ , each point influences only its close neighbourhood and the surface changes rapidly to the trend between the points. In 2D analogy,  $T$  tunes the interpolation surface from a stiff plate to an elastic membrane [Neteler and Mitasova, 2002]. On the other hand,  $S$  allows the surface to deviate from the data points in an effort to minimize its energy. Low (high)  $S$  implies that the interpolation function passes close to (deviates more from) the data points.  $S$  is important when using low  $T$  because it prevents overshoots (unusually high or low

values);  $S$  also removes noise that may be present in the data [Neteler and Mitasova, 2002].

The optimal values of these parameters were chosen by minimization of the predictive error estimated by a Cross-Validation ( $CV$ ) procedure [Tomczak, 1988; Neteler and Mitasova, 2002], which is also incorporated in the `v.vol.rst` module [GRASS Development Team, 2008]. In this approach, one data point was eliminated at a time, and the interpolation was performed using the remaining points. Then the residual between the actual value of the eliminated point and the value estimated (interpolated) at this point was computed. This procedure was repeated subsequently for all the data points. This resulted in the same number of residuals as input data points. Then the overall performance of the interpolation was evaluated as the root mean of squared residuals (Root Mean Square Error, RMSE). This step was repeated for a range of values of  $T$  and  $S$  (0.01–0.09) and the combination that yielded the lowest RMSE was chosen as the optimal set of interpolation parameters. The entire procedure was carried out for a domain larger than the model domain (Figures 3.1 and 1.7). The locations and heights were specified based on the GLOBE DEM grid, but these values were almost the same as the in-situ locations and heights given by IMD. (The averaging over a grid cell in the DEM implies that the height at a location in the DEM will not be equal to the IMD height in a region with complex terrain. The GLOBE values were preferred to the in-situ values for interpolation because the rainfall in any cell represents an average over the cell and is therefore not the same as the in-situ measurement using a rain gauge.)

The  $CV$  method provides an objective criterion to evaluate the selection of the interpolation parameters. Although there are many issues involved with the  $CV$  procedure, the final assessment of the spatial estimate of precipitation and its consistency should be judged by the discharge simulations, which provide an independent spatial climate element [Daly, 2006].

**Figure 3.1** The topography of the region as in the edited GLOBE DEM. The outer and inner rectangles denote the interpolation and THMB model domains; rainfall interpolation was performed over a larger domain in order to include more rain gauges to map the variation. The black jagged line is the ridge separating the windward and leeward sides of the Sahyadris. Rain-gauge stations on the windward (leeward) sides are marked in black (white).



## 3.2 Application to the Mandovi basin

We first interpolated the rainfall for 1981–1998 using the rain-gauge data from 20 stations in and around the Mandovi basin (Figure 3.1). Of the 20 stations, data for only six (Castle Rock, Mormugao, Panaji, Sanguem, Khanapur, Kalasai, and Kumbarwada) were available over the entire analysis period (Table 3.1). All available data, however, were used for interpolation in order to generate the best possible map for each month. The entire region ( $15^{\circ}$  N –  $15^{\circ} 48'$  N and  $73^{\circ} 36'$  E –  $74^{\circ} 34'$  E) in the GLOBE DEM was divided into  $96 \times 116$  grid cells with a resolution of 30 arc seconds.

The  $T$  and  $S$  were varied in the range 0.01–0.09 to obtain optimal parameters by minimising the RMSE obtained through the  $CV$  procedure; the range for  $T$  and  $S$  was arrived at subjectively after a few interpolations. The RMSE for the optimum  $T$  and  $S$  (Figure 3.2) varied between 5.01 and 92.3 cm during the peak rainfall months (June–September). The resulting rainfall maps were unable to capture the large gradients expected in the vicinity of the Sahyadris (Figure 3.3) owing to the poor rain-gauge coverage in the regions with large rainfall gradients, i. e., the ridge and the slopes of the Sahyadris. This poor coverage resulted in undershoots (low values) and overshoots (high values) when we tried to simulate the large rainfall gradient by reducing the smoothness of the rainfall surface (by lowering  $S$ ). Hence, smoother surfaces had to be fitted to the rain-gauge data, resulting in the inability to simulate the large spatial gradients. When these rainfall maps were used to force THMB, the error in the simulated discharge at Ganjem, though now less than when the IMD data were used, was still too large ( $\sim 14$ – $44\%$ ) (see Table 3.2).

### 3.2.1 Separate interpolation for windward and leeward sides

The reason for the large errors in interpolation is the sparse distribution of rain gauges. This poor spatial sampling did not permit a clear separation between the windward and leeward sides,

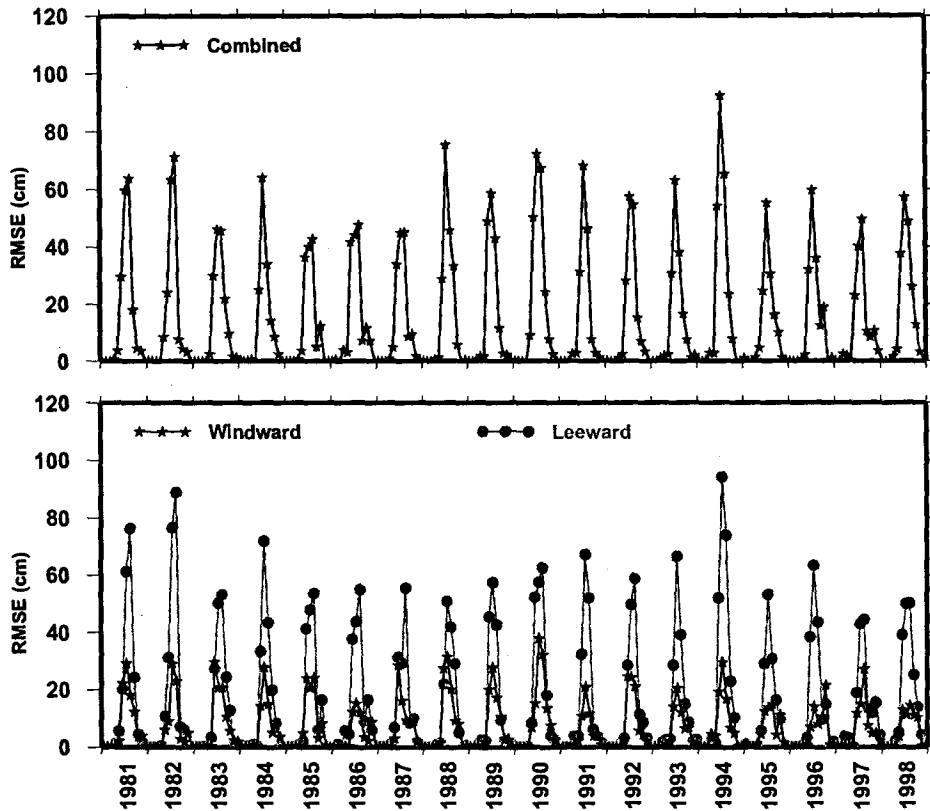
**Table 3.1** Name, location (latitude (longitude) in degrees north (east)) and height (m) of the rain-gauge stations, along with a summary of the annual rainfall statistics (mean and SD; cm year<sup>-1</sup>). Stations in the top (bottom) half of the table are from the windward (leeward) side of the Sahyadris. Column 5 lists the years for which data were not available (at least for the monsoon months).

Station	Longitude	Latitude	Height	Missing years	Mean	SD
Castle Rock	74.35	15.4	559	—	597.8	93.1
Gavali	74.26	15.6	744	1982–85	661.1	172.7
Madgaon	73.96	15.28	10	1988,1998	292.8	58.2
Mhapsa	73.8	15.59	22	1988–89,1998	303.1	57.6
Mormugao	73.79	15.41	22	—	270.9	39.9
Panaji	73.81	15.48	1	—	286.0	45.0
Ponda	74.02	15.4	32	1988,1998	332.0	61.6
Quepem	74.06	15.21	48	1987–89, 1998	357.3	83.8
Sanguem	74.15	15.23	52	1998	361.7	50.3
Valpoi	74.13	15.55	67	1988,1993–95,1998	413.2	56.2
Asoga	74.36	15.6	692	1997	160.5	49.5
Desur	74.5	15.75	732	1997	143.8	34.5
Jamagaon	74.48	15.55	673	1982,1984–85	394.0	96.7
Khanapur	74.51	15.63	646	—	183.0	42.8
Londa	74.5	15.45	650	1984–85,1987–89,1997	227.8	93.5
Akhetai	74.42	15.75	766	1987	519.2	101.1
Jagalpet	74.5	15.25	515	1987,1998	256.2	61.2
Kalasai	74.42	15.07	640	—	327.3	59.3
Kumbarwada	74.46	15.14	614	—	366.9	100.1
Kundar	74.35	15.14	666	1989	498.8	121.7

which is obvious in the large-scale rainfall distribution, to emerge naturally from the data. Hence, in order to overcome this problem, we interpolated the rainfall separately for the windward and leeward sides. We defined a ridge separating the windward and leeward sides, choosing, as a first approximation, the location of maximum elevation along a latitude circle as the ridge. This ridge was then subjectively edited where river valleys (like the Mandovi; see Figure 1.7) cut through the Sahyadris. This subjective editing was necessary to ensure a “reasonably” smooth and continuous ridge. This definition separated the domain into a high-rainfall windward side and a low-rainfall



**Figure 3.2** RMS error (RMSE, in cm) for obtaining optimal tension and smoothing parameters to be used in rainfall interpolation. The top panel shows the RMSE when interpolation was done for windward and leeward stations combined (discharge  $S_C$  in Table 3.2); the bottom panel shows the RMSE for separate interpolation for windward and leeward sides (discharge  $S_{W+L}$  in Table 3.2).

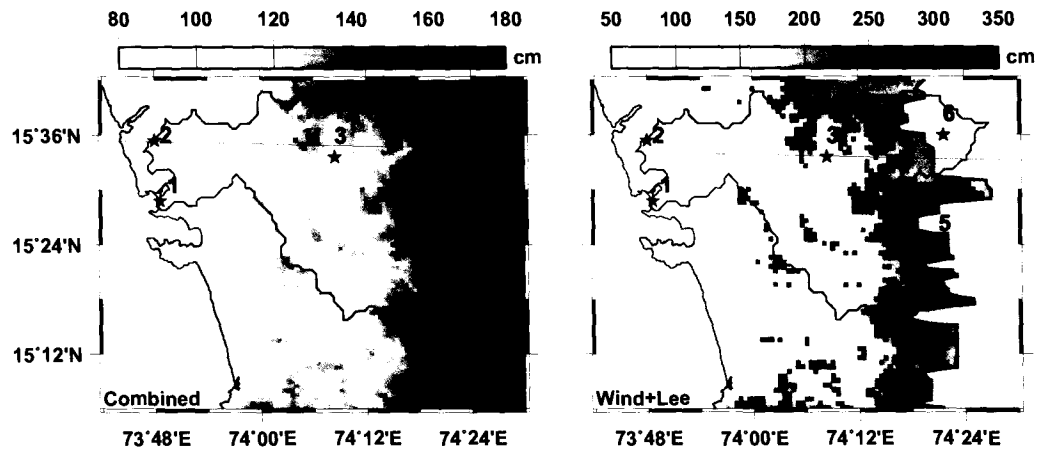


leeward side, with 10 rain-gauge stations on both sides (Table 3.1). We then used the *CV* procedure to map the rainfall separately for each side; on both sides, the optimal  $T$  and  $S$  ranged between 0.01 and 0.09. The two maps were then merged together to obtain the rainfall map.

Suprit and Shankar [2008] used a 3-point smoothing for merging leeward and windward side map:

$$R_i = (R_{i-1} + R_i + R_{i+1})/3, \quad (3.1)$$

**Figure 3.3** Interpolated rainfall maps for August 1982. The left (right) panel is for simulation  $S_C$  ( $S_{W+L}$ ). The black curve is the Mandovi basin. The ridge separating the windward and leeward sides is shown by the black curve in the right panel. The six rain-gauge stations (1–6) are the ones for which estimated and observed rainfall are compared in Figure 3.4.



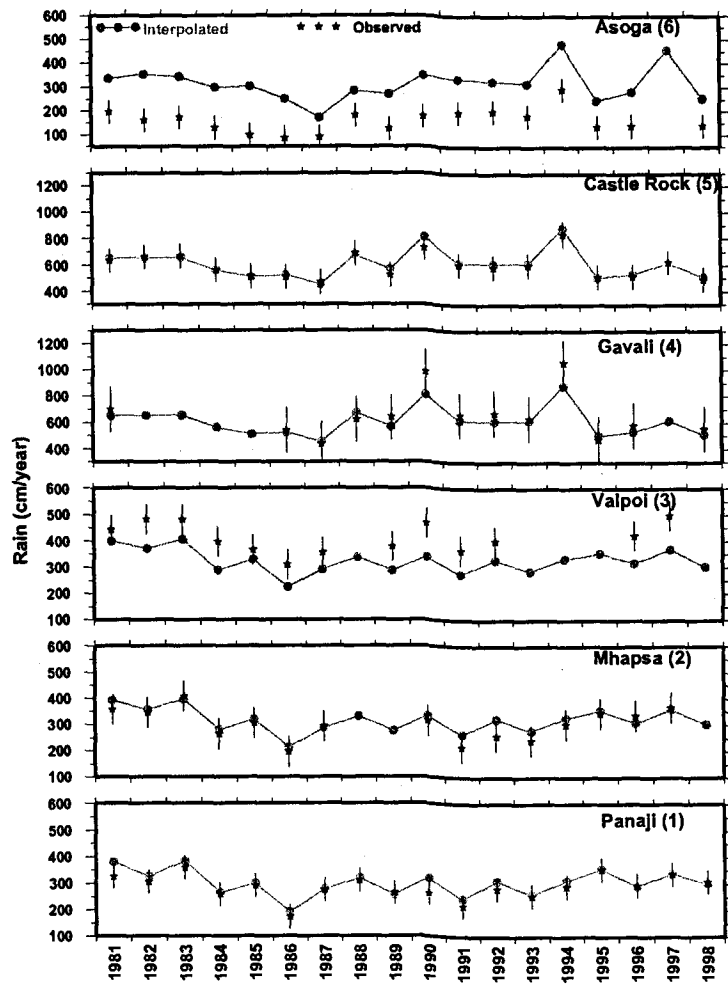
where  $R_i$  is the rainfall in the first grid cell on the leeward side,  $R_{i+1}$  the (adjacent) leeward cell to its east and  $R_{i-1}$  the (adjacent) windward cell to its west; here,  $i$  is the zonal index. This smoothing was done to ensure a smoother transition from the high rainfall on the windward side to the low rainfall on the leeward side, but this smoothing causes overestimation of rainfall on the leeward side. As rainfall is generally underestimated, on monthly rainfall maps this improves the results a little. On the leeward sides, however, interpolated rainfall is already heavily overestimated (See Figure 3.4 for Asoga (top panel)) and this smoothing adds to this overestimation.

The RMSE for the windward (leeward) side was 0–37.8 (0–94.2) cm (Figure 3.2). The reason for the larger error on the leeward side could not be ascertained, but we suspect the complex relation between rainfall and elevation and the clustering of rain gauges into two groups on the leeward side (Figure 3.1). The errors were, however, lower when the windward and leeward sides were mapped separately; note also that the leeward side constitutes a much smaller fraction of the catchment of the Mandovi at Ganjem, ( $\sim 21\%$  by area and on the average 13.8–20.4% by rainfall; see Table 3.1). The RMSE values still seem large, but they are unavoidable in a data-sparse region

**Table 3.2** Comparison of simulated and observed discharges at Ganjem; all the discharges are in  $\text{Mm}^3$ . Column 2 ( $O_G$ ): Observed discharge at Ganjem ( $O_G$ ); C3: simulated discharge at Ganjem for forcing with interpolated (windward and leeward sides combined) rainfall ( $S_C$  is the simulated discharge for this experiment); C4: as in C3, but with the rainfall interpolation done separately for the windward and leeward sides ( $S_{W+L}$  is the simulated discharge for this experiment); C5: observed discharge at Kulem; C6: as in C4, but for Kulem ( $S_K$  is the simulated discharge at Kulem for separate interpolation experiment). In columns 3, 4 and 6 the numbers in parenthesis denote percentage error (simulated minus observed discharge). Columns 7 ( $P_W$ ) and 8 ( $P_L$ ) are the areal rainfall (in  $\text{Mm}^3$ ) over the windward and leeward parts, respectively, over the catchment area at Ganjem for the forcing used in C4 ( $S_{W+L}$ ). The last two rows of table show the mean (percentage error in parentheses) and standard deviation (SD) of the respective variables.

Year	( $O_G$ )	$S_C$	$S_{W+L}$	( $O_K$ )	( $S_K$ )	$P_W$	$P_L$
1981	3895	3001 (-22.9)	3513 (-9.8)	456	429 (-5.9)	3585	770
1982	4214	2522 (-40.2)	3528 (-16.3)	530	455 (-14.2)	3631	757
1983	3787	2648 (-30.1)	3558 (-6.0)	640	444 (-30.7)	3587	740
1984	3540	2003 (-43.4)	2750 (-22.3)	635	358 (-43.6)	2887	634
1985	3171	2115 (-33.3)	2838 (-10.5)	599	349 (-41.7)	2943	637
1986	2543	1678 (-34.0)	2443 (-3.9)	440	335 (-24)	2620	555
1987	2275	1768 (-22.3)	2219 (-2.5)	331	287 (-13.4)	2531	404
1988	4187	2353 (-43.8)	3193 (-23.7)	474	426 (-10.0)	3309	643
1989	2762	2102 (-23.9)	2863 (3.7)	401	370 (-7.8)	2986	603
1990	4018	2552 (-36.5)	3578 (-10.9)	610	483 (-20.8)	3823	804
1991	3305	2203 (-33.3)	2957 (-10.5)	458	389 (-15.2)	3092	726
1992	3326	2346 (-29.5)	3028 (-9.0)	431	381 (-11.5)	3189	714
1993	3333	2113 (-36.6)	2851 (-14.5)	457	381 (-16.7)	3046	682
1994	4718	3140 (-33.4)	4018 (-14.8)	614	532 (-13.3)	4021	1025
1995	2940	1964 (-33.2)	2501 (-14.9)	400	310 (-22.4)	2806	542
1996	2557	2193 (-14.2)	2877 (12.5)	418	356 (-14.8)	3026	620
1997	3721	2673 (-28.2)	3466 (-6.9)	514	430 (-16.3)	3451	884
1998	2906	1877 (-35.4)	2387 (-17.9)	423	302 (-28.7)	2686	559
<b>Mean</b>	3400	2292 (-31.9)	3032 (-9.9)	491	390 (-19.5)	3179	683
<b>SD</b>	648	391	480	91	63	414	137

Figure 3.4 Interpolated and observed rainfall (in  $\text{cm year}^{-1}$ ) at the stations marked in Figure 3.3; note that Castle Rock is not in the Mandovi basin, but is the only station on the ridge for which data were available. The vertical bars are a measure of the variability in the observed rainfall; the length represents one standard deviation on either side of the observed rainfall.



like this: we have no means of comparing the RMSE with any other studies in the region. The *CV* method also usually overestimates the interpolation error because the estimate is being computed at a location where data are genuinely available, and lack of data points aggravate this further [Hofierka et al., 2005].

The interpolated rainfall compared well with observed rainfall at the rain-gauge stations in the basin and at Castle Rock, the station nearest the ridge (but outside the Mandovi basin) (Figure 3.1 and Figure 3.4). The interpolation procedure captured the sharp increase in rainfall on the slopes (see panel for Gavali), but the rainfall was consistently underestimated on the windward side. On the leeward side (see panel for Asoga), the rainfall was consistently overestimated. This error was due to the curve tending to become smooth (in order to avoid overshoots) in regions that are data-sparse but have large gradients. The resulting rainfall maps were nevertheless able to catch the sharp increase in rainfall on the slopes of the Sahyadris, with the rainfall maximum hugging the Sahyadris (Figure 3.3). For the peak rainfall months, we obtained similar maps for all the years.

### 3.3 Simulation results and discussions

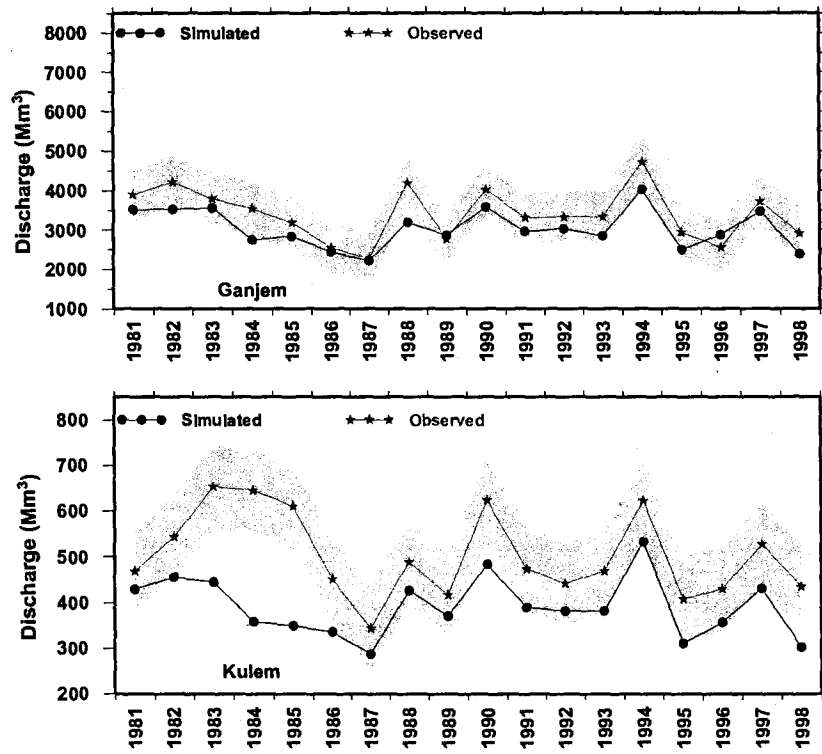
THMB was then forced with the new rainfall maps. The simulated discharge compared well with the observed discharge at Ganjem (Figure 3.5 and Table 3.2). The error in simulated discharge was within the natural variability in the system (except in 1984 and 1988). The annual discharge error was less than 20% for 16 of 18 years; the average error over the 18 years was 10%. This is comparable to the measurement errors involved with discharge observations, which is of the order of  $\sim 15$  to 25% [Dickinson, 1967; Cogley, 1989; Coe, 2000; Di Baldassarre and Montanari, 2009]. Except in two years, the simulated discharge was lower than observed. This was due to the underestimation of rainfall at Gavali and Valpoi, which are representative of the heavy rainfall on the hill slopes. The percentage error was higher at Valpoi (often greater than 20%), but the much higher mean rainfall at Gavali implied that the smaller percentage error there led to a higher

absolute rainfall error. Rain-gauge data for Gavali (Valpoi) were not available for 1984 (1988); these were the two years in which the discharge error (underestimate) exceeded 20% (Table 3.2). The larger simulation errors occur in years when data for Gavali or Valpoi are missing (Table 3.1 and Table 3.2). The large error in 1998 is owing to data for six of the 10 windward stations not being available. Note, however, that (as may be expected with the *CV* procedure) the RMSE is the error in rainfall at a station (Figure 3.4) and bears no obvious relation to the error in simulated discharge (Table 3.2 and Figure 3.5).

The simulated discharge showed larger errors when compared with the discharge measurements at Kulem on the Khandepar (Figure 3.5, Table 3.2). One reason for this larger simulation error is the much lower discharge of the Khandepar. Another reason is the absence of critical data. The discharge errors are largest (greater than 30%) during 1983–1985, when the observed discharge was high and rainfall data for Gavali were missing. (Note that data for several stations were missing in 1998, another year with a large error.) There are no rain-gauge stations on the slopes in the Khandepar basin, implying a high impact of Gavali and Castle-Rock rainfall on the discharge simulated at Kulem. Absence of data at Gavali therefore leads to an underestimate in basin rainfall, the error being larger when the rainfall is high because the highest rainfall (and the highest standard deviation) is on the slopes of the Sahyadris (Table 3.1). Note, however, that the discharge during 1983–1985 at Ganjem was closer to the mean discharge, suggesting an unmapped, higher-than-normal rainfall in the Khandepar basin. Since the available data do not suggest a north-south trend during these years, it is likely that the excess rainfall in the Khandepar basin was restricted to it. The absence of a rain gauge in the basin makes it impossible to resolve the spatial variation any better than done above. Hence, the method is only as good as is the distribution of data: sparsity of data implies larger errors in smaller sub-basins.

Nevertheless, the mean simulated discharge was lower at both Ganjem and Kulem. The simulated variance was also lower than the observed variance. Both point to a smoother rainfall map than probably exists in nature, with the sparse coverage of the basin, especially on the hill slopes,

**Figure 3.5** Simulated discharges at Ganjem and Kulem (bottom panel). The observed discharge is plotted for comparison. The shaded area is a measure of the variability in the observed discharge; the shading is done for one standard deviation on either side of the observed discharge. The black curve is the simulated discharge. Note the negligible impact of evapotranspiration (indicated by the thickness of the black curve) and that the error in simulated discharge is within the natural variability of the system (except in 1984 and 1988, where the black curve falls just outside the shaded region).



resulting in a lower estimate of basin rainfall than observed. A consequence of this sparse coverage is the lack of variation in rainfall between Gavali and Castle Rock, which are separated by  $\sim 25$  km (Figure 3.1). Though Gavali is at a higher elevation (Table 3.1), Castle Rock is on the ridge and Gavali on the slopes. The observed rainfall is higher at Gavali than at Castle Rock, but the sparsity of rain gauges masks this spatial gradient. Data from south of Goa also show that, in accordance with theory [Sarkar, 1966, 1967], the maximum rainfall occurs on the windward slope of the Sahyadris (Gavali, for example), not on the ridge (Castle Rock, for example) [Basappa and Jose, 2008]. Hence, sparsity of data, which is common in the vicinity of the Sahyadris, will imply a similar rainfall underestimate all along the Indian west coast.

The results did not show an obvious relationship between the rainfall RMSE and the discharge errors: the correlation between the two errors is low. It is known, however, that the *CV* method does not provide optimum parameters in all cases, and is dependent on the density and homogeneity of data points [Hofierka et al., 2002; Daly, 2006]. The THMB simulations were able to capture the variability in discharge observations reasonably well on the annual scale (Figure 3.5), and since the discharge is an independent measure of the rainfall interpolation, it is a more stringent test of the rainfall interpolation [Daly, 2006].

### 3.3.1 Rainfall mapping on higher temporal scale

Simulations forced with interpolated annual rainfall, however, resulted in larger errors: though the interpolation error was lower for annual rainfall, the discharge error was higher because the annual-rainfall map was much smoother and it underestimated the rainfall over the Sahyadris.

Simulations on higher temporal scale (e. g., on daily time scale) require rainfall mapping on daily time scale. The method outlined above for mapping monthly rainfall is also applicable for daily rainfall [Hofierka et al., 2002]. The GRASS GIS routine, *v.vol.rst*, used to perform the RST interpolation is embedded within the GRASS environment, but the process was slow owing to the internal GRASS GIS computational overheads. Since daily forcing would increase the compu-



tational load, the C routines used for the interpolation were extracted from the GRASS GIS and converted to a stand-alone program that was used to determine the optimum  $T$  and  $S$ . Generation of the rainfall-forcing maps requires only the DEM, the rain-gauge data, and the optimum  $T$  and  $S$ ; hence, the rainfall-mapping procedure was integrated with THMB, allowing rainfall maps for a given day to be generated online within THMB during the simulation.

### 3.3.2 Discussion

We have shown that an interpolation algorithm that includes elevation as a co-variate yields a better rainfall map for the Mandovi basin than an algorithm that ignores elevation. This improvement is due to the influence of orography on the rainfall on the Indian west coast. The IMD interpolation [Rajeevan et al., 2006a,b], which did not account for elevation, also excluded several stations that did not have a long record in order to produce a consistent estimate of the rainfall. Hence, the interpolated IMD rainfall underestimated the rainfall over the Mandovi basin. A key result is that in data-sparse regions with a complex mountainous terrain (like the Mandovi basin), it is better to extract the ridge line *a priori* and map the windward and leeward sides separately. This separate mapping reduces the underestimation of rainfall by ensuring that the sharp decline in rainfall across the ridge, which does not emerge naturally from a combined mapping of the entire basin, is now guaranteed to the extent that rain-gauge data are available on the slopes and the ridge. Note that such subjectivity is common in geostatistical techniques like kriging.

The resolution of the interpolation also matters. The CRU data set also includes elevation as a co-variate, but the  $0.5^\circ$  resolution of the data set was too crude for it to resolve the sharp rainfall gradient induced by the Sahyadris. Interpolating the rainfall at a high resolution and then downscaling the interpolated rainfall to a coarser grid also proved superior to an interpolation at a coarse resolution. We downscaled the rainfall interpolated at 30 arc seconds to a  $0.25^\circ$  grid and then forced THMB (at a 30 arcseconds resolution) with the resulting rainfall map. The rainfall forcing, as with the TRMM/CRU/IMD data sets, was now invariant over the larger  $0.25^\circ$  grid,

but the results were superior to those obtained with the other data sets: the average discharge error was 4.8% (underestimate), as opposed to 10% when THMB was forced with the interpolated rainfall at 30 arc-seconds resolution without any rescaling (Table 3.2). (The lower error does not imply that rescaling is better. For the Mandovi basin, the positioning of the low-resolution and high-resolution grids means higher rainfall from outside the basin *spilled* into the basin, resulting in a positive rainfall error that countered the overall underestimation of basin rainfall.) When the terrain is complex and data are sparse, it is important to grid the rainfall at a high resolution even if the final resolution at which data are required is much lower. Hence, if hydrological consistency is an objective, mapping at different resolutions in different regions may be necessary, the maps being subsequently rescaled to the common desired resolution. In other words, the IMD data set [Rajeevan et al., 2006b] might have benefited from a higher resolution of the mapping grid along the Indian west coast; the coarser grid is probably sufficient in the low-gradient terrain common over most of India. The final data set could always be prepared at a common resolution by downscaling the high-resolution maps to the lowest common resolution possible.

The results presented here are significant. It is impossible to understand the hydrology of the Indian west coast without resolving the variability of rainfall. The rainfall mapping algorithm was validated by discharge simulations, an independent measure. The interpolated monthly rainfall, when used to force THMB, produced an annual discharge estimate within 15–25% of the observations. Further, the mapping algorithm has been incorporated into THMB framework, making simulation experiments faster and seamless on daily time scales. But, on the daily time scale there is much more variability in the discharge and rainfall (Figure 1.9). Hence, simulating the daily discharge of the Mandovi will present a challenge to resolve this variability, which forms the basis of the next chapter (Chapter 4).

## Chapter 4

# Rainfall-runoff modelling

### 4.1 Introduction

The highest temporal resolution of data available with us was on daily time scale. Hence, our next step was to simulate the daily discharge in the Mandovi river. The method discussed in Chapter 3 for mapping monthly rainfall is applicable for daily rainfall also. The THMB framework now incorporates the interpolation algorithm, where daily rainfall forcing maps from rain gauges are generated on the fly. Simulating the daily discharge of the Mandovi will, however, present another challenge. The seasonality of rainfall over the Indian west coast, with almost no rain during January–April and November–December (Figure 1.8), implies that the result of each year is independent of that of the preceding years: the system has no memory as far as annual discharge is concerned and there is no correlation between the discharge of two successive years. Physically, the land dries up soon after the rains cease, and the rains of the next year fall on empty surface and subsurface reservoirs. Hence, the annual discharge curve starts at almost zero each year (and is almost zero till April). Therefore, the integral of monthly discharge for each year is independent of the details of the discharge curve and is a function of only the total rainfall over (and evapotranspiration from) the basin. Hence, the details of model parameterisation were not important for

simulating the annual discharge: model parameters could be held constant (as in the simulations of Coe [2000], Shankar et al. [2004] and Suprit and Shankar [2008]) without affecting the results.

With daily discharge, however, this will no longer hold true. On the daily time scale, there is a large temporal variability embedded in the seasonal variation. There is a large variability of rainfall, and hence of runoff (and discharge), on daily time scale (Figure 1.9). This variability is also evident in the daily rainfall forcing maps generated by THMB (Figure 4.1), where observed discharge is compared with the integral of the rainfall over the catchment at Ganjem (area 872 km<sup>2</sup>). A simple parameterisation like  $\alpha$  ( $\alpha = 0.3$ , a constant) that partitions rainfall minus evapotranspiration ( $P - E$ ) into subsurface runoff  $(1 - \alpha)(P - E)$  and surface runoff  $\alpha(P - E)$  will not work. On daily time scales, this constant partitioning can no longer be held valid.

In other words, a more complex rainfall-runoff model than the one used earlier in THMB is required. In this chapter, incorporation of a rainfall-runoff model into THMB for daily discharge simulations is discussed in detail.

We forced THMB with the daily rainfall maps and analysed the results for 1981–1998. The simulated discharge for three years, 1986, 1990 and 1992, is shown in Figure 4.2. The simulated discharge at Ganjem is compared with the observed discharge and catchment integrated rainfall. As in Suprit and Shankar [2008] and Shankar et al. [2004], the seasonal cycle is poorly simulated. Discharge is underestimated during the peak monsoon months (July–August), and overestimated during the onset (May–June) and post-monsoon phases (September–November). Changing the value of  $\alpha$  did not improve the simulations. On decreasing (increasing)  $\alpha$  to 0.1 (0.7), the simulated discharge improved (deteriorated) in the onset period, but deteriorated (improved) in the peak-monsoon period (Figure 4.2). The cause of this poor simulation is the constant  $\alpha$ . The strong seasonal cycle in rainfall and soil moisture, and hence in runoff, in the Mandovi basin implies a time-dependent  $\alpha$ .

**Figure 4.1** Daily observed discharge (black curve, in  $\text{Mm}^3$ ) at Ganjem and the rainfall integrated over the catchment (blue curve, in  $\text{Mm}^3$ ) for May–October (a) 1981, (b) 1982, (c) 1983, and (d) 1984. Daily rainfall maps obtained by interpolating the rain-gauge data were integrated over the catchment area at Ganjem to obtain the catchment-integrated rainfall. The bold tick marks on the abscissa indicate beginning and end of a month.

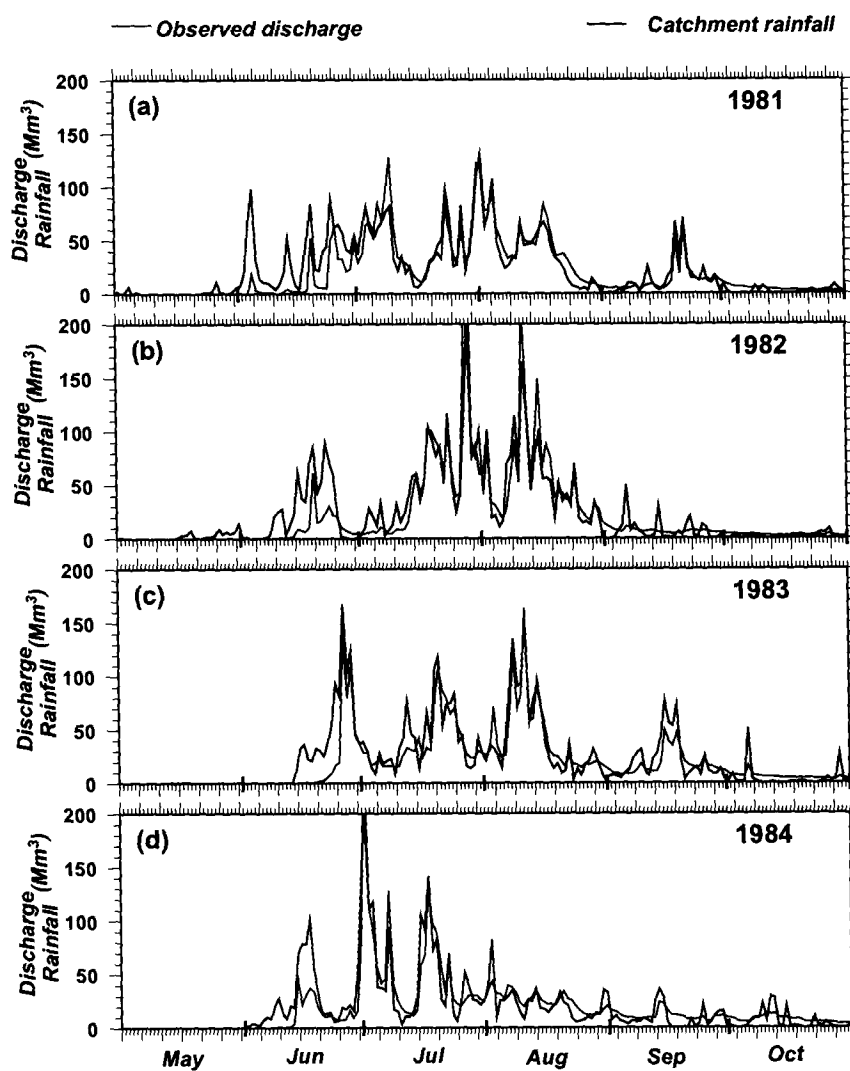


**Figure 4.1** (continued) Daily observed discharge (black curve, in  $\text{Mm}^3$ ) at Ganjem and the rainfall integrated over the catchment (blue curve, in  $\text{Mm}^3$ ) for May–October (a) 1985, (b) 1986, (c) 1987, and (d) 1988. Daily rainfall maps obtained by interpolating the rain-gauge data were integrated over the catchment area at Ganjem to obtain the catchment-integrated rainfall. The bold tick marks on the abscissa indicate beginning and end of a month.

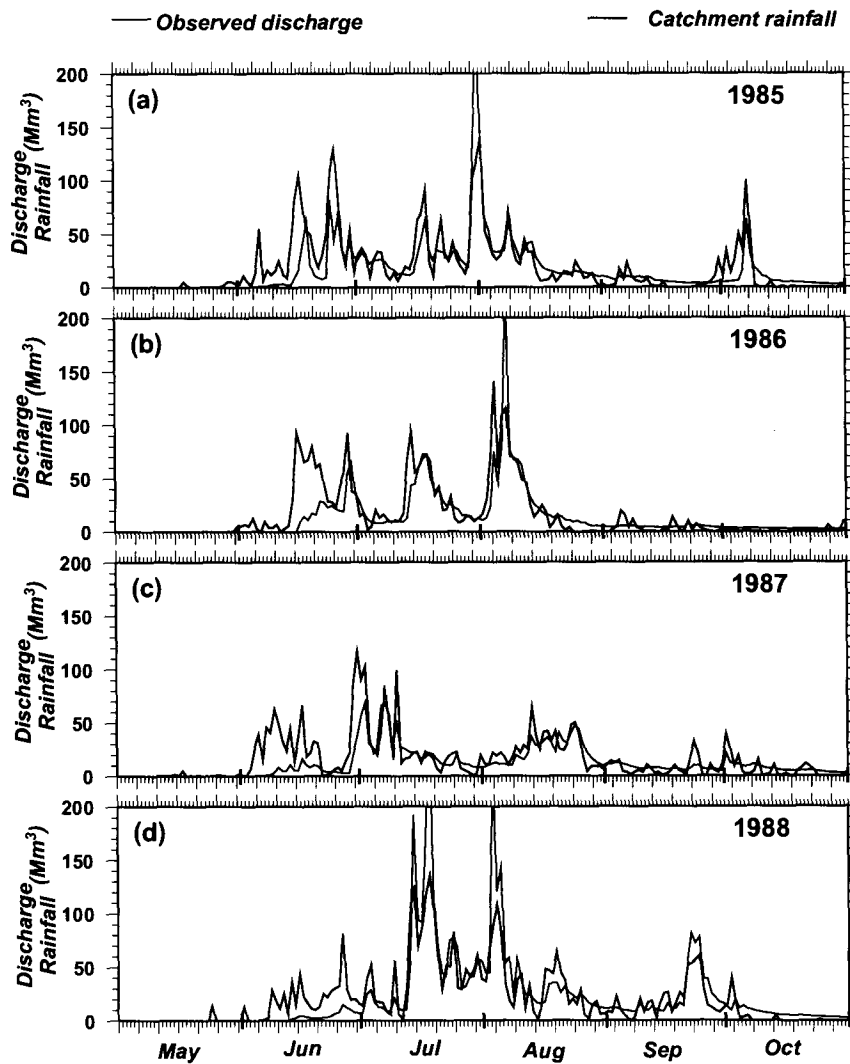


**Figure 4.1** (continued) Daily observed discharge (black curve, in  $\text{Mm}^3$ ) at Ganjem and the rainfall integrated over the catchment (blue curve, in  $\text{Mm}^3$ ) for May–October (a) 1989, (b) 1990, (c) 1991, and (d) 1992. Daily rainfall maps obtained by interpolating the rain-gauge data were integrated over the catchment area at Ganjem to obtain the catchment-integrated rainfall. The bold tick marks on the abscissa indicate beginning and end of a month.

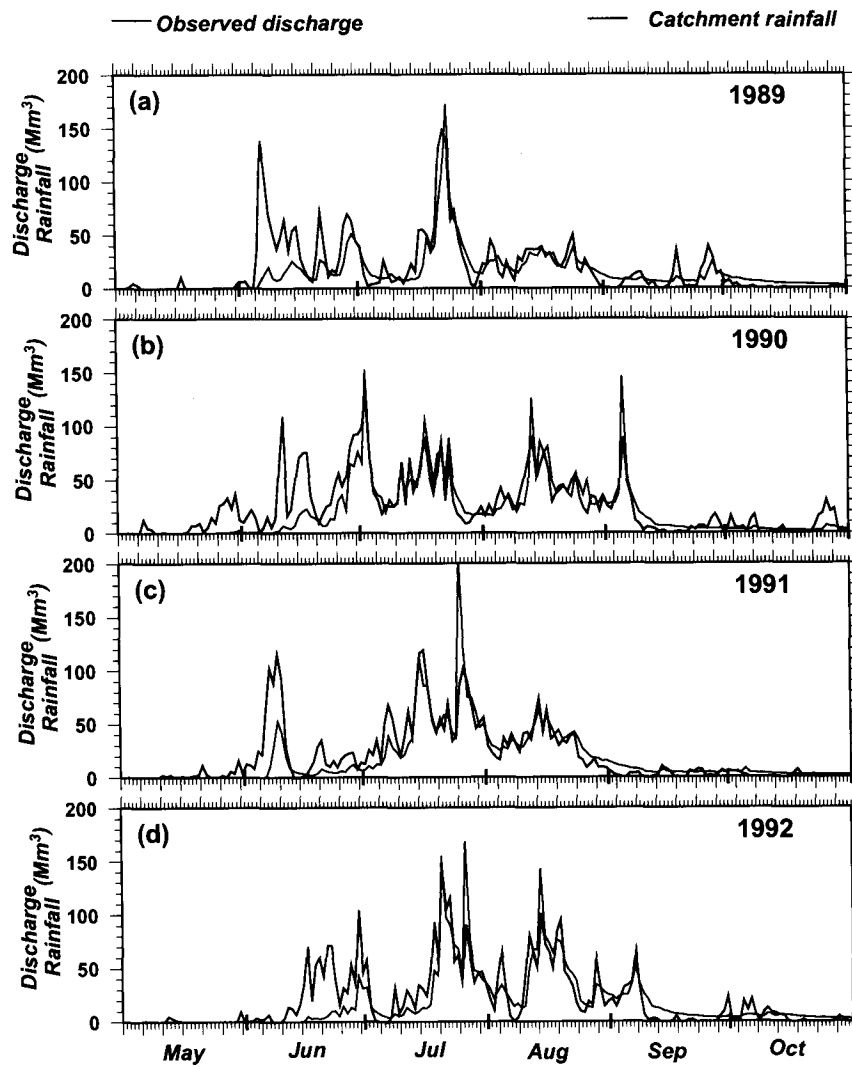


**Figure 4.1** (continued) Daily observed discharge (black curve, in  $\text{Mm}^3$ ) at Ganjem and the rainfall integrated over the catchment (blue curve, in  $\text{Mm}^3$ ) for May–October (a) 1993, (b) 1994, (c) 1995, and (d) 1996. Daily rainfall maps obtained by interpolating the rain-gauge data were integrated over the catchment area at Ganjem to obtain the catchment-integrated rainfall. The bold tick marks on the abscissa indicate beginning and end of a month.

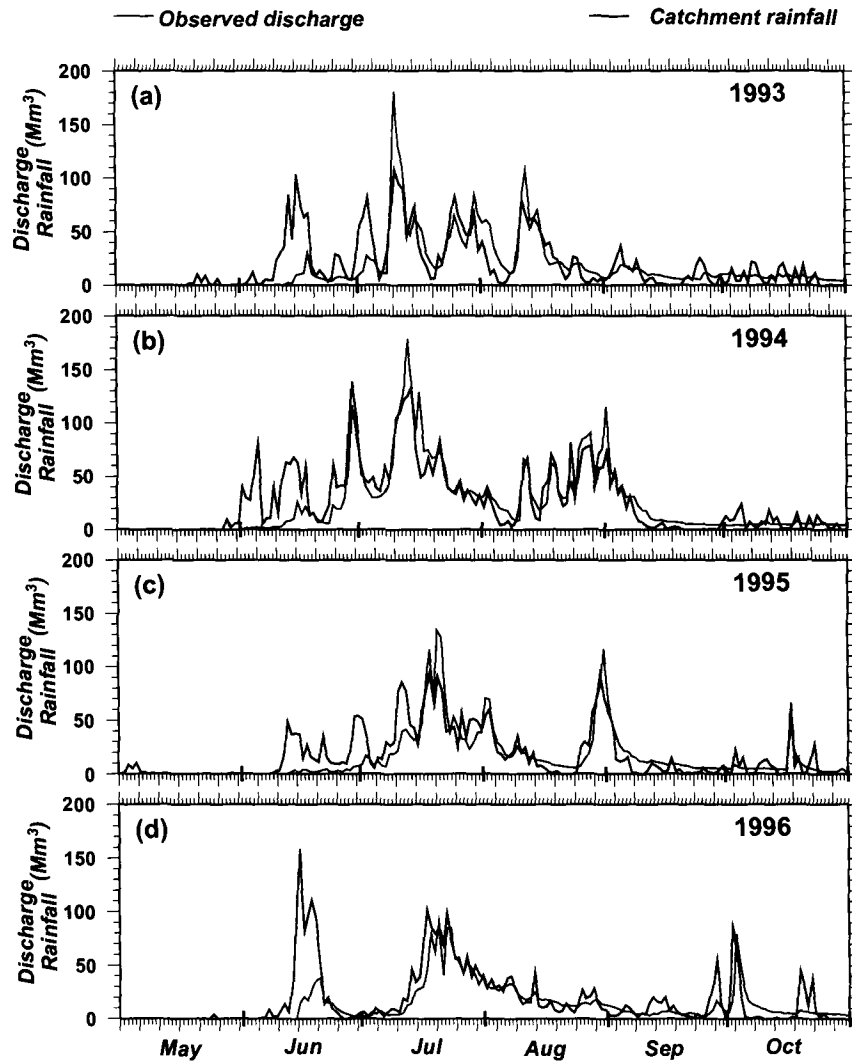




**Figure 4.1** (continued) Daily observed discharge (black curve, in  $\text{Mm}^3$ ) at Ganjem and the rainfall integrated over the catchment (blue curve, in  $\text{Mm}^3$ ) for May–October (a) 1997, and (b) 1998. Daily rainfall maps obtained by interpolating the rain-gauge data were integrated over the catchment area at Ganjem to obtain the catchment-integrated rainfall. The bold tick marks on the abscissa indicate beginning and end of a month.

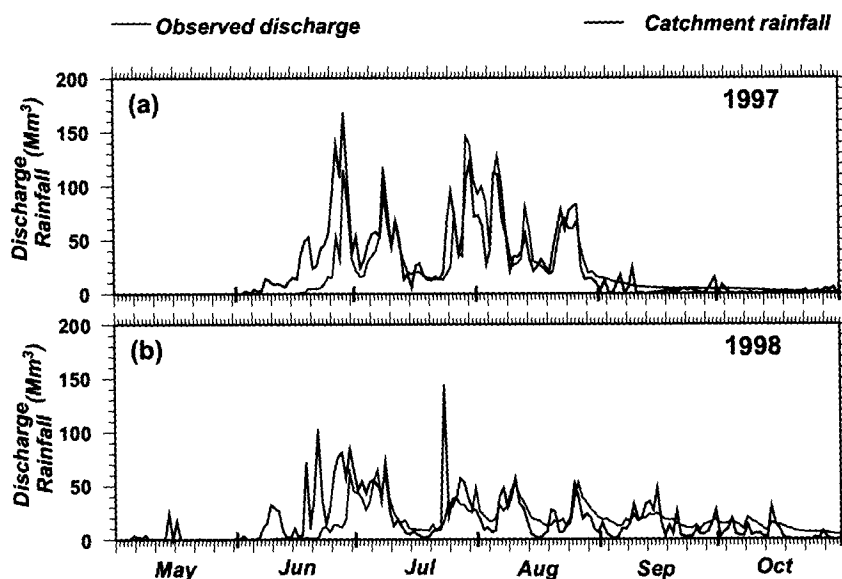
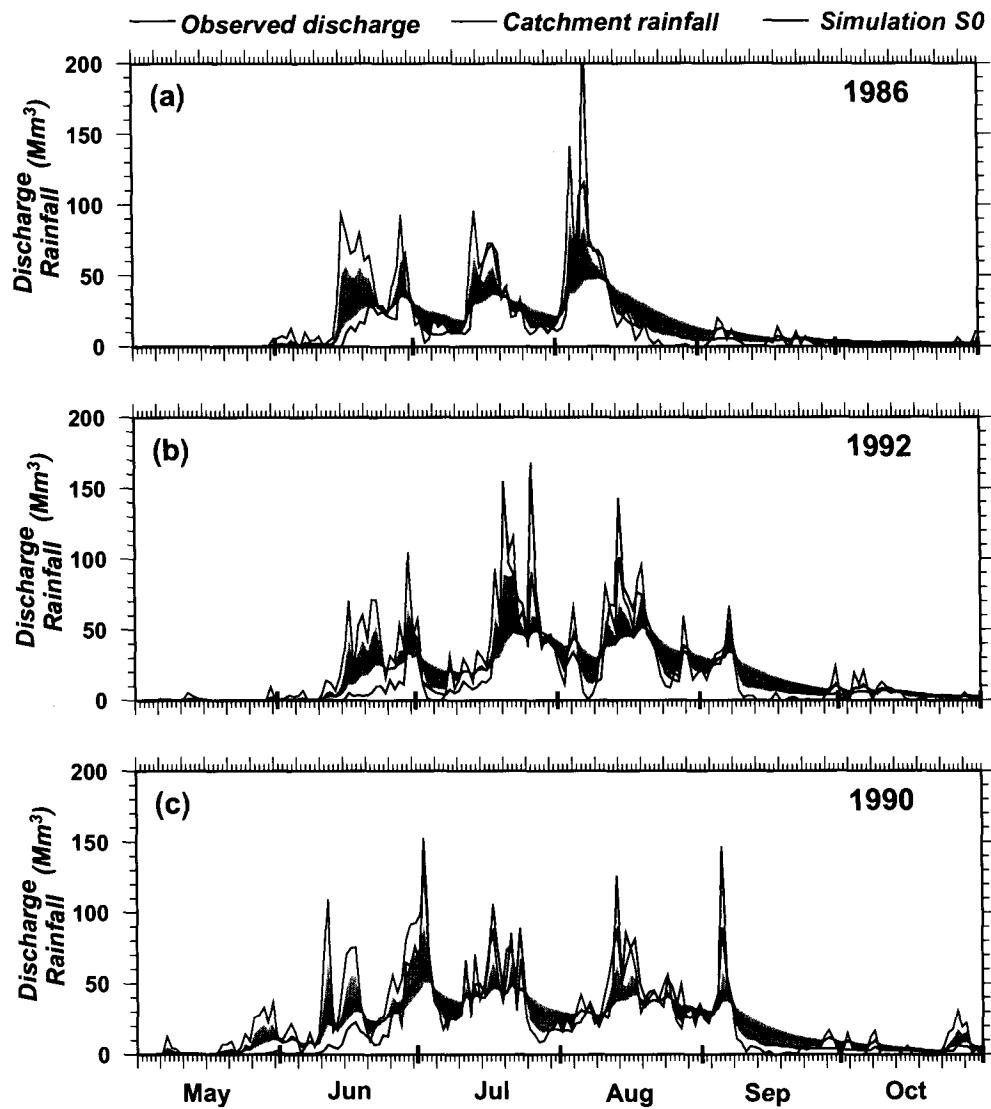


**Figure 4.2** Observed discharge (black), discharge simulated by Simulation *S0* (red), and the catchment-integrated rainfall at Ganjem (blue). (a) 1986. (b) 1992. (c) 1990. The units are  $\text{Mm}^3$ . The bold tick marks on the abscissa indicate beginning and end of a month. The grey band shows the variation in simulated discharge when  $\alpha$  is varied over the range 0.1–0.7;  $\alpha = 0.3$  in Simulation *S0*



#### 4.1.1 Limitations of the framework: Model parameterisation

Thus, simulation of daily discharge requires realistic estimates of surface and subsurface runoff on this time scale. Constant partitioning of rainfall into runoff smoothens the observed variability in discharge because this parameterisation is simplistic and ignores the differing hydrological response to differences in geographical and climatic conditions, i.e., it ignores variations in space and time. The hydrological processes, in turn, affect the generation of runoff, implying the need for a new, but simple, rainfall-runoff model to calculate the runoff required to force THMB. This rainfall-runoff model has to be simple enough to work with the meagre available data, but complex enough to account for the basic hydrological processes involved in the hydrological response of the Mandovi basin to the rainfall forcing.

#### 4.1.2 Rainfall-runoff model

Hydrological systems are very difficult to observe owing to limited measurement techniques and range of measurements. This is especially true for a complex process like conversion of rainfall into runoff. The flow of water on the surface through soil, until it appears in a stream, is a very complex and nonlinear process. Hydrological models represent the relation between total rainfall and runoff generated during the event and also route the runoff to the outlet point of the watershed. Almost always, errors involved in routing are much less than in the process of runoff generation. The generated runoff depends upon the rainfall and antecedent conditions of the watershed.

There exist many hydrological models, of varying complexities, to convert the rainfall into runoff [Chow et al., 1988; Wanielista, 1990; Beven, 2001]. Rainfall-runoff processes are very complex and numerous modelling strategies are used to tackle the problem, such as black-box, analytical, empirical, and conceptual approaches. Furthermore, a model can be either *lumped* or *distributed*, or even the two combined. Lumped models average the input and output variable over the watershed area, treating it as a single unit. Distributed models take spatial variability into

account, most commonly by dividing the region into grid cells. Furthermore, most of the hydrological models are *deterministic*, producing a single output from a single set of input variables and parameters. They are different from the less common *stochastic* models, which allow uncertainty and give a probabilistic output. Apart from these approaches, there are models based on techniques as varied as ANN (Artificial Neural Network), fuzzy logic, and SVM (Support Vector Machines).

The THMB framework, shorn of biogeochemistry, is basically a routing algorithm. For daily discharge simulation, it requires a rainfall-runoff model. According to our objectives, the model should be freely available. The challenge is to select a model that represents reasonably a fair approximation of the hydrological processes that culminate in generating runoff from rainfall. Another major constraint is the availability of data: the model should not be data-intensive. The only observational data available in the Mandovi basin are rainfall and discharge, making the choice of a usable model more difficult. It is also worth noting that discharge data are not available for most of the west-coast rivers, ruling out the use of the discharge data in the model parameterisation.

## 4.2 Soil Conservation Service (SCS) method

The Soil Conservation Service Curve Number (SCS-CN) method is one of the most popular models available for converting rainfall into runoff. An empirical model, the SCS-CN method, was derived from the analysis of runoff volumes from several experimental catchments maintained by the United States Department of Agriculture [Mockus, 1949]. The method requires only rainfall as the input data and uses a single parameter called Curve Number (*CN*) that defines the antecedent conditions. Since its simplicity matches that of the existing modelling framework, we adopt the SCS-CN method (hereafter referred to as just the SCS method) to parameterise the separation of runoff into surface and subsurface runoff.

Despite its inherent limitations [Lyon et al., 2004; Michél et al., 2005; Ponce and Hawkins, 1996], the SCS method (or a variant) is used in all types of hydrological modelling systems like

the water-yield models like SWAT, CREAMS, AGNPS, etc. [Arnold et al., 1993; USDA, 1980; Young et al., 1989], continuous hydrological simulation models [Geetha et al., 2007; Choi et al., 2002; Mishra and Singh, 2004], and grid-based and GIS-based models [White, 1988]. However, the SCS method is a purely conceptual model derived empirically from the rainfall-runoff data. It has been shown subsequently by various authors [Hawkins et al., 2001; Mishra and Singh, 1999; Yu, 1998; Steenhuis et al., 1995] that the method can be derived through process based approach. This physical basis and empirical soundness, combined with the underlying simplicity, makes the SCS method probably the most widely used hydrological-process model in hydrological modelling systems [Smith and Thomas, 2008].

The SCS method was developed as an event-based model to generate the direct runoff from the rainfall excess due to the rainfall event [Ponce and Hawkins, 1996]. To use the model in the THMB framework, a day's rainfall is considered as an event and the runoff is generated for the day (e. g., Choi et al. [2002]; Geetha et al. [2007]). The temporal variations are introduced by taking into account the moisture condition prevailing before the event (day). Although the shortcomings of this assumption, which extends the event-based SCS method to continuous, long-term hydrological modelling, have been pointed out by various authors (e. g., Ponce and Hawkins [1996]), it has been applied with success in many continuous-modelling studies [Choi et al., 2002; Geetha et al., 2007; Mishra and Singh, 2004].

The SCS method is a conceptual model and is therefore not limited by the size of the watershed [Mishra et al., 2003]. By itself, however, it does not take into account spatial variations because it was developed as a lumped model, in which the basin-runoff-generation processes are lumped into a single mechanism. Distributed or cell-based models like THMB, which require the input data and parameters to be specified for each grid cell, have become the preferred choice for modelling because of the observed spatial variability. In the THMB framework, rainfall is mapped onto the grid cells defined by the DEM, and the runoff forcing is generated for each grid cell. In the rest of this section, we incorporate the SCS method into the THMB framework to parameterise the

rainfall-runoff relationship.

According to the SCS method, the ratio of the actual runoff to potential runoff is equal to the ratio of the amount of water detained in the basin and the maximum storage in the watershed [Mishra and Singh, 2003]. For  $P > I_a$ ,

$$\frac{F_a}{S} = \frac{R_s}{P - I_a}, \quad (4.1)$$

where  $F_a$  is the water detained in the basin,  $S$  the storage or potential maximum detention in the basin,  $P$  the rainfall,  $R_s$  the direct or surface runoff, and  $I_a$  the initial abstraction or amount of rainfall for which there is no runoff. All the above quantities are in mm. Then, the water-budget (or mass-conservation) requirement implies

$$P = R_s + I_a + F_a. \quad (4.2)$$

From Equations (4.1) and (4.2), we obtain

$$R_s = \frac{(P - I_a)^2}{(P - I_a + S)}. \quad (4.3)$$

A part of the water (detained in the basin) that infiltrates the surface layer is stored as soil moisture, a part penetrates to recharge the groundwater, and the rest flows as subsurface runoff towards a river or water body. As data on infiltration are meagre, estimation of infiltration, and therefore of the subsurface runoff, is difficult. The subsurface runoff is defined as in Geetha et al. [2007] as

$$R_D = bF_a, \quad (4.4)$$

where  $b$  is the base flow index, which varies between 0 and 1. Since baseflow is small in the Mandovi basin, we assumed that all the water that infiltrates contributes to the subsurface runoff, i. e.,  $b = 1$ . Hence, as in the original THMB formulation, there is no groundwater-recharge term in the model and the only loss term is the initial abstraction (evapotranspiration). The direction of flow of this subsurface runoff is assumed to be the same as that of the surface runoff; only the

time scale associated with this subsurface flow is greater than that associated with the surface flow.

Then, from Equations (4.2) and (4.4),

$$R_D = P - R_s - I_a. \quad (4.5)$$

Equations (4.3) and (4.5) give the surface and subsurface runoff ( $R_S$  and  $R_D$ ), which are used to force THMB. Thus, we have replaced THMB's original  $\alpha$  parameterisation with the SCS method. This is a very important addition to THMB, and this model is called hereafter THMB-SCS. Once the SCS parameters are estimated, THMB-SCS (see the modelling framework schematic in Figure 4.3) can be used for discharge simulations.

#### 4.2.1 Parameters of the SCS method

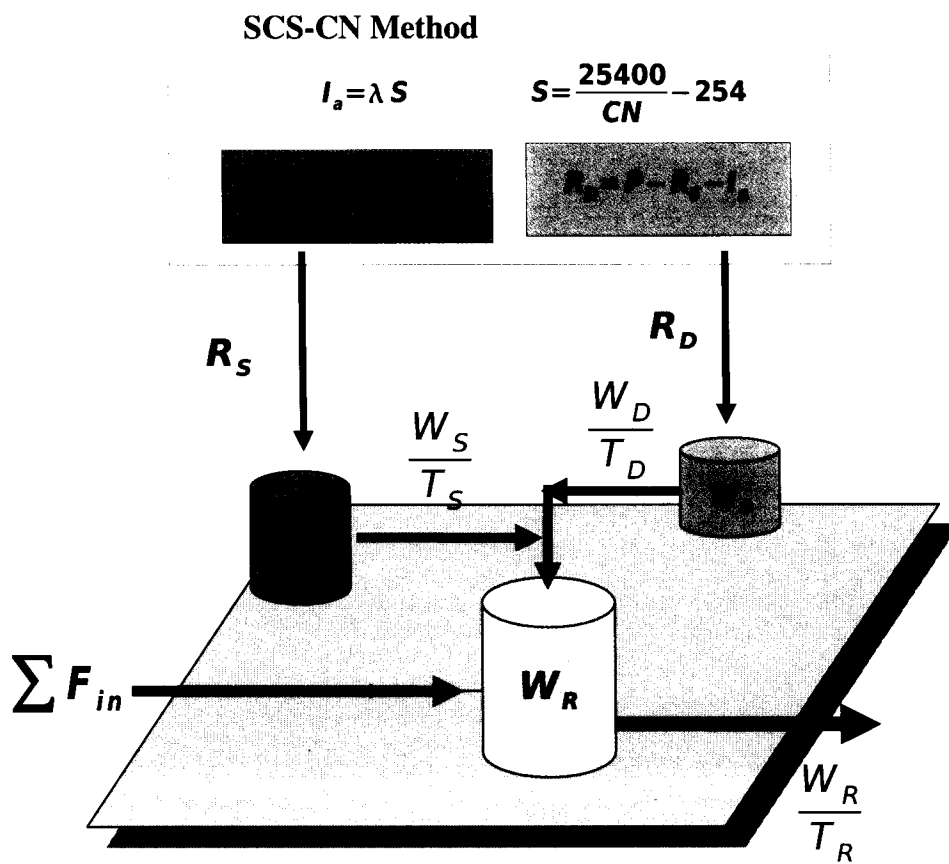
The two unknown quantities in Equations (4.3) and (4.5) are  $I_a$  and  $S$ , which are parameterised by the SCS using two dimensionless quantities called initial abstraction coefficient  $\lambda$  and Curve Number ( $CN$ ).

#### Model calibration and validation

Before going into the details of the estimation of parameters, it is necessary to address the problem of parameter calibration. The optimum values of parameters are derived by comparing the discharge simulations with the observed discharge. For most of the west-coast rivers, however, the observed discharge data are not available. Hence, parameter calibration should not be based on a mere comparison of simulated and observed discharge: it should be process-oriented. Therefore, observed discharges are not used in the THMB-SCS parameterisation.

Furthermore, instead of employing global optimum parameters (derived using all the years of observed data), we used a calibration and validation approach. Only a part of the observations are used for model calibration; the rest are used for validating the parameterisation. To build the model parameterisation, or to calibrate the model, we use three of the available 18 years (1981–

**Figure 4.3** Schematic representation of the THMB-SCS. The Soil Conservation Service Curve Number (SCS) method was incorporated to parametrise the rainfall-runoff relationship. The top panel shows how the surface (subsurface) runoff  $R_S$  ( $R_D$ ) are parameterised using the SCS method.  $R_S$  and  $R_D$  derived from the SCS method, then used to force THMB. THMB schematic is same as in Figure 2.2.





1998) of rainfall and discharge data. The remaining 15 years are used subsequently to validate the model. The three years (1986, 1990 and 1992) chosen to calibrate the model represent the inter-annual variability of the data: they are years of low, high, and average rainfall respectively (see Figure 4.4). These are also three of the six years for which rainfall data are available for all 20 stations (Table 3.1), thus yielding the best possible spatial rainfall maps. A Kolmogorov-Smirnov test (e. g., see Papoulis and Pillai [2002]) shows that the data for these three years are only qualitatively representative of the inter-annual variability (Figure 4.5). The inter-annual variability is much more than can be statistically represented by a small subset of the 18-year data set. Increasing the number of sample years, however, does not lead to an improvement in the parameterisation because the number of potential variables is very high and the information available is very low. Hence, we use only these three years as the test data for calibration.

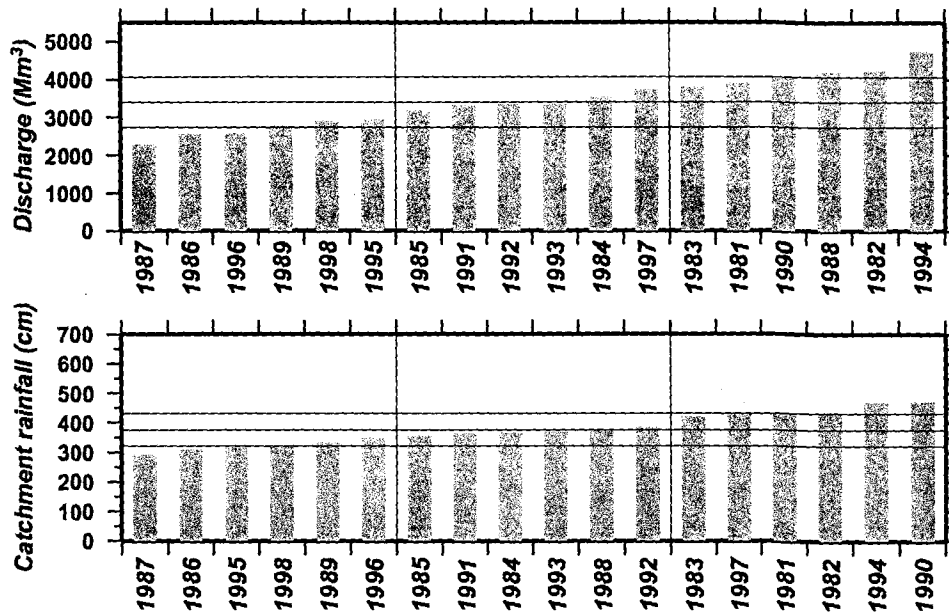
#### Initial abstraction coefficient, $\lambda$

The initial abstraction represents the minimum amount of rainfall required to generate surface runoff. To simplify estimation of runoff, the SCS proposed a linear relation between  $S$  and  $I_a$  on the basis of empirical evidence. Hence,

$$I_a = \lambda \times S, \quad (4.6)$$

where  $\lambda$  is the initial abstraction coefficient, a dimensionless quantity that conceptually represents the loss term in the model. The losses consist of surface detention, interception, and infiltration, all of which finally evaporate or transpire to the atmosphere. Therefore, the initial abstraction term as well as the storage in the basin are a function of evapotranspiration. The SCS recommends using  $\lambda = 0.2$  even though theoretically  $\lambda$  can vary from zero to infinity [Mishra and Singh, 2003]. The empirical basis for this choice of  $\lambda$  are the experiments carried out in watersheds in the United States [SCS, 1985; Mishra and Singh, 2003] that yield a scatter of values, 50% of which lie in the range 0.095–0.38. Though the SCS recommends a constant  $\lambda$ , it is a space-time varying parameter

Figure 4.4 Annual observed discharge (top, in  $\text{Mm}^3$ ) and the catchment-integrated rainfall normalised by the catchment area (bottom, in cm); the abscissa shows the year. The discharge and rainfall increase monotonically over the abscissa. The two vertical lines divide the 18 years into three bands: low rainfall, average rainfall, and high rainfall. 1986, 1992, and 1990 are representative of these three bands, respectively. The central horizontal line marks the mean discharge or rainfall and the other two horizontal lines mark one standard deviation from this mean.



depending on the geographic and climatic conditions of the watershed [Ponce and Hawkins, 1996; Mishra and Singh, 2003]. A wide range of  $\lambda$  (0–1) has been reported in the hydrology literature related to models based on the SCS method (see Table 4.1).

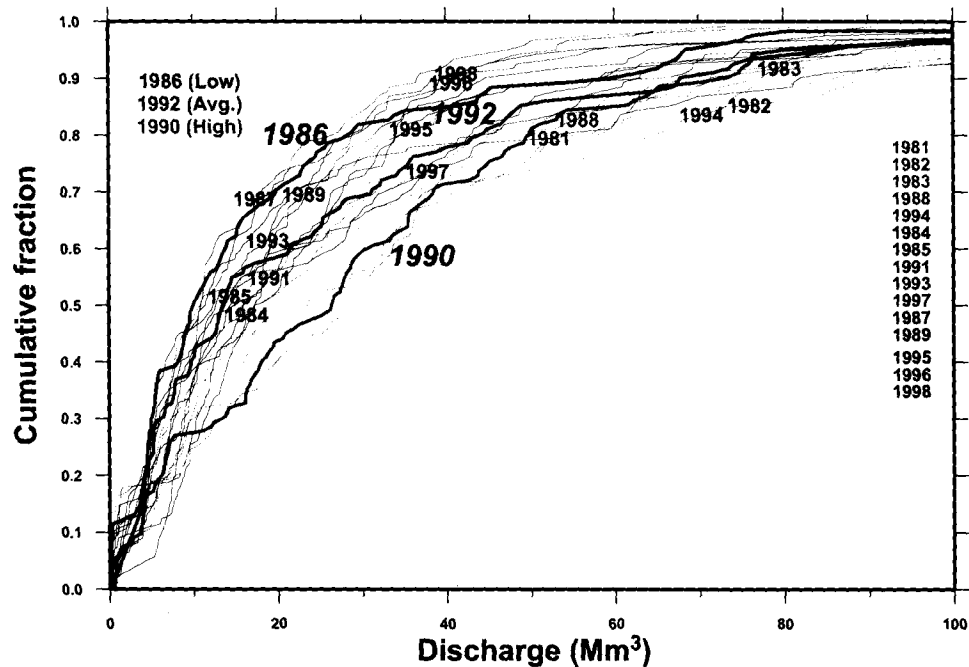
#### Storage $S$ and Curve Number $CN$

The storage  $S$  is mapped onto a dimensionless quantity called Curve Number ( $CN$ ), which is given by:

$$S = \frac{25400}{CN} - 254, \quad (4.7)$$

where  $S$  is in mm. Since higher (lower) storage implies lower (higher) surface runoff, higher (lower)  $CN$  implies higher (lower) discharge.  $S$  depends on the physical properties of the wa-

**Figure 4.5** Kolmogorov-Smirnov diagram showing the cumulative distribution plot for daily discharge during June–September for all 18 years (red curves for high-rainfall years, black curves for average-rainfall years and blue curves for high-rainfall years). Though 1986, 1992, and 1990 represent the low-, average-, and high-rainfall years, the spectrum of variability is too high for any reasonable sample of the data to be representative of the whole.



tershed, and therefore  $CN$  depends on the soil type, vegetation cover, land use, and hydrological and moisture conditions.  $CN$ , as defined in Equation (4.7), varies from 0–100, with a value of 0 implying infinite storage (capacity) and therefore no runoff, and a value of 100 implying that all the rainfall runs off because there is no storage in the basin. A more practical range for  $CN$ , however, is defined by various authors to be 40–100, implying a range of 0–381 mm for  $S$ .

The values of  $CN$  for basins having different physical characteristics (soil type, land use, vegetation cover, hydrologic conditions) have been prepared and tabulated by the SCS [Mishra and Singh, 2003]. These  $CN$  values are based on the rainfall-runoff calculations done over a large number of watersheds in the United States. Only a subset of this table is relevant for the Mandovi and these

**Table 4.1** A wide range of  $I_a$  is used in the models based on the SCS method.

Range (Mean)	References	Region	Remarks
0–0.26	Springer et al. [1980]	USA	Small humid and arid catchment
0–0.3	Cazier and Hawkins [1984] and Bosznay [1989]		
0.05	Hawkins et al. [2001]	USA	Useful in lower rainfall depths or lower $CN_s$
0.014–0.037	Baltas et al. [2007]	Greece	Experimental watershed
0.01–0.154	Shi et al. [2009]	China	Three Gorges Area of China
0–1 (0.06)	Mishra et al. [2005]	USA	Basins classified into 5 categories
0–1 (0.06)			$P \leq 12.7$ mm
0–1 (0.17)			$12.7 \leq P \leq 25.4$ mm
0–1 (0.37)			$25.4 \leq P \leq 38.1$ mm
0–1 (0.2)			$38.1 \leq P \leq 50.8$ mm
			$P \geq 50.8$ mm

$CN$  values are listed in Table 4.2, based on which we pick 60–90 as the possible range of  $CN$  for the Mandovi basin.

#### Antecedent Moisture Conditions (AMC)

The  $CN$  values given by SCS represent an average hydrologic condition in the basin, i. e., they do not account for the variability in antecedent conditions. The variability in the antecedent moisture conditions translates into the basin's runoff generation potential and thus to variability in  $CN$ . This variability is incorporated in the SCS method by a simple parameterisation scheme called AMC (Antecedent Moisture Conditions) to differentiate dry and wet soil conditions from normal or average soil condition [Chow et al., 1988; Mishra and Singh, 2003]. The  $CN$  for dry AMC is usually denoted as  $CN(I)$  and that for wet AMC as  $CN(III)$ ;  $CN(II)$  is the  $CN$  for average AMC. Thus,  $CN(II)$  (written simply as  $CN$ ) represents the central tendency in the rainfall-

**Table 4.2** A subset of the Curve Number ( $CN(II)$ ) classification.  $CN$  for different hydrological characteristics in humid range lands or agricultural uncultivated lands has been adapted from Mishra and Singh, (2003). Although these  $CN$ s are based on basins in the United States, similar ranges of  $CN$  are applicable to India, especially in the Sahyadris (see Tables 1 and 2 in Mishra et al. [2008]).

Land use description	Hydrologic condition	Hydrological soil group			
		A	B	C	D
Woods or forest land	Poor	45	66	77	83
	Fair	36	60	73	79
	Good	25	55	70	77
Wood-grass combination	Poor	57	73	82	86
	Fair	43	65	76	82
	Good	32	58	72	79

runoff data, and  $CN(I)$  and  $CN(III)$  represent the two extremities of the dispersion in the data [Mishra and Singh, 2003].  $CN(I)$  and  $CN(III)$  are calculated from the normal AMC  $CN$  by the empirical expressions given below [Chow et al., 1988]:

$$CN(I) = 4.2 \times \frac{CN(II)}{10 - 0.58CN(II)}; \quad (4.8a)$$

$$CN(III) = 23.0 \times \frac{CN(II)}{10 + 0.13CN(II)}. \quad (4.8b)$$

For example, if  $CN(II) = 90$ , implying a basin with low storage capacity, then  $CN(I) = 79$  and  $CN(III) = 95$ . Thus, once the central  $CN$  is determined for a watershed on the basis of its soil type, etc., the impact of differing hydrological conditions (dry to wet) is determined using Equation (4.8). All that needs to be determined is how to assess what type of moisture condition is prevalent at any given time, i. e., we need to determine the rainfall thresholds for the AMC.

The most popular method to determine the AMC thresholds is based on the amount of the rainfall in the preceding five days (5-day antecedent rain), called the antecedent precipitation index (API). Although the term antecedent does not specify a limit on the number of days, the AMC is determined based on a range of from 5 to 30 days [Mishra and Singh, 2003]. SCS [1971]

uses the 5-day rainfall for the AMC thresholds. Other methods similar to API include antecedent baseflow index (ABFI), soil moisture index (SMI), and the more recent antecedent runoff condition [Mishra and Singh, 2003]. Nevertheless, the 5-day AMC remains the most popular, owing to its simplicity and applicability [Mishra and Singh, 2003]. Although SCS [1971] gives the 5-day rainfall value to determine the AMC for watersheds in the United States, it also recommends developing separate AMC criteria for different watersheds [see also Ponce and Hawkins, 1996]. As an example, we note that the factors for converting  $CN(II)$  to  $CN(I)$  and  $CN(III)$  differ from Equation (4.8) [Mishra et al., 2008].

### 4.3 Application to the Mandovi basin

Application of the above parameterisation (with the 5-day AMC thresholding) to the Mandovi demands estimation of the optimum values of the SCS parameters:  $CN$ ,  $\lambda$ , and the AMC thresholds. An inherent assumption in optimization is that the observations, with which simulations are compared, are without error and that the model is a true representation of data. Obviously, both these assumptions are not correct: hence, it is important to check the sensitivity of simulations to the SCS parameters.

#### 4.3.1 Sensitivity to $CN$

For the  $CN$  range 60–90, we carried out simulations to test the sensitivity of the simulated discharge to  $CN$  (Figure 4.6). In all these experiments, the initial abstraction coefficient  $\lambda$  was set to 0.2 (SCS-recommended), and the lower and upper AMC thresholds were 100 and 250 mm respectively. Five-day antecedent rainfall less (greater) than 100 (250) mm is equivalent to lower or dry (upper or wet) AMC and correspondingly  $CN(I)$  ( $CN(III)$ ) is used. Moreover, the AMC setting was also constant for the basin. The correlation between the simulated and observed discharge was comparable across this  $CN$  range, but was highest for  $CN = 80$ . The results were

similar to Simulation *S0* in the sense that higher (lower) *CN* values resulted in higher (lower) simulated discharge irrespective of seasonality.

The range of *CN* values for the above experiments was based on the different soil and hydrological characteristics in the basin. In spite of its small size, the Mandovi basin shows a great degree of variability in these characteristics. On one hand, the regime of the Sahyadris, with steep slopes and hard soils, implies large *CN* values; on the other hand, the coastal sandy area implies low *CN*. Therefore, an average value of *CN* ( $CN = 70$ ) was considered representative of the entire basin.

#### Sensitivity to $\lambda$

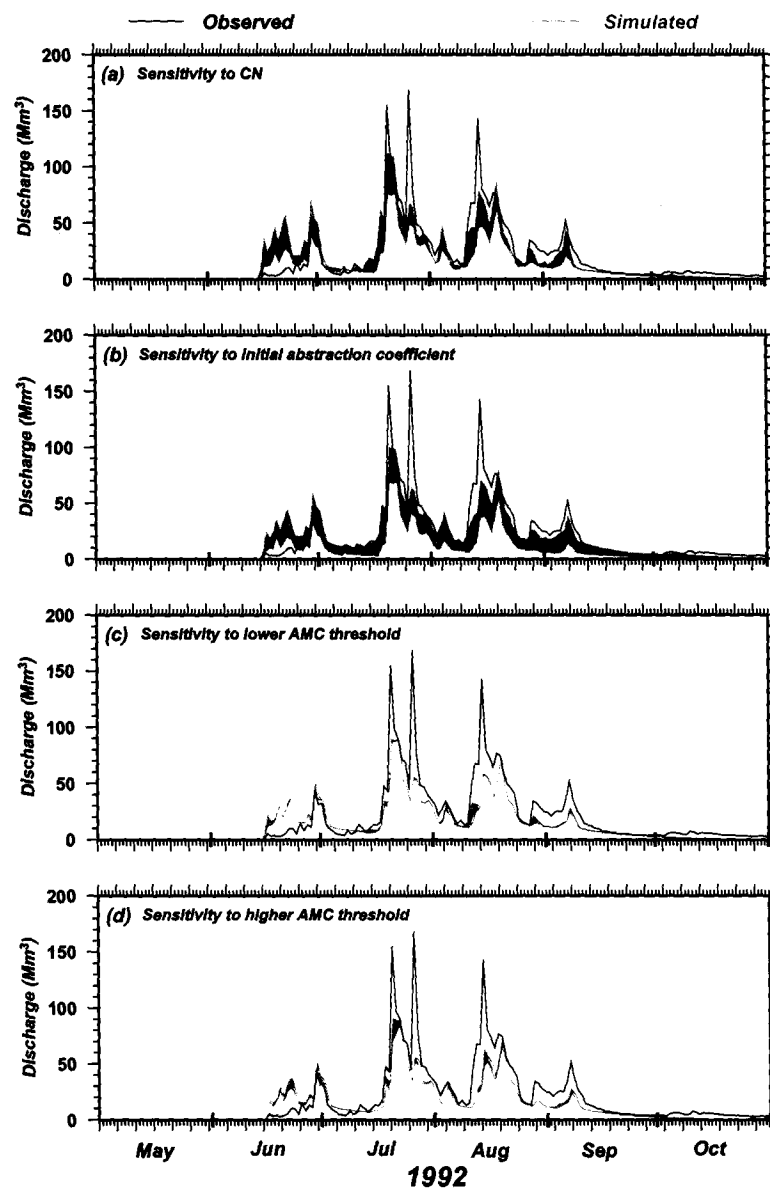
The initial abstraction coefficient  $\lambda$  also depends on the geographical and climatic conditions in the watershed. Simulations were done for different values of  $\lambda$ : 0.05, 0.2, 0.3, and 0.6. For all these simulations, *CN* was fixed at 70 for the entire basin and the AMC thresholds were also fixed as in the *CN* sensitivity tests. The results (Figure 4.6) show that the simulated discharge is not as sensitive to  $\lambda$  as it is to *CN*. Note that in these sensitivity tests,  $\lambda$  varied by over 100% in comparison to the  $\sim 10\%$  variation in the *CN* sensitivity tests.

#### Sensitivity to AMC thresholds

Sensitivity tests were carried out by varying the lower AMC threshold between 50 and 150 mm and the upper AMC threshold between 200 and 400 mm. The other two parameters, *CN(II)* and  $\lambda$ , were set to 70 and 0.2, respectively. The simulations show (Figure 4.6) that the simulated discharge is not sensitive to the definition of the AMC thresholds.

A histogram and a cumulative frequency curve (Figure 4.7) of the 5-day-rainfall pick 100 and 250 mm as the appropriate lower threshold (distinguishing the dry and average AMC) and upper threshold (distinguishing the average and wet AMC), respectively. These thresholds were chosen such that  $1/e$  (36%) of the days had rainfall above the lower threshold and  $1/e^2$  ( $\sim 14\%$ ) of the

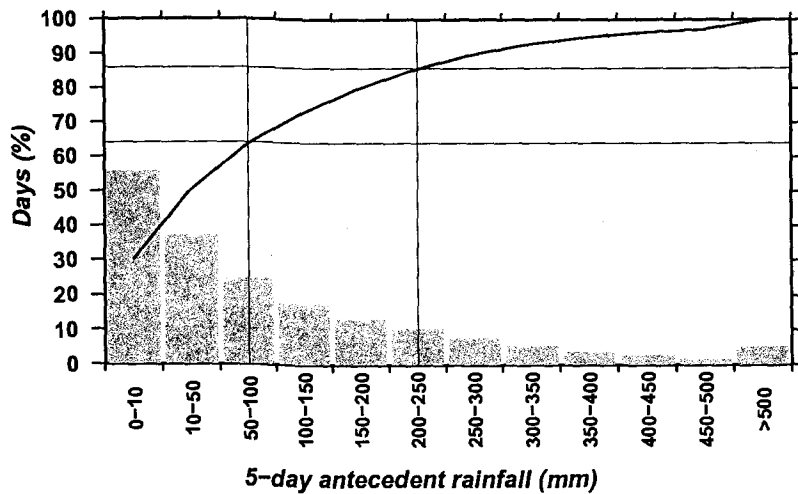
**Figure 4.6** The SCS parameters were constant in space and time. The black (red) curve shows the observed (simulated) discharge and the light grey band shows the range of the simulated discharge over the parameter range in the sensitivity test; the units are  $\text{Mm}^3$ . The bold tick marks on the abscissa indicate beginning and end of a month. (a) Sensitivity to  $CN(II)$ .  $CN(II)$  was varied in the range 60–90; for all the experiments, we set  $\lambda = 0.2$  and the AMC thresholds to 100 and 250 mm.  $CN(I)$  and  $CN(III)$  were estimated using Equation (4.8). The simulated discharge was higher for higher values of  $CN(II)$ . (b) Sensitivity to initial abstraction coefficient  $\lambda$ , which was varied in the range 0.05–0.6. For all the experiments,  $CN(II)$  was set to 70 and the AMC thresholds to 100 and 250 mm. The simulated discharge was higher for lower values of  $\lambda$ . (c) Sensitivity to the lower AMC threshold, which was varied in the range 50–150 mm. For all the experiments,  $CN(II)$  was set to 70 and  $\lambda = 0.2$ . The simulated discharge was higher for lower values of this threshold. (d) Sensitivity to the upper AMC threshold, which was varied in the range 200–400 mm. For all the experiments,  $CN(II)$  was set to 70 and  $\lambda = 0.2$ . The simulated discharge was higher for lower values of this threshold.





days had rainfall over the upper threshold;  $\sim 22\%$  of the days experienced the “average” rainfall. The hydrologic rationale for these numbers is as follows. The soil and land are expected to adjust to the normal or expected runoff over most of the rainy season. Hence, we assume that the dry  $CN$ , implying greater storage and lower runoff, would hold for  $(1 - 1/e)$  of the days and that the average  $CN$  would hold for  $(1 - 1/e)$  of the remaining  $1/e$  days, leaving  $1/e^2$  of the days in the higher-than-average-rainfall band. The simulations also suggest that this argument is reasonable: the best results are obtained for these thresholds of 100 and 250 mm. Therefore, these were the AMC values used for the  $CN$  and  $\lambda$  sensitivity tests.

**Figure 4.7** Determination of the AMC thresholds for Simulation *S1*. The histogram shows the percentage of the total days (during May–October) that had a 5-day antecedent rainfall in the rainfall bands (mm) marked on the abscissa. The histogram was drawn by averaging the number of days in each band over the entire basin and summing over the three years 1986, 1992, and 1990. The curve is the cumulative fraction. The vertical lines represent the lower and upper thresholds. The lower (upper) threshold at 100 (250) mm; the cumulative fraction curve shows that  $1/e$  ( $\sim 36\%$ ; bottom horizontal line) of the days had rainfall above the lower threshold and  $1/e^2$  ( $\sim 14\%$ ; top horizontal line) of the days had rainfall over the upper threshold.

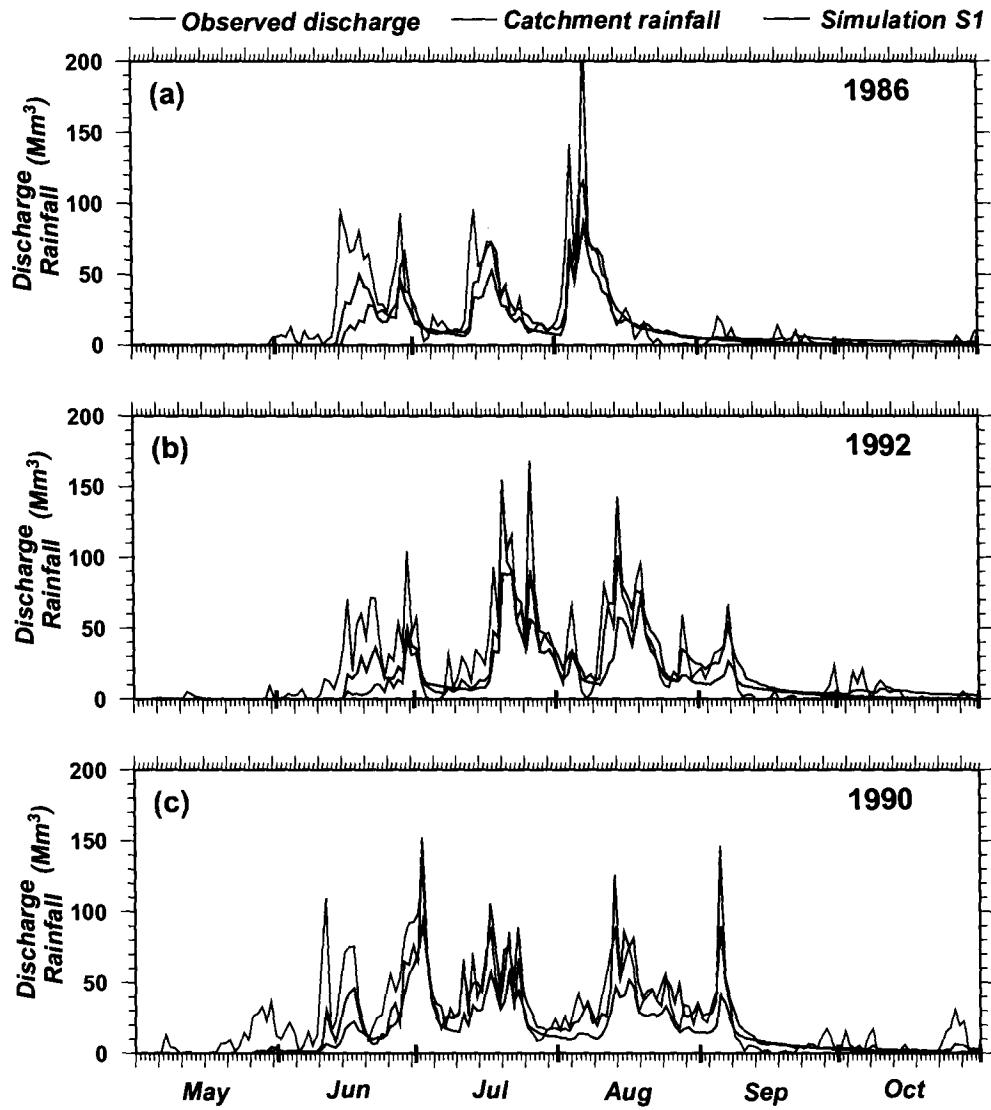


#### 4.4 Results and discussion

We use  $CN = 70$ ,  $\lambda = 0.2$ , and AMC thresholds of 100 and 250 mm as the optimum basin-average values to simulated discharges (Simulation *S1*) for 18 years (1981–1998). The simulations showed marked improvement; there were two major improvements in *S1* over *S0* (Figures 4.8 and 4.2). First, as expected, the baseflow decreased during the weak spells of the peak-monsoon season (July–August). Second, as with the observed discharge, there was greater variability in the simulated discharge in Simulation *S1* than in Simulation *S0*. The reason for these improvements is that the high  $CN$  values in the average and wet periods lead to a dominance of surface runoff at these times and the relatively low  $CN$  during the dry periods allows much of the rainfall to be abstracted.

One drawback of Simulation *S1* is the underestimation of the discharge following the peak of the monsoon, i. e., the simulated baseflow in September is lower than observed. The main drawback, however, lies in the simulated discharge being much higher than the observed discharge during the onset phase of the monsoon in May–June (Figure 4.2). One possible reason is an overestimate of the runoff on the lee side, which is drier than the windward side and should therefore have lower  $CN$  values compared to the slopes of the Sahyadris. The SCS parameters in Simulation *S1* were, however, constant across the basin, and did not account for such spatial or geographical differences. Another possible reason is that the onset-phase  $CN$  is overestimated on the windward side too. The basin is much drier before the monsoon than after onset, and the storage capacity should therefore vary accordingly. The SCS parameters in Simulation *S1* did not, however, vary with season, leading to a possible overestimate of the onset-phase surface runoff. The sensitivity of the simulations to the SCS parameters implies a large potential variation in the rainfall-runoff relationship across the basin, and possibly also in time. In other words, the 5-day AMC used in *S1* is not sufficient to capture the spatial and temporal variations that are likely in the SCS parameters even within this small basin. Nevertheless, incorporating the SCS method

Figure 4.8 Observed discharge (black), discharge simulated by Simulation *S1* (red), and the catchment-integrated rainfall(blue) at Ganjem for May–October, (a) 1986, (b) 1992, and (c) 1990. The units are  $\text{Mm}^3/\text{day}$ . The bold tick marks on the abscissa indicate beginning and end of a month.



into THMB does improve the simulated discharge, suggesting that this simple parameterisation is useful. Further improvements can be made by incorporating spatial and temporal variations in the SCS parameters. The challenge is to incorporate these variations in a manner that is not only physically reasonable, but also simple. Incorporating spatial and temporal variations in the SCS parameters is the subject of the next chapter.

## Chapter 5

# Spatio-temporal variability in rainfall-runoff model

### 5.1 Introduction

Simulation *S1* was a major improvement over *S0*. The reason for this improvement was incorporation of the SCS method into THMB: THMB's simple parameterisation (a single parameter  $\alpha$ ) was replaced by the more complex parameterisation of the SCS method (*CN*,  $\lambda$ , and AMC thresholds). In Simulation *S1*, the SCS parameters used were constant in both space and time. Constant parameters represent an average condition of the basin. This parameterisation ignores spatial and temporal variability in rainfall (see Figures 3.3 and 4.1). It also ignores spatial variability of other runoff-generating parameters (such as soil, land cover and use and other physical properties of the basin). This variability in runoff-generating parameters implies a spatio-temporal variability in runoff and therefore in the SCS parameters. Incorporation of this spatio-temporal variability in SCS parameters in order to improve the discharge simulations is the subject of this chapter<sup>1</sup>.

---

<sup>1</sup>Work reported in this chapter is compiled in a manuscript for publication [Suprit et al., 2011].

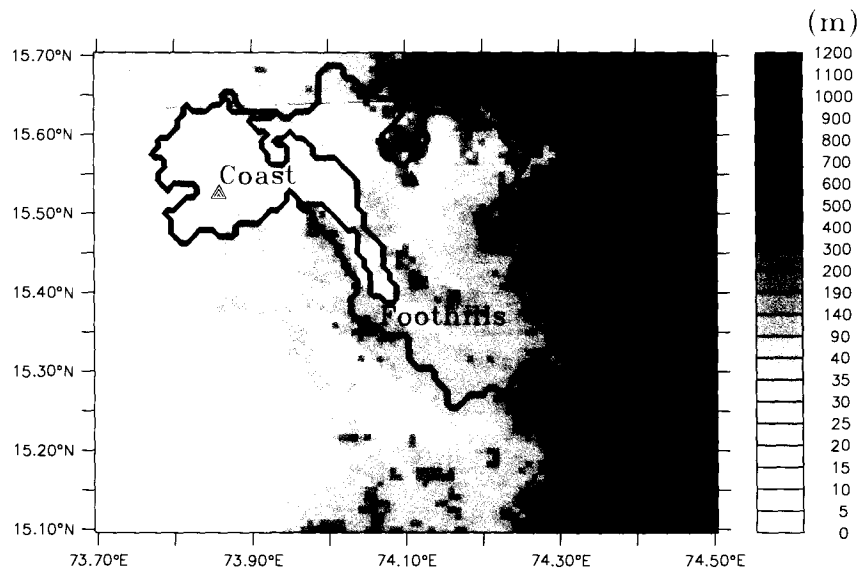
## 5.2 Spatial variations

Ideally, estimating the SCS parameters requires rainfall and runoff data from the catchment area, or, in the case of a distributed model like THMB, from each grid cell. Though the rainfall-mapping procedure provides rainfall information for each grid cell, we do not have runoff information for the cells. The only information available on runoff is the discharge at Ganjem and Kulem. THMB is a distributed model, but we do not have the runoff data in the same distributed sense in order to build an empirical, cell-based parameterisation of the SCS parameters. Hence, for incorporating spatial variability into these parameters, we take recourse to a semi-lumped approach, wherein the basin is divided into four sub-basins or hydrologically coherent regions.

### 5.2.1 Regionalisation

The reason for spatial variation in the SCS parameters ( $CN$ ,  $\lambda$  and AMC thresholds) is the spatial variation in soil type, vegetation cover, land use, and hydrological and moisture conditions. As with runoff, we do not have cell-specific information for these characteristics: the only cell-based data available are elevation and rainfall. Hence, we use the elevation to divide the basin into four hydrological regions: the leeward side of the Sahyadris (*Lee*), the ridge and the windward slope above 200 m (*Ridge*), the foothills of the Sahyadris or the region on the windward side between elevation contours 40 and 200 m (*Foothills*), and the coastal plains or the region at an elevation below 40 m (*Coast*). (The names in the parentheses are used to refer to these regions.) The regions were delineated using the 40 and 200 m contours on the smoothed (using 5 cells  $\times$  5 cells averaging) DEM. The resulting regions were made uniform by eliminating pockets or enclosures. Thus, the basin was divided into four contiguous regions (Figure 5.1), and the SCS parameters were determined for each of these regions. It is evident from Figure 5.1 that the sharp change in elevation that marks the Sahyadris occurs around the 200-m contour. Likewise, the 40-m contour separates the low-lying Coast region from the relatively higher Foothills.

**Figure 5.1** The four spatial regions, *Coast*, *Foothills*, *Ridge*, and *Lee*, in the Mandovi basin (region bounded by black curve). The regions were defined by smoothing the GLOBE DEM over 25 cells (5 cells  $\times$  5 cells). The *ridge* (blue curve; Figure 3.1) separates the regions *Lee* and *Ridge*, the smoothed 200 m (green) contour separates the regions *Ridge* and *Foothills*, and the smoothed 40 m (purple) contour separates the regions *Foothills* and *Coast*. Elevation is in metres. The filled triangles mark the cells used for plotting Figures 5.4 and 5.6.



### 5.2.2 Estimation of parameters

The  $CN$  was estimated on the basis of the runoff-generation capacity of the soil in a region because detailed information on soil cover was not available. The dominant soil type and land usage for the four regions are listed in Table 5.1. The *Ridge* region is dominated by forests with a thin layer of laterite soil over an impervious layer of rock [Gokul et al., 1985], implying that it belongs to Soil Group *D*. As the hydrologic condition of the *Ridge* region is not known, we average the  $CN$  over the three types of hydrologic conditions tabulated by SCS (Table 4.2), yielding  $CN = 75$ . From the soil type listed in Table 5.1, it is evident that the *Ridge* region has the maximum runoff-generation capacity, followed by *Foothills*, *Lee*, and *Coast*.

The estimation of  $\lambda$  was done similarly. The minimum value used in the literature (Table 4.1)

**Table 5.1** Basin soil and hydrologic characteristics and SCS parameters for Simulation *S2* (SCS parameters allowed to vary in space).

Parameter		Lee	Ridge	Foothills	Coast	Remarks
Soil type		Red, laterite	Shallow soils over rock	Red, Sandy loam	Sandy soil,	Representative
Hydrologic soil group		B/C	D	C	A	—
<i>CN(II)</i>		65	75	70	60	—
AMC (mm)	Dry	< 100	< 150	< 100	< 100	5-day antecedent rainfall
AMC (mm)	Wet	> 100	> 400	> 250	> 200	
$\lambda$		0.3	0.05	0.1	0.3	SCS value (0.2)

was used for the *Ridge* region because of its steep slopes and impervious, rocky soil. The highest value of  $\lambda$  (0.3) was used for Lee (Table 4.1) because of its gentle topography and Soil Group (*B* and *C*), which would allow more of the rainfall to be abstracted. The same value was used for *Coast* because it belongs to Soil Group *A*, which implies low runoff, and has a gentle topography.

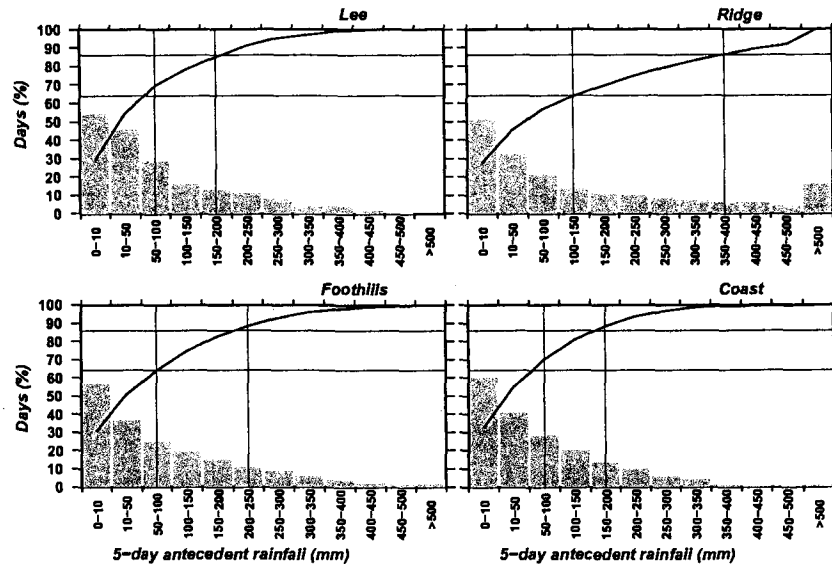
As with *CN* and  $\lambda$ , the AMC thresholds were prescribed for each of the four regions. The antecedent rainfall, however, was computed separately for each grid cell and the condition (dry or average or wet) is determined for each cell. As done earlier for the entire basin, the AMC thresholds for each of the four regions were determined on the basis of a histogram of rainfall during May–October and a cumulative frequency curve of the 5-day rainfall (Figure 5.2): the thresholds, listed in Table 5.1, were chosen such that  $\sim 36\%$  ( $\sim 14\%$ ) of the days had rainfall above the lower (higher) threshold.

### 5.2.3 Simulation *S2*

We extended the SCS parameterisation in THMB to permit spatial variation in the SCS parameters (Simulation *S2*, Table 5.1). The simulated discharge (Figure 5.3) is similar to that in Simulation



Figure 5.2 As in Figure 4.7 but for Simulation S2, in which the AMC thresholds depend on the spatial region: *Lee* (top left) or *Ridge* (top right) or *Foothills* (bottom right) or *Coast* (bottom left).

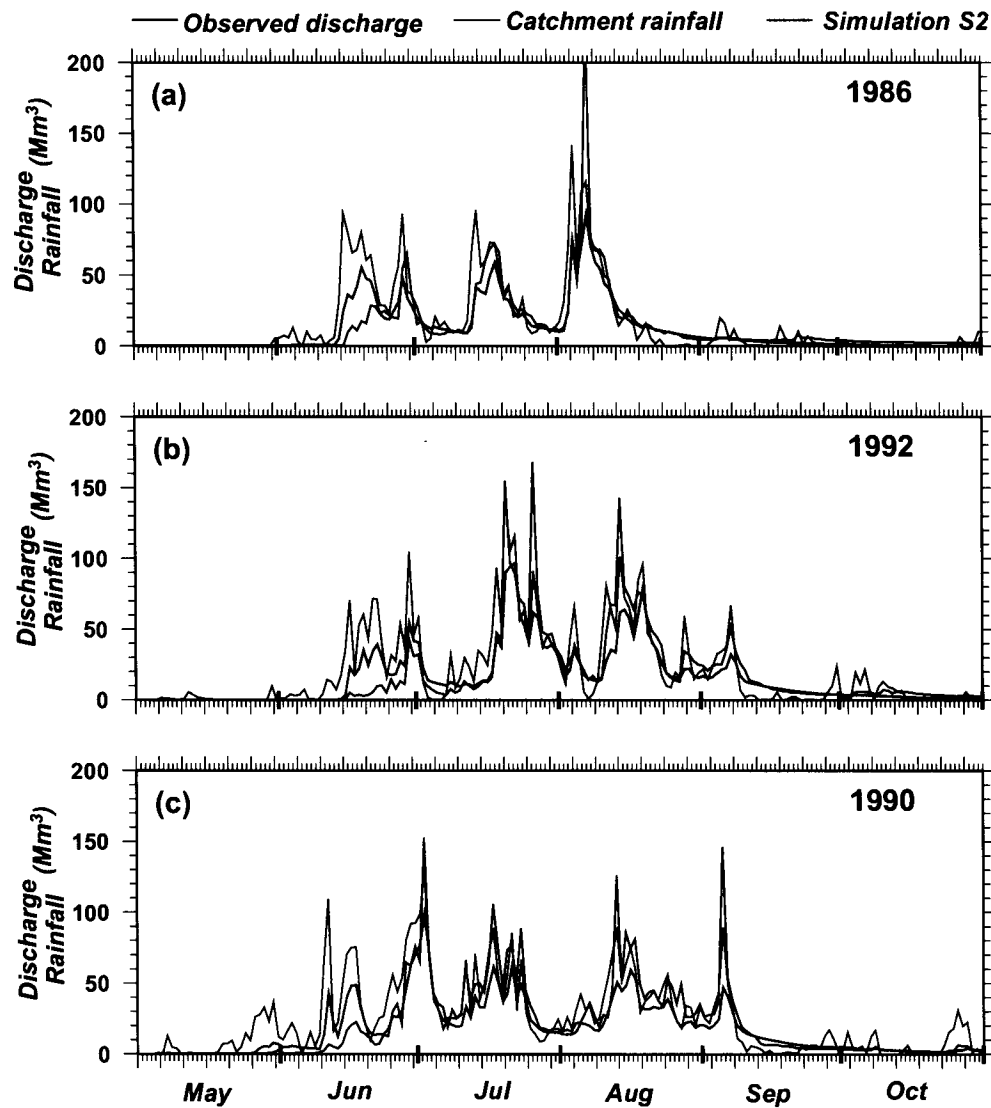


S1 (Figure 4.8): the spatial variation of the SCS parameters has but a minor impact on the simulated discharge at Ganjem. The higher  $CN(II)$  (75) in the high-rainfall Ridge region leads to an improvement in the simulated discharge during July–September: the peak discharge increases, and so does the baseflow during the weak spells and following the monsoon peak in September. This increase in the Ridge  $CN(II)$ , however, leads to an increase in the overestimate of discharge during the onset phase in May–June. Thus, only spatial variation of the SCS parameters is not sufficient to simulate the Mandovi discharge accurately. So, we explore the impact of the temporal variation of the SCS parameters on the generation of runoff.

### 5.3 Temporal variations

As discussed earlier, most of the west-coast rainfall ( $\sim 90\%$ ) occurs during the summer monsoon (June–September), with negligible rainfall during December–April (Figure 1.8). Correspondingly,

**Figure 5.3** Observed discharge (black), discharge simulated by Simulation *S2* (red), and the catchment-integrated rainfall (blue) at Ganjem for May–October. (A) 1986. (B) 1992. (C) 1990. The units are  $\text{Mm}^3/\text{day}$ . The bold tick marks on the abscissa indicate beginning and end of a month.



the daily discharge during December–April is of the order of  $0.1 \text{ Mm}^3$  in contrast to the  $100 \text{ Mm}^3$  discharge observed in bursts during the peak of the summer monsoon (July–August, Figure 4.1).

The transition from the dry to the wet season occurs in May–June. There is considerable rainfall during this onset of the summer monsoon, but there is no hydrological response: the discharge remains low, responding only to rainfall bursts during this onset phase (Figure 4.1). Even during these bursts, however, the discharge is much lower than the catchment-integrated rainfall. Thus, most of the rainfall during the onset phase is abstracted or lost to the river flow.

After some time following the onset of the monsoon, the discharge starts mirroring the rainfall. The sharp discharge peaks observed during June–August coincide with the rainfall peaks, as is evidenced by the lack of any time lag between the rainfall and discharge on the daily time scale (Figure 4.1). This coincidence of peaks has two implications. First, surface runoff or overland flow dominates following the onset of the monsoon, and there is practically no subsurface runoff or baseflow. The Mandovi originates on the lee side of the Sahyadris and flows for  $\sim 37 \text{ km}$  before reaching the gauging station at Ganjem. The time taken for this flow to reach Ganjem is just 2–3 hours, leading to the coincidence of rainfall and discharge peaks. Second, success in simulating the peak discharge during June–August is contingent on success in mapping these rainfall peaks accurately. As shown in Figure 4.1, the peak summer-monsoon discharge, even allowing for a 15% error in the discharge measurement, is invariably greater than the catchment-integrated rainfall. The rainfall-mapping algorithm is unable to resolve the peak rainfall events and underestimates the rainfall during these bursts. The cause of this underestimation lies in the sparsity of rain gauges (see Figure 3.1): there are too few gauges for an accurate mapping of the strong rainfall gradients across the Sahyadris and this problem is exacerbated for the shorter time scales. This underestimation of rainfall has implications for the simulated discharge.

Though the baseflow is negligible in the Mandovi, there are two seasons when it makes a contribution. First, the negligible discharge during the lean season (December–April) comprises primarily of baseflow. Second, the discharge during early September, at the conclusion of the

peak-monsoon season, exceeds the catchment-integrated rainfall (see Figure 3.1). This excess flow is also probably sustained by baseflow resulting from the heavy rainfall during the preceding bursts.

Therefore, our objective for incorporating temporal parameterisations is to focus on three aspects of the discharge in the Mandovi. First, we seek an improved simulation of the observed discharge throughout the rainy period from the onset of the monsoon in late May or early June to the end of October, by when the baseflow declines to negligible levels beyond the scope of this model. Second, though the baseflow following the peak monsoon is small, it is almost two orders of magnitude larger than the lean-season flow and is therefore significant enough ( $\sim 10 \text{ Mm}^3$ ) to merit better simulation. Third, the large abstraction during the onset phase of the monsoon is important, but neither Simulations *S1* nor *S2* could simulate it correctly: simulating this large abstraction is important.

### 5.3.1 The seasonal change in abstraction

The excess rainfall in the Mandovi basin appears neither as streamflow (immediately following the rain) nor as baseflow (appearing after a lag) (Figures 1.9 and 4.1). This excess rainfall must therefore either recharge the groundwater or be returned to the atmosphere through evapotranspiration. On the catchment scale, groundwater recharge is a small quantity [Coe, 2000; Maréchal et al., 2009] and has been neglected in the THMB formulation. Evapotranspiration is therefore the only loss term in this model and it is parameterised using the initial abstraction, which is a function of  $CN$  and  $\lambda$  in the SCS method. In any case, evapotranspiration observations are rare in the region [Maréchal et al., 2009], and estimates of initial abstraction are non-existent.

Before monsoon onset, the soil is dry, temperature is high, and relative humidity is low. Transpiration through the vegetation canopy also leads to a loss of water from the basin [Maréchal et al., 2009]. Therefore, there exists a large potential for initial water retention and evapotranspiration whenever moisture becomes available. These conditions prevail till the system changes from a

moisture-deficient state to a moisture-saturated state. The rate at which these changes occur depends on the process of monsoon onset, i. e., fewer rainy days in June make this transition slow, allowing more abstraction.

The basin characteristics change dramatically once the monsoon sets in. The soil begins to soak up moisture, temperature decreases, and relative humidity increases. Evapotranspiration is highest during this transition period. It is higher than during the preceding dry season because the actual evapotranspiration is limited by the amount of water available. Hence, abstraction is at its peak during the onset phase. Not accounting for this high abstraction leads to an overestimate of the discharge at this time (Figures 4.8 and 5.3).

During the peak-monsoon season, availability of water is no longer a limiting factor, but lower temperatures and high relative humidity, in combination with the increase in the number of rainy days, ensure low evapotranspiration and low initial abstraction.

Immediately after the monsoon peaks, the soil is still saturated. Hence, the runoff responds rapidly to rainfall and the abstraction remains low. Therefore, the catchment rainfall at this time is comparable to the observed discharge (Figures 4.8 and 5.3), but the runoff generated in the model is low, leading to an underestimate of the discharge even if the SCS parameters are allowed to vary spatially (Figure 5.3). Later the soil dries out, but the availability of water becomes the limiting factor and abstraction remains low till the following year's monsoon onset.

Thus, the SCS parameters exhibit an inherent seasonality that cannot be accounted for by the 5-day AMC parameterisation. In other words, there is a difference between a dry (or wet) spell, based on the 5-day antecedent rainfall, in the dry and wet seasons. Hence, temporal variation of the SCS parameters needs to be incorporated into the rainfall-runoff model.

One way to incorporate seasonality in the SCS parameters is implementing a similar parameterisation like AMC, but for a longer time scale of 30 days. The idea is that a 30-day parameterisation for  $CN(II)$  and  $\lambda$  might be able to capture seasonal or low-frequency variations by accounting for rainfall over a longer time scale in addition to the higher frequency variations. The

basis for this assumption lies in the lower rainfall in May–June compared to August–September, implying a lower (higher)  $CN$  during monsoon onset (post-monsoon) for the same 5-day antecedent rainfall. This 30-day AMC-like parameterisation was used in addition to the 5-day AMC. The simulation is better than Simulation  $S2$  over only a part of the rainy season, but it is worse at other times.

The reasons for the inability of a second, longer, AMC-like parameterisation to account for the low-frequency variability are the rapid decrease in rainfall following the peak of the monsoon and the sudden increase in rainfall during onset. The soil also does not seem to dry as much during the weak phases of the peak-monsoon season. Such weak spells are different from a similar rainfall regime either during the onset or following the peak monsoon. In other words, it is not enough that a longer, 30-day window is used for determining the runoff: equally important is the location of this window in the seasonal cycle of rainfall. Hence, the temporal parameterisation has to incorporate the seasonal cycle of soil moisture in order to generate the appropriate runoff.

### 5.3.2 Seasonal variation of SCS parameters

In order to build a time-dependent parameterisation of the SCS parameters, we need to distinguish the different rainfall-runoff regimes during the seasonal cycle and define objective criteria for transition from one regime to another. The only data available, however, are the daily rainfall used to force the model and the observed daily discharge. We use both rainfall and discharge to describe these temporal regimes, but use only the rainfall and its accumulation over the year, which we call *cumulative rainfall* (CR), as the criteria for transition from one regime to another.

### 5.3.3 The temporal regimes

The temporal regimes are described in Table 5.2 and depicted graphically in Figure 5.4. The discharge, rainfall, and CR curves show that there exist five distinct temporal regimes in the Mandovi basin. The first regime is the *Lean-Season* Regime ( $A$ ) at the beginning and end of a calendar

**Table 5.2** Classification of hydrological regimes (temporal) and of the transitions from one regime to the next. See Figure 5.4 for the corresponding graph.

Classification	Condition	Rain	CR	Discharge
<i>A Lean-Season</i>	Very dry (scanty rainfall)	Very small	No discharge	
	Transition <i>AB</i>	First spells of rain	Small inflection	—
<i>B Onset-Monsoon</i>	Wet unsaturated	Rain in bursts or continuous rain peaks	Rising	Does not respond to rain
	Transition <i>BC</i>	Bigger burst that continues into peak-monsoon (3–6 days into the burst)	First large up-slope inflection	Starts responding to rain
<i>C Peak-Monsoon</i>	Very wet	Intense and continuous	Rising rapidly (with plateaus during weak spells)	Follows rainfall curve
	Transition <i>CD</i>	Rain break (little or no rainfall) for 5 (more) days	Second large downslope inflection	Recedes exponentially
<i>D End-Monsoon</i>	Wet saturated	late-monsoon active period or rain bursts	Flattening out some bumps	Still responds big rain bursts
	Transition <i>DE</i>	Longer break of 10–15 days		Smooth decline continues
<i>E Post-Monsoon</i>	Moist unsaturated	Scattered bursts of low rain	Plateau	Stops responding to the rain
	Transition <i>EA</i>	30 days of no rainfall	Maximum	—
<i>A Lean-Season</i>	Very Dry	No or scanty rainfall	Maximum	No discharge

year. This regime is very dry and the discharge is due to a baseflow that is three orders of magnitude smaller than the peak discharge during the year. The transition (called *AB*) to the second regime, which is the *Monsoon-Onset* Regime (*B*), is marked by the first spells of rain. Regime *B* is wet, but the soil is unsaturated. In other words, while there is frequent rainfall, the discharge does not respond to the rainfall. The transition (*BC*) to the third regime, which is the *Peak-Monsoon* Regime (*C*), is marked by a big rainfall burst and a sharp inflection of the CR curve; the soil is saturated by now and the discharge starts responding to the rainfall during this transition (instantaneous pooling). Rainfall is more sustained during this transition and lasts a few days, leading to a different slope for the CR curve during this regime in comparison to the Regime *B*. The transition (*CD*) to the next regime, called the *End-Monsoon* Regime (*D*), is marked by a break in rainfall. There is little or no rainfall for five or more days, the CR curve plateaus off (marking a second major inflection point), and the discharge recedes exponentially. During Regime *D*, there are some rainfall bursts, but they are weaker than during Regime *C*, and the discharge still responds to these bursts because the soil is wet and saturated. The transition (*DE*) to the next regime, called the *Post-Monsoon* Regime (*E*), is marked by a longer rainfall break, which lasts for 10–15 days. During this regime, the soil is moist (but unsaturated), and the discharge stops responding to the weak and scattered rainfall. The last transition (*EA*) is back to Regime (*A*): it occurs towards the end of the calendar year and is marked by a longer (~ 30 days) rainfall break.

#### 5.3.4 Objective criteria for transition

The transitions described above need quantification, i. e., a set of objective criteria are needed to determine the period of transition. The criteria we use (see discussion below and Table 5.3) are applied to each grid cell of the Mandovi basin. Hence, a transition can occur on different days for different cells within a spatial region. The rainfall data, however, indicate that the transition occurs for most cells within a week of the first transition in the region.

The rainfall is cumulated starting in January every year because Transition *EA*, marking the



**Figure 5.4** The temporal regimes, *A–E*, and the inter-regime transitions. The vertical lines mark the transition from one regime to the next. The observed discharge (dotted curve, in  $Mm^3$ ), daily rainfall over one grid cell in a region (solid black curve, in mm), and the cumulative rainfall (CR; solid red curve, in mm) in the cell are shown. The cell chosen has the average rainfall in a region during May–October and is marked by the filled triangle in Figure 5.1. The four panels are for the *Ridge* (first), *Foothills* (second), *Coast* (third), and *Lee* (fourth) regions during 1992.

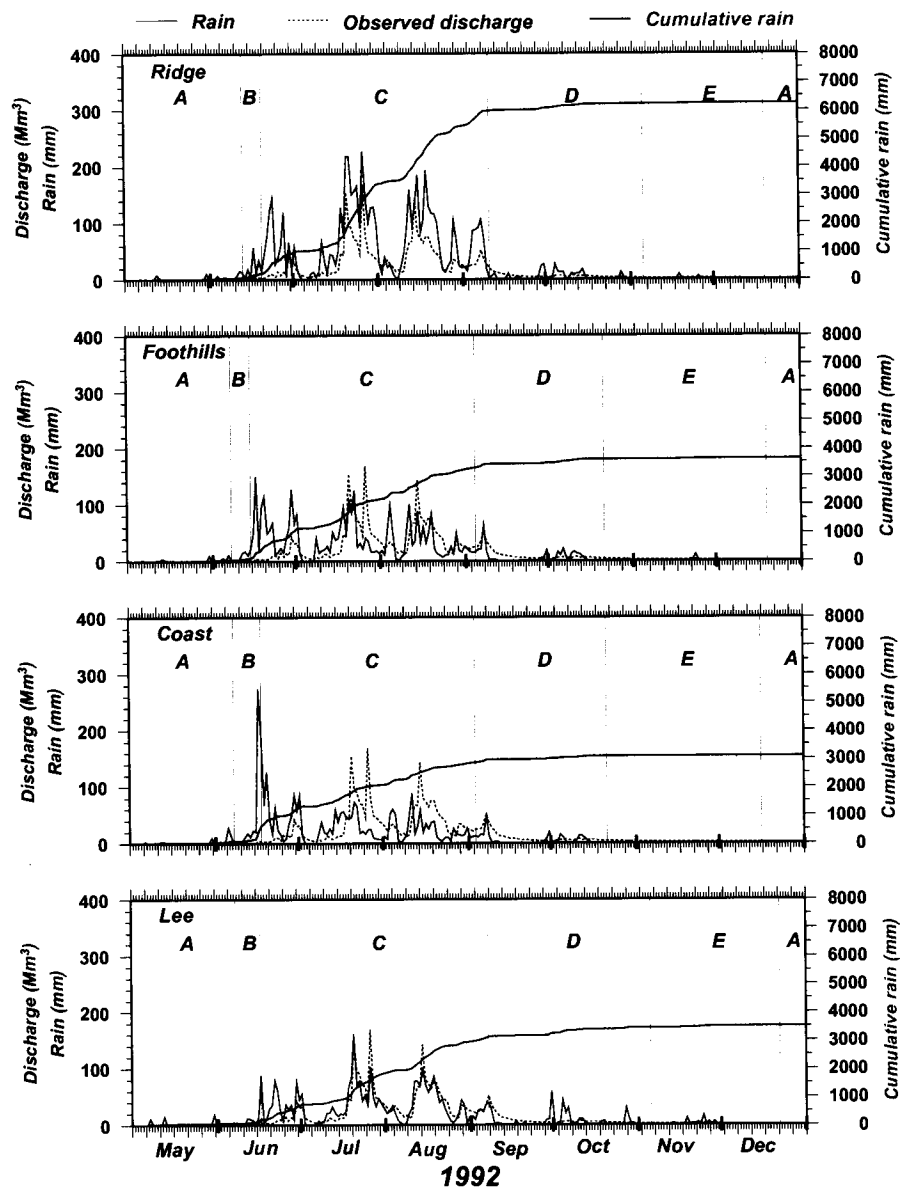


**Table 5.3** Objective criteria for transition from one regime to the next. Note that CR is estimated starting from the beginning of a year.

	AB	BC	CD	DE	EA
CR	$\geq 75$ mm	CR1	CR2	—	—
AMC	—	—	—	AMC $\leq 30$ mm for 5 consecutive days	—
P	(1) Sum of 3-day $P \geq 30$ mm. (2) $P \geq 5$ mm on each of 3 days	$P \geq 150$ mm	$P \leq 5$ mm for one day	$P \leq 5$ mm for 15 consecutive days	$P \leq 1$ mm for 30 consecutive days
Note	Both conditions	(1) If P condition true, transition after 5 days. (2) If not, then CR1 condition. (3) Transition if one of the above is true	CR2 condition first and then rain. The AMC applied only once, then P applied	AMC first, and then P.	Transition in December
CR1	Fit a straight line to the CR data and compare the deviation of the curve from the line. Transition occurs if the deviation ( <i>concave-up inflection</i> ) exceeds one and half standard deviation for five consecutive days				
CR2	Fit a straight line to the CR data and compare the deviation of the curve from the line. Transition occurs if the deviation ( <i>concave-down</i> ) exceeds one and half standard deviation for five consecutive days.				

start of the lean-season regime, occurs in December. The first transition to be determined is  $AB$ , i. e., the onset date (phase) of the monsoon. Since scattered pre-monsoon showers may occur in April and May, the first condition is that the cumulative rainfall (CR) should exceed 75 mm. A second condition to ensure that an isolated event is not taken to herald the monsoon onset, is that the accumulated rainfall over three consecutive days has to exceed 30 mm and the rainfall on each of these three days has to exceed 5 mm. This latter condition is similar to that used by IMD to determine the date of onset of the monsoon over Kerala [Ananthakrishnan et al., 1968; Pai and Nair, 2009]. A more complex criterion recently adopted by IMD results in a similar date for monsoon onset [Pai and Nair, 2009]. These two conditions constitute the criterion for Transition  $AB$  (Table 5.3).

The second transition,  $BC$ , is marked by a sharp increase in rainfall, and the CR curve shows a sharp, concave-upward inflection (Figure 5.4), which we capture by noting the deviation of the curve from a line fitted to the CR curve over Regime  $B$ . This procedure is implemented as follows.

1. First, Regime  $B$  is assumed to last at least  $LC$  (least count, set to 5) days. From the starting point ( $SP$ ) of Regime  $B$ , a least-squares regression line is fitted to the CR curve.
2. Once Regime  $B$  is  $LC$  days long, a comparison is made between the actual deviation ( $AD$ ) of the curve from this line with the positive standard deviation ( $PSD$ ) of the fitted line; the difference between these two deviations ( $IC$  is  $AD$  minus  $PSD$ ) is a measure of the concave-up inflection of the CR curve.
3. If  $IC$  exceeds zero for a minimum number of days ( $MD$ ), then transition is declared on the last of these  $MD$  days.

$LC$  and  $MD$  are determined by the typical time scale associated with these rain events. Rainfall observations suggest that the time scale for this period is  $\sim 5$  days, the typical time scale for dry and wet spells [Kulkarni et al., 2006]. Thus, we set the minimum number of days for both

$LC$  and  $MD$  to 5. It is worth mentioning here that  $MD$  is not equated to one so as to prevent an isolated rain event from determining the transition. Such an isolated event can, however, change the hydrological characteristics of the cell if the rainfall associated with this event exceeds some threshold. Hence, if the rainfall on some day during Regime  $B$  exceeds 150 mm, transition  $BC$  is assumed to take place five days after this event. Thus, two conditions constitute the criterion for  $BC$ , but only one of these two conditions has to be fulfilled for the transition to take place (Table 5.3).

The third transition,  $CD$ , is opposite to  $BC$ . The CR curve plateaus off, resulting in another sharp inflection, but now in the opposite direction, i. e., the inflection is concave-down (Figure 5.4). Regime  $C$  is assumed to last at least 60 days. This is a reasonable time-period since the core of the summer monsoon lasts through July and August. The procedure to detect  $CD$  remains similar, but opposite to that used for  $BC$ . In other words, if  $IC$  is less than zero for  $MD$  consecutive days and rainfall is less than or equal to 5 mm for a day, then transition  $CD$  is deemed to occur. As done for transition  $BC$ ,  $MD$  was set to 5 for  $CD$ . The second condition, that rainfall is less than or equal to 5 mm for a day, is needed to ensure that the transition does not take place during a rainfall burst, even if it is a weak event (Table 5.3).

Once Regime  $D$  sets in, the CR curve is too flat to be used as a criterion to determine Transition  $DE$  (Figure 5.4). Hence, the following two conditions constitute the  $DE$  criteria. First, the 5-day antecedent rainfall has to be less than 30 mm for five consecutive days. Once the first condition is fulfilled, then the rainfall has to be less than 5 mm for 15 consecutive days for Transition  $DE$  to occur. Once the first condition is fulfilled, if the rainfall exceeds 5 mm after (say) 10 days, then only the second condition is used again: the first condition is applied only once, but the second is used more than once, if necessary, to determine the transition (Table 5.3).

The transition to the lean-period regime,  $EA$ , is deemed to occur if the daily rainfall is equal to or less than the trace rainfall (1 mm) for 30 consecutive days. Transition  $EA$  occurs in December, and from January, the next year's CR is computed (CR is reset to 0 on 1 January) and the process

is repeated.

### 5.3.5 Estimation of the SCS parameters

The SCS parameters have to be estimated for each regime for each of the four regions. The AMC thresholds were determined the same way as done for  $S1$  and  $S2$  (Figures 4.7 and 5.2):  $1/e$  ( $\sim 36\%$ ) of the days in a regime had rainfall above the lower threshold and  $1/e^2$  ( $\sim 14\%$ ) of the days had rainfall over the higher threshold;  $\sim 22\%$  of the days experienced the “average” rainfall. The AMC thresholds are listed in Table 5.4.

The exceptions to this rule were Regimes  $B$  and  $C$ . During Regime  $C$ , the Peak-Monsoon Regime, it rains on most days and the soil is wet and saturated. Therefore, the discharge curve follows closely the rainfall curve (Figure 4.1), and almost all the rain is expected to run off on most days even if the rainfall is relatively low. Hence, the thresholds for Regime  $C$  (Table 5.4) were determined using an inversion of the exponential cut-offs used earlier. We assumed that only  $1/e^2$  ( $\sim 14\%$ ) of the days were dry, or had rainfall below the lower threshold ( $CN(I)$ ), and  $1/e$  ( $\sim 36\%$ ) of the days were wet, or had rainfall below the higher threshold. Thus,  $\sim 22\%$  of the days had average rainfall ( $CN(II)$ ) and  $\sim 64\%$  of the days had rainfall over the higher threshold ( $CN(III)$ ).

During Regime  $B$  (onset of monsoon), the discharge does not correspond to the rainfall curve. Since it needs to rain more for the rain water to run off during this regime, we assumed that  $1/e^2$  ( $\sim 14\%$ ) of the days had rainfall over the lower threshold and  $1/e^3$  ( $\sim 5\%$ ) of the days had rainfall over the upper threshold. Thus,  $\sim 9\%$  of the days in this regime experienced average rainfall,  $5\%$  heavy rainfall, and  $\sim 86\%$  low rainfall; hence, most days in this regime were set to  $CN(I)$ .

Just as the AMC thresholds show considerable variation with season, so must  $CN$  and  $\lambda$ . We used the “mean conditions” to define the average basin  $CN(II)$  and used this  $CN(II)$  to estimate the dry-period and wet-period  $CN(II)$ . The average conditions are represented for the Mandovi by Regime  $E$ , the post-monsoon season, when the soil is still moist but unsaturated.

Hence, the average  $CN(II)$  used for the four regions were applied to this regime. We used this  $CN(II)$  and Equation (4.8a) to estimate the dry-period  $CN(II)$ , which was applied to Regime *B*, the monsoon-onset phase, and used it and Equation (4.8b) to estimate the wet-period  $CN(II)$ , which was applied to Regime *D*, the end-monsoon phase. Regime *A* is even drier and represents an extreme case in which there is little spatial variation in the basin's hydrological characteristics: hence, the lowest  $CN(II)$  value (40) noted in the literature [Mishra and Singh, 2003] was applied to all regions in this regime. There is less spatial variation during the extremely wet and extremely dry periods in comparison to the moderately wet periods. Regime *C* is also an extreme case and almost all the rainfall is converted to surface runoff because the soil is completely saturated. Hence, for this regime, we set the  $CN(II)$  for all four regions to 90. Empirical estimates of  $CN(II)$  for Indian watersheds spanning a range of hydrological regimes suggest that a high value is appropriate during rainfall events [Mishra and Singh, 2003]. The  $CN(II)$  values we use are comparable to, but less than, the ones reported by Mishra and Singh [2003] because their estimates were based on very few events.

Thus,  $CN(II)$  varies in both space and time. The spatial variation for selected days during each regime is shown in Figure 5.5 and the temporal variation at the four locations marked in Figure 5.1 is shown in Figure 5.6.

Shankar et al. [2004] and Suprit and Shankar [2008] also noted that another variable that might require parameterisation is the residence time for the subsurface-runoff reservoir ( $T_D$  in Figure 2.2). Their conjecture was that the residence time was likely to vary in space and time, just as  $\alpha$  seems to do. Simulations show, however, that the small baseflow in the Mandovi basin implies a minor role for  $T_D$  in the water balance. Hence, for all the simulations, we keep  $T_D$  constant (15 days).

**Figure 5.5** Variation of  $CN$  in the basin on selected days during each temporal regime in 1992 . Regimes *A* (top left), *B* (top right), *C* ((middle left), *D* (middle right), *E* (bottom left) and back to regime *A* (bottom right). Note that the scales are different .

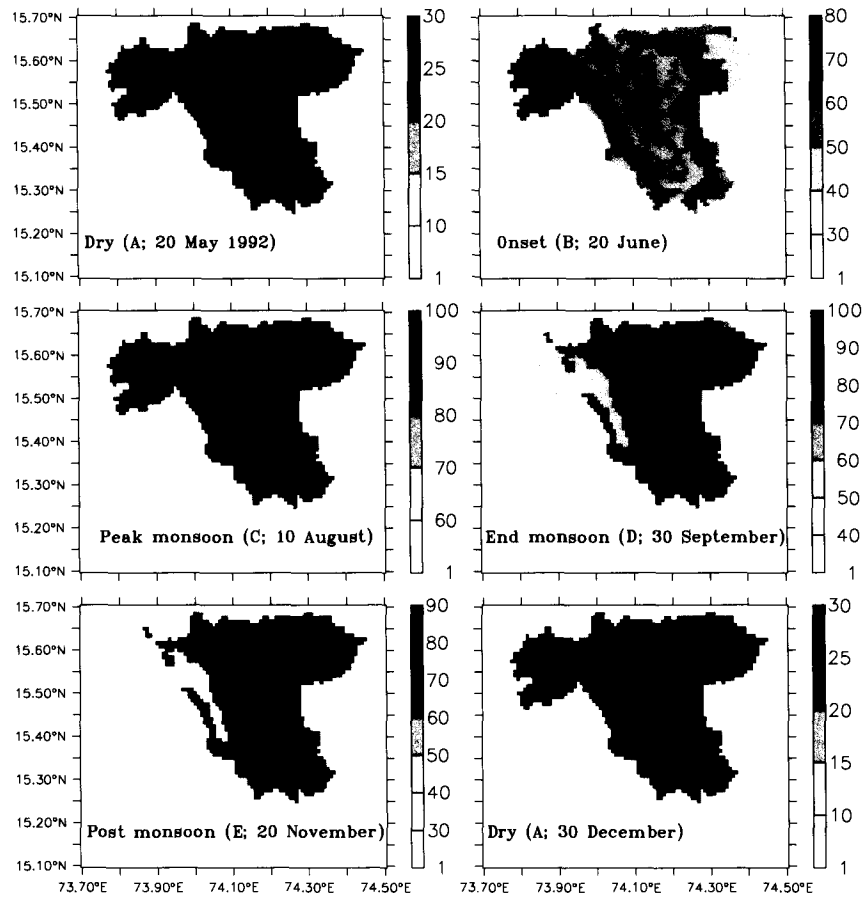
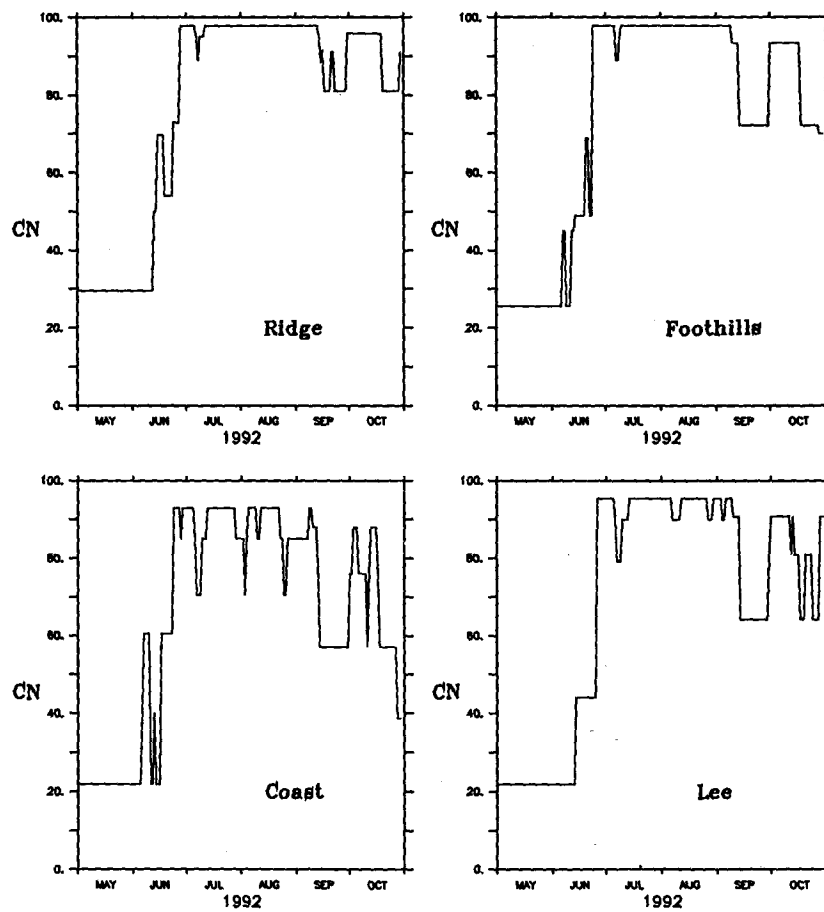


Figure 5.6 Variation of CN in time for the four regions. The locations are marked by the filled triangles in Figure 5.1.





## 5.4 Results and discussion

### 5.4.1 Simulation *S3*

Simulation *S3* was made using the spatio-temporally varying parameters listed in Table 5.4. The results (Figure 5.7) show a significant improvement over Simulation *S2* (and Simulations *S0* and *S1*; Figure 5.8). The simulated discharge matches the observed discharge better across a range of conditions. Specifically, the simulated discharge increases during the rainfall bursts in July, August, and September, resulting in a better match with observations. The increase in discharge, however, is also seen during the weak spells in early July, when Simulation *S3* performs worse than Simulation *S2*. The sharp increase in *CN* with Transition *BC* increases the discharge even during the weak spells. It also leads to an erroneous increase in the discharge during the second rainfall burst at the time of transition: the lower *CN* in Simulation *S2* leads to the simulated discharge being closer to that observed. The results for the other two years, 1986 and 1990, are similar (Figure 5.7).

The correlation for Simulation *S3* is comparable to that for Simulation *S2* (Table 5.5). Error histograms for Simulations *S1*, *S2*, and *S3* show that the major improvement in *S3* is the lack of underestimation of discharge (Figure 5.9). Though Simulation *S3* has a greater tendency to overestimate the discharge during June–August, there is an overall improvement. Figure 5.8 shows that Simulation *S3* is much better than *S0*, *S1*, and *S2*. It captures the variability better over the range of temporal hydrological regimes.

### 5.4.2 Evapotranspiration and abstraction

The initial abstraction represents the minimum amount of rainfall required to generate surface runoff. It is the only loss term in the model and represents the water lost to the atmosphere owing to evaporation and transpiration (evapotranspiration). In the model, this abstraction is a function of the initial abstraction coefficient ( $\lambda$ ) and Curve Number (*CN*); the *CN*, in turn, depends on the

**Table 5.4** SCS parameters for Simulation S3 (spatial and temporal variation). The numbers in parentheses in the first column represent the parameter choices for Simulation S2; these parameters are used for Regime E. The  $CN(II)$  for Regime B is computed using Equation (4.8a) and the  $CN(II)$  for Regime E, and the  $CN(II)$  for Regime D is computed using Equation (4.8b) and the  $CN(II)$  for Regime E. Regime E therefore represents the average or central hydrologic regime, Regimes B and D the dry and wet regimes, and Regimes A and C the extremely dry and wet regimes.

	Lean period (A) Very dry	Onset Monsoon (B) Wet (Unsaturated)	Peak Monsoon (C) Very wet	End Monsoon (D) Wet (Saturated)	Post Monsoon (E) Moist (Unsaturated)
<b>Region</b>	<b>Curve Number <math>CN</math></b>				
<i>Lee</i> (65)	40	44	90	81	65
<i>Ridge</i> (75)	40	56	90	87	75
<i>Foothills</i> (70)	40	49	90	84	70
<i>Coast</i> (60)	40	40	90	78	60
<b>Region</b>	<b>Initial abstraction coefficient (<math>\lambda</math>)</b>				
<i>Lee</i> (0.3)	0.3	0.2	0.05	0.2	0.3
<i>Ridge</i> (0.05)	0.3	0.2	0.05	0.05	0.2
<i>Foothills</i> (0.1)	0.3	0.2	0.05	0.05	0.2
<i>Coast</i> (0.3)	0.3	0.2	0.05	0.2	0.3
<b>Region</b>	<b>AMC (5-day antecedent rainfall range in mm)</b>				
<i>Lee</i> (100–200)	30–40	200–250	50–100	20–40	5–20
<i>Ridge</i> (150–400)	40–70	300–450	100–200	30–60	5–20
<i>Foothills</i> (100–250)	50–70	350–450	50–100	20–50	5–20
<i>Coast</i> (100–200)	50–60	400–450	50–100	20–50	5–20

**Figure 5.7** Daily observed discharge (black), discharge simulated by Simulation S3 (red), and the catchment-integrated rainfall (blue) at Ganjem for May–October for three validation years. (A) 1986. (B) 1992. (C) 1990. The units are  $\text{Mm}^3/\text{day}$ . The bold tick marks on the abscissa indicate beginning and end of a month.

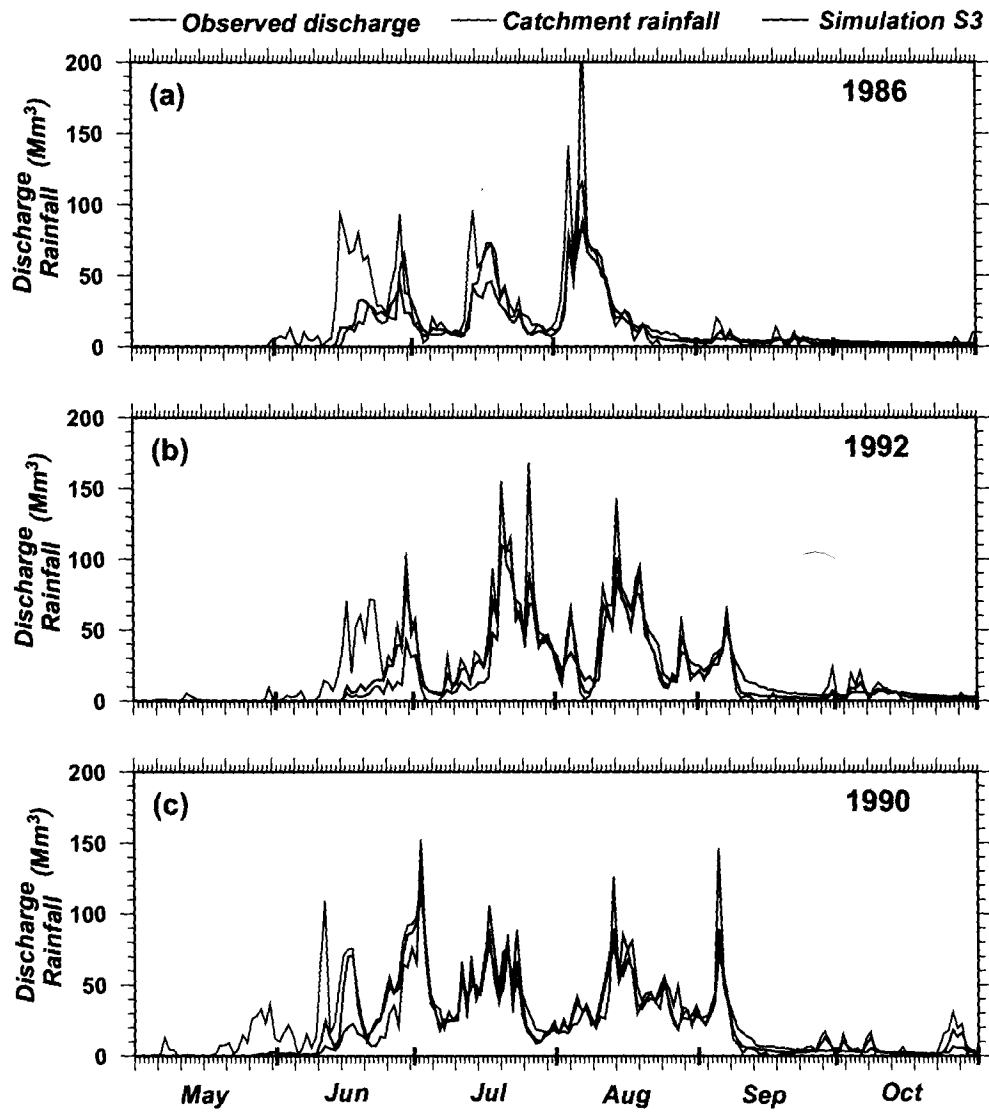
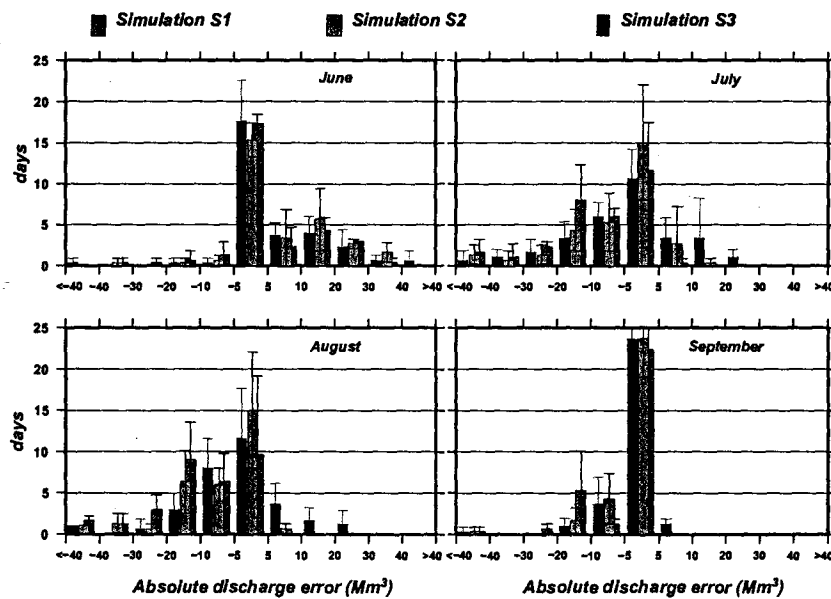


**Table 5.5** A brief description of the simulations and their results (Figure 5.8). The last column lists the square of the correlation between the simulated and observed discharge over the period May–October. The first number is the correlation for the three years (1986, 1990, and 1992) used to calibrate the model; the second number (in parentheses) is for the other 15 years (model validation). The major improvement occurs with the inclusion of the SCS method in Simulation *S1*. The other refinements — spatial and temporal variation of the parameters — result in improvements over a part of the simulation, but the overall May–October correlation does not improve any more.

Simulation	Detail	Parameters	Simulated discharge	$r^2$
<i>S0</i>	Only THMB (No SCS)	$\alpha = 0.3$	Figure 4.2	0.68 (0.67)
<i>S1</i>	THMB+SCS simulation (constant parameters)	$CN(II)$ (70) $\lambda$ (0.2) AMC (100–250 mm)	Figure 4.8	0.78 (0.76)
<i>S2</i>	THMB+SCS simulation (spatially varying parameters)	Table 5.1	Figure 5.3	0.78 (0.77)
<i>S3</i>	THMB+SCS simulation (spatio-temporal varying parameters)	Table 5.4	Figure 5.7	0.79 (0.80)

**Figure 5.9** Absolute error histograms showing the difference between simulated and observed discharge ( $Mm^3$ ) for the Simulations *S1*, *S2* and *S3*. Histograms are drawn for the three calibrations year 1986, 1992, and 1990 during the summer monsoon (June–September). The ordinate shows number of days averaged over three years. The vertical lines indicate the standard deviation.



average-condition  $CN$  ( $CN(II)$ ) and the AMC thresholds.

The simulations suggest high abstraction during the monsoon-onset regime ( $B$ ) (Figure 5.10). Abstraction decreases sharply following monsoon onset and increases again slightly after the monsoon. It is low in the dry season because the limiting factor then is the availability of moisture. It is shown by Shankar et al. [2004] and Suprit and Shankar [2008] in their annual simulation that evapotranspiration is very small compared to rainfall. Therefore, in the Mandovi basin, the net fractional abstraction during the year is low because the abstraction is negligible when the rainfall peaks. It is only during the onset phase that the fraction of rainfall abstracted ( $\sim 68\%$  over the 18 years for June) matches the high values suggested for India by some recent studies [Jain et al., 2007; Narasimhan, 2008]. Similar profiles have been estimated for evapotranspiration using the Penman method for some west-coast cities [Krishna Kumar et al., 1987] and for reference (or potential) evapotranspiration using satellite data for the Krishna basin (Musi River) [Bouwer et al., 2008]. It is also evident from the simulations that large-scale data sets like those based on the NCEP-NCAR (National Center for Environmental Prediction/National Center for Atmospheric Research) Reanalyses [Kalnay et al., 1996] considerably underestimate the abstraction (Figure 5.10).

### 5.4.3 Discussion

We built the model parameterisation using data for only three of the 18 years (Figure 4.4) for which rainfall and discharge data are available. Validation of the model is done using the data for the other 15 years. The error histogram for these 15 years (Figure 5.11) is similar to that for the three years (Figure 5.11). The results of Simulation  $S3$  for all the 15 other years are shown in Figure 5.12. The model parameterisation works as well for the entire data set as it does for the three calibration years (Table 5.5). Indeed, the strength of Simulation  $S3$  lies in its ability to simulate the discharge better across the spectrum of variability from the seasonal to the inter-annual (Figure 5.13). The simpler 5-day AMC parameterisation fails to account for this spectrum

of variability not only over a season, but also across years.

Nevertheless, there is a tendency to overestimate the discharge at some times in some years. In 1990 and 1995 (Figures 5.7 and 5.12), Transition *BC* occurs a little earlier than it probably should, the peak-monsoon regime sets in early, and the simulated discharge is higher at the beginning of Regime *C*. In 1992 and 1998 (Figures 5.7 and 5.12), there is a long break during the peak-monsoon season and the soil probably becomes unsaturated; hence, the discharge is overestimated. Other than these discrepancies, the model performance is remarkable, and the simulated discharge correlates well with the observed discharge across all the regimes (Table 5.5). Note that the major improvement in the correlation (Table 5.5) was achieved by incorporating the SCS method, i. e., the correlation increased significantly from Simulation *S0* to *S1*, but there was not much change in correlation from Simulation *S1* to Simulation *S3*. The improvement brought about by incorporating the spatio-temporal variation is more subtle: the temporal variation helps improve the discharge simulation across *all* temporal regimes, and though it is not possible to verify it, the spatial variation probably helps improve the simulation across *all* regions.

In summary, even for a small basin like the Mandovi, the variations in space and time are significant enough for them to be incorporated in the rainfall-runoff model. Since the Mandovi is a typical west-coast river, our framework has major implications for the hydrology of other west-coast rivers. A discussion on the strengths and caveats of the framework, and of its applicability to other west-coast rivers is the topic of the next chapter.

**Figure 5.10** Abstraction (blue curve) during May–October in Simulation *S3*. The observed discharge (black curve) and the evapotranspiration from the NCEP-NCAR Reanalysis (red curve) are also plotted. The units are  $\text{Mm}^3$ . The bold tick marks on the abscissa indicate beginning and end of a month. (a) 1992. (b) 1986. (c) 1990.

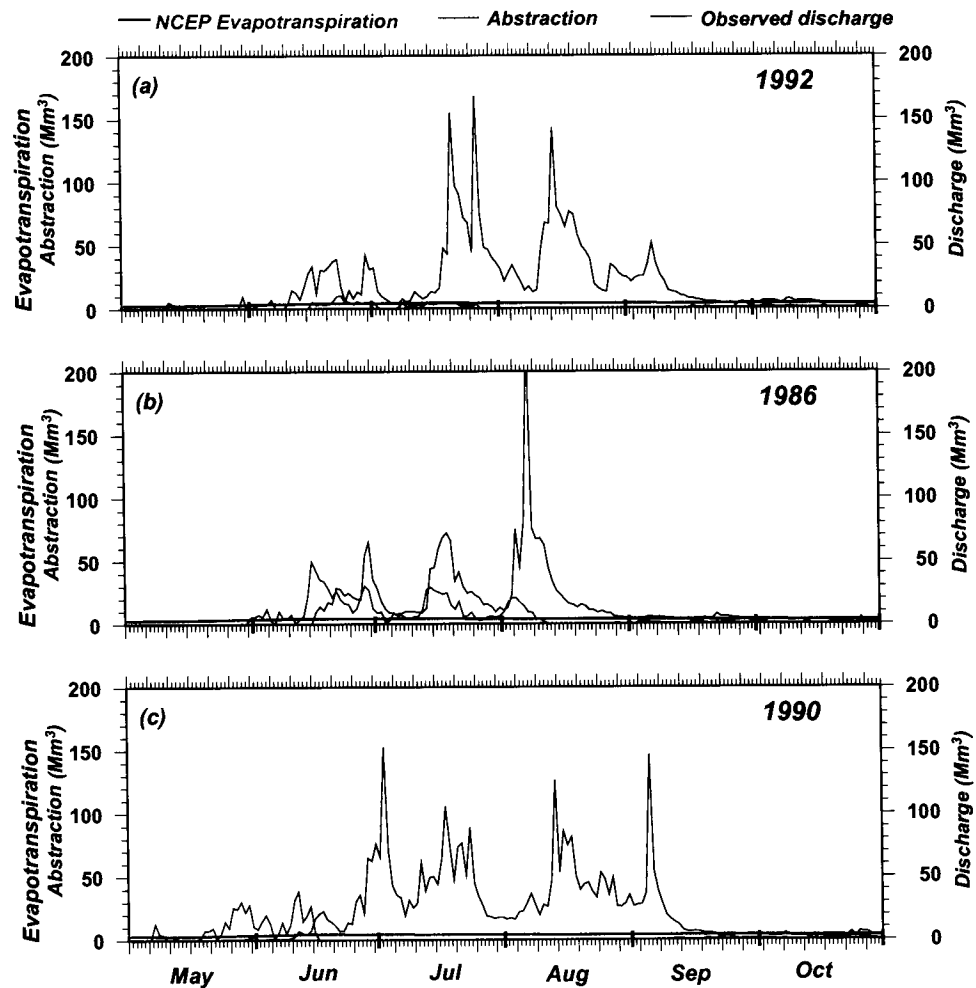




**Figure 5.11** Absolute error histograms showing the difference between simulated and observed discharge ( $Mm^3$ ) for the Simulations *S1*, *S2* and *S3*. Histograms are drawn for the 15 validation years (1981–1998 excluding years 1986, 1992, and 1990) during the summer monsoon (June–September). The ordinate shows number of days averaged over 15 years. The vertical lines indicate the standard deviation.

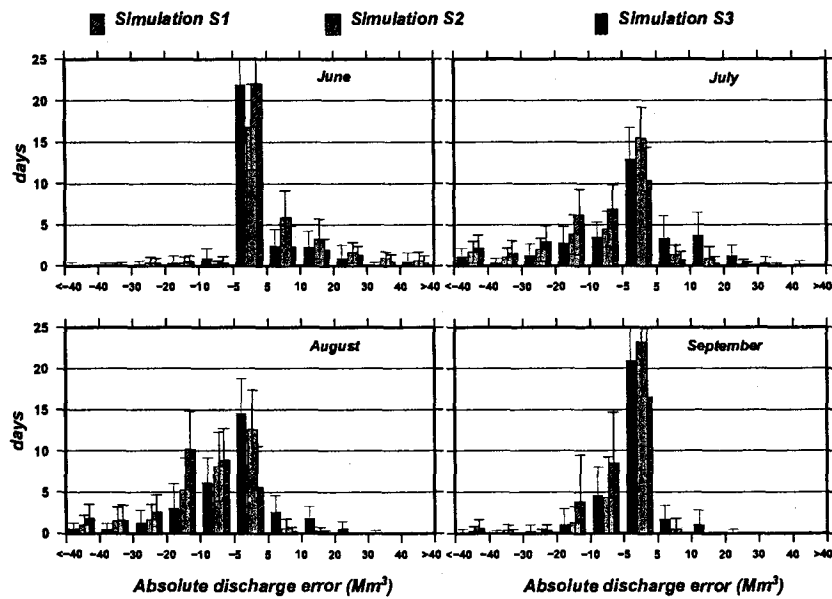


**Figure 5.12** Daily observed discharge (black), discharge simulated by Simulation *S3* (red), and the catchment-integrated rainfall at Ganjem (blue) for May–October (a) 1981, (b) 1982, (c) 1983, and (d) 1984. The units are  $\text{Mm}^3$ . The bold tick marks on the abscissa indicate beginning and end of a month.

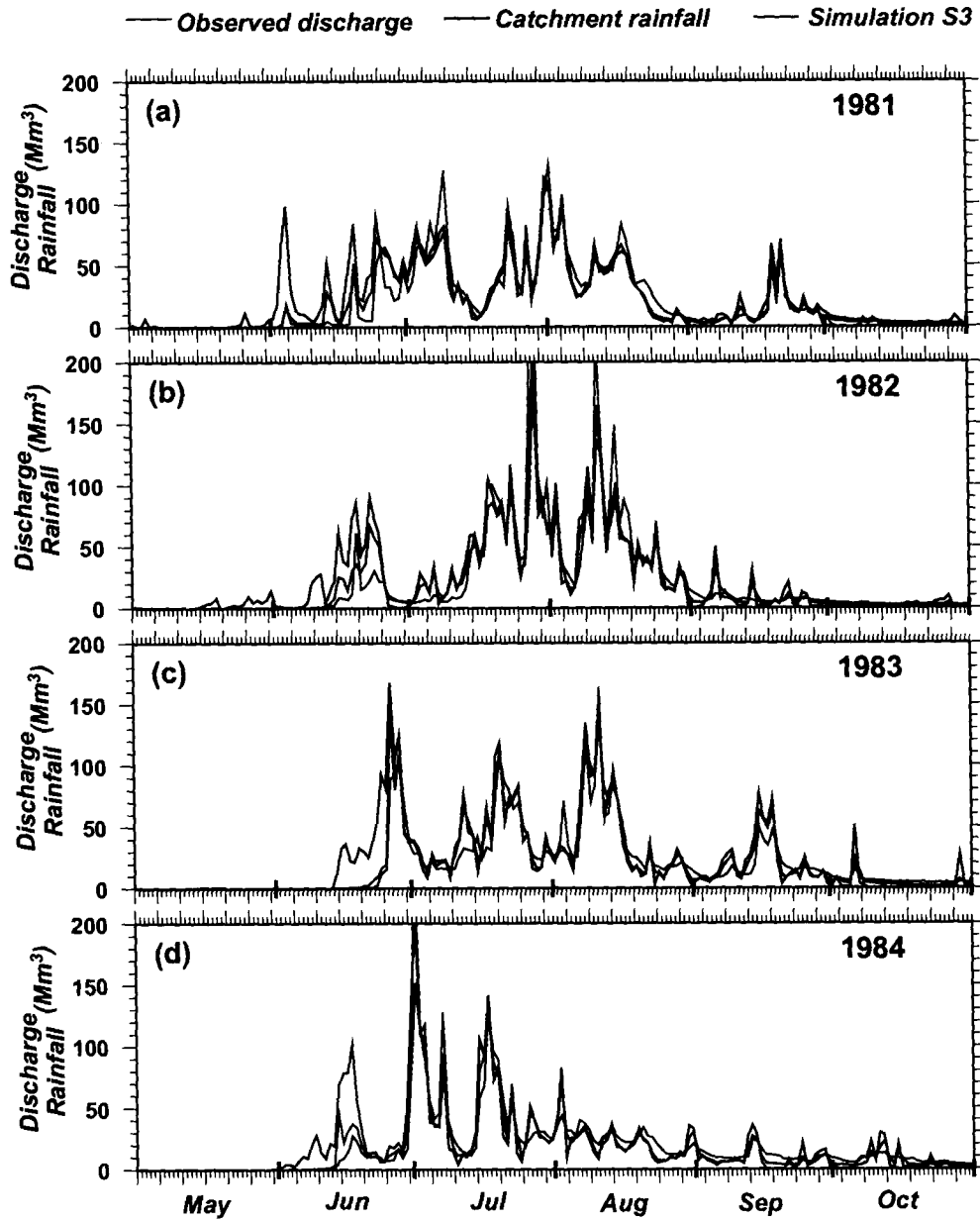


**Figure 5.12** (continued) Daily observed discharge (black), discharge simulated by Simulation *S3* (red), and the catchment-integrated rainfall at Ganjem (blue) for May–October (a) 1985, (b) 1987, (c) 1988, and (d) 1989. The units are  $\text{Mm}^3$ . The bold tick marks on the abscissa indicate beginning and end of a month.

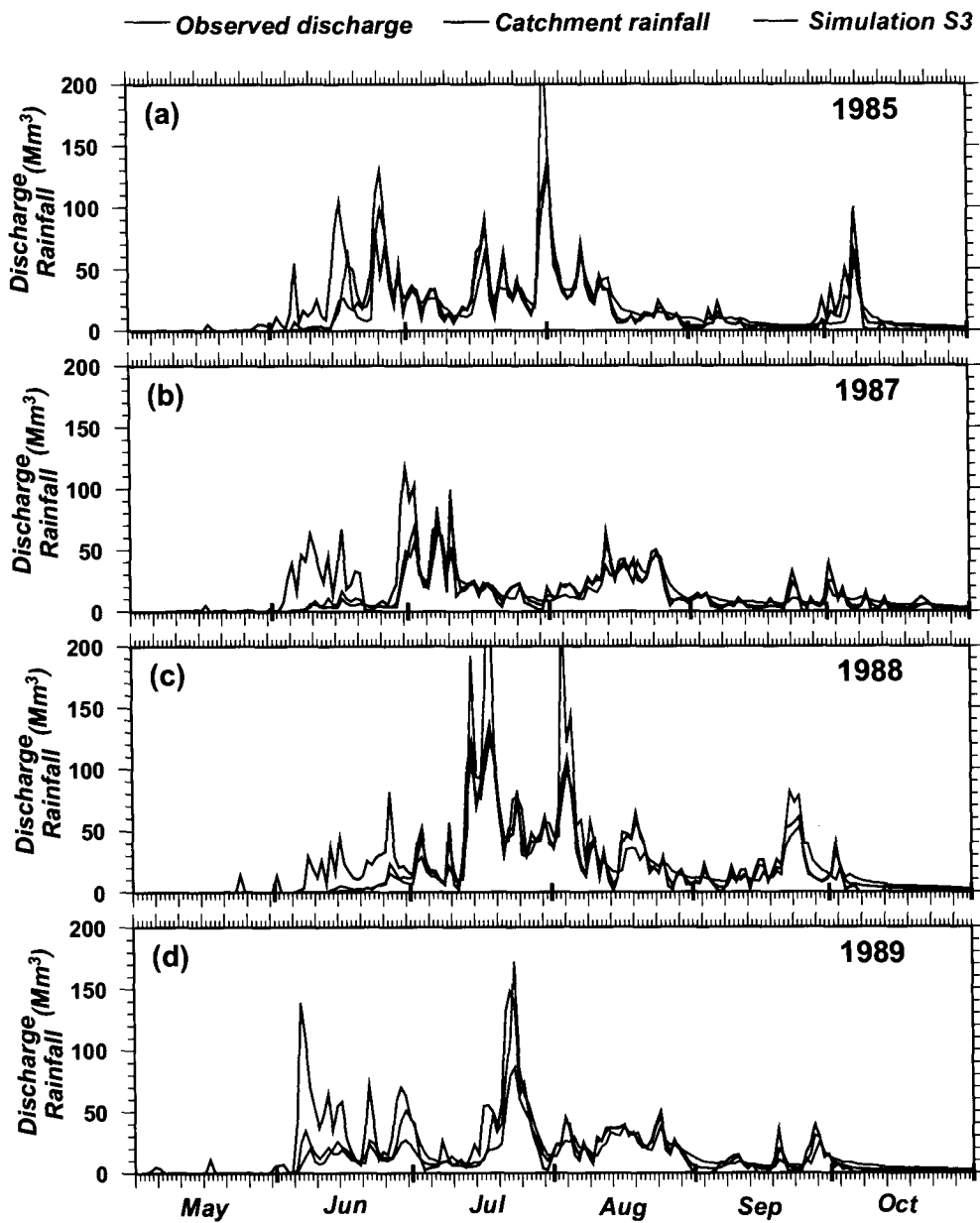


**Figure 5.12** (continued) Daily observed discharge (black), discharge simulated by Simulation S3 (red), and the catchment-integrated rainfall at Ganjem (blue) for May–October (a) 1991, (b) 1993, (c) 1994, and (d) 1995. The units are  $\text{Mm}^3$ . The bold tick marks on the abscissa indicate beginning and end of a month.

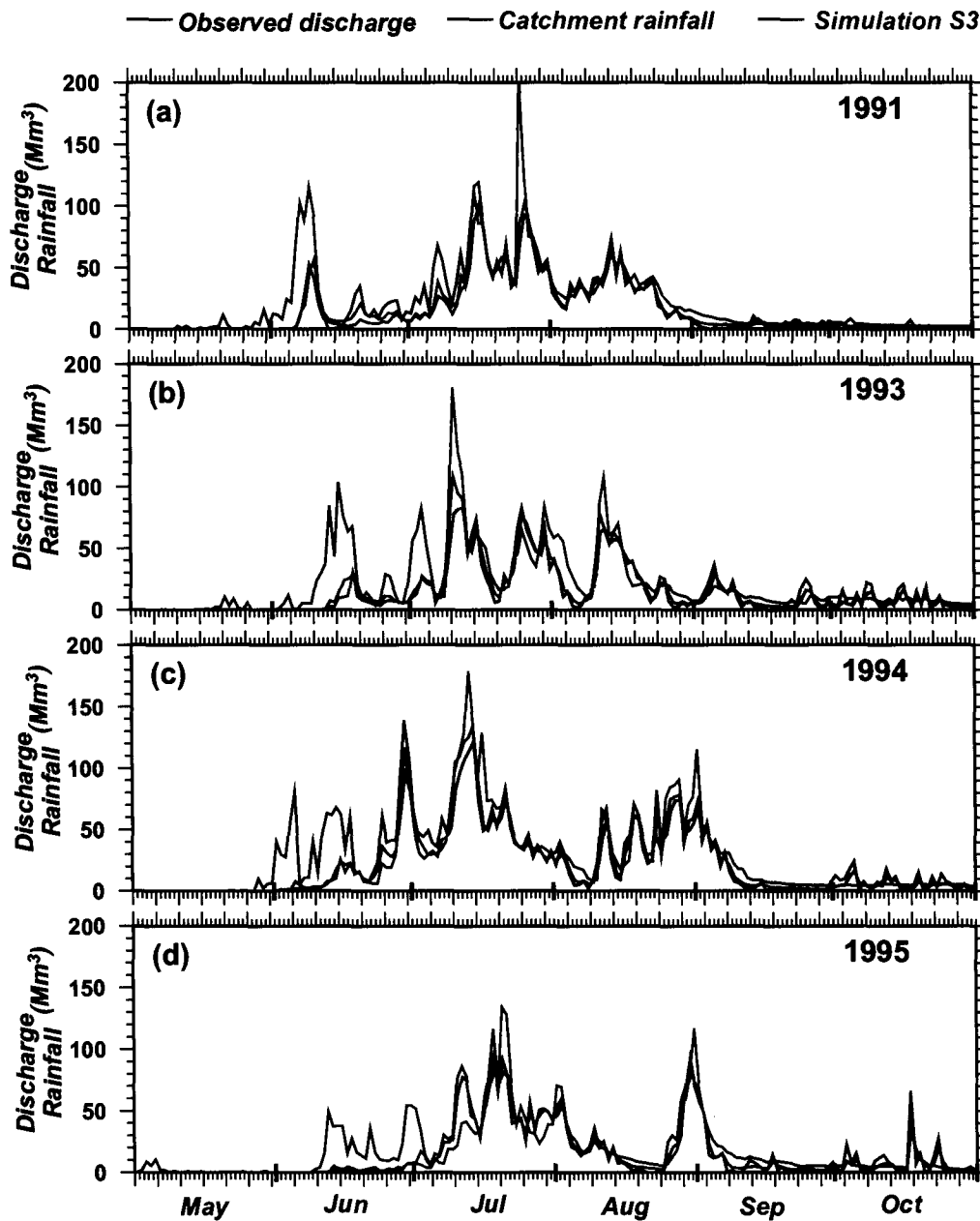


**Figure 5.12 (continued)** Daily observed discharge (black), discharge simulated by Simulation S3 (red), and the catchment-integrated rainfall at Ganjem (blue) for May–October (a) 1996, (b) 1997, and (c) 1998. The units are  $\text{Mm}^3$ . The bold tick marks on the abscissa indicate beginning and end of a month.

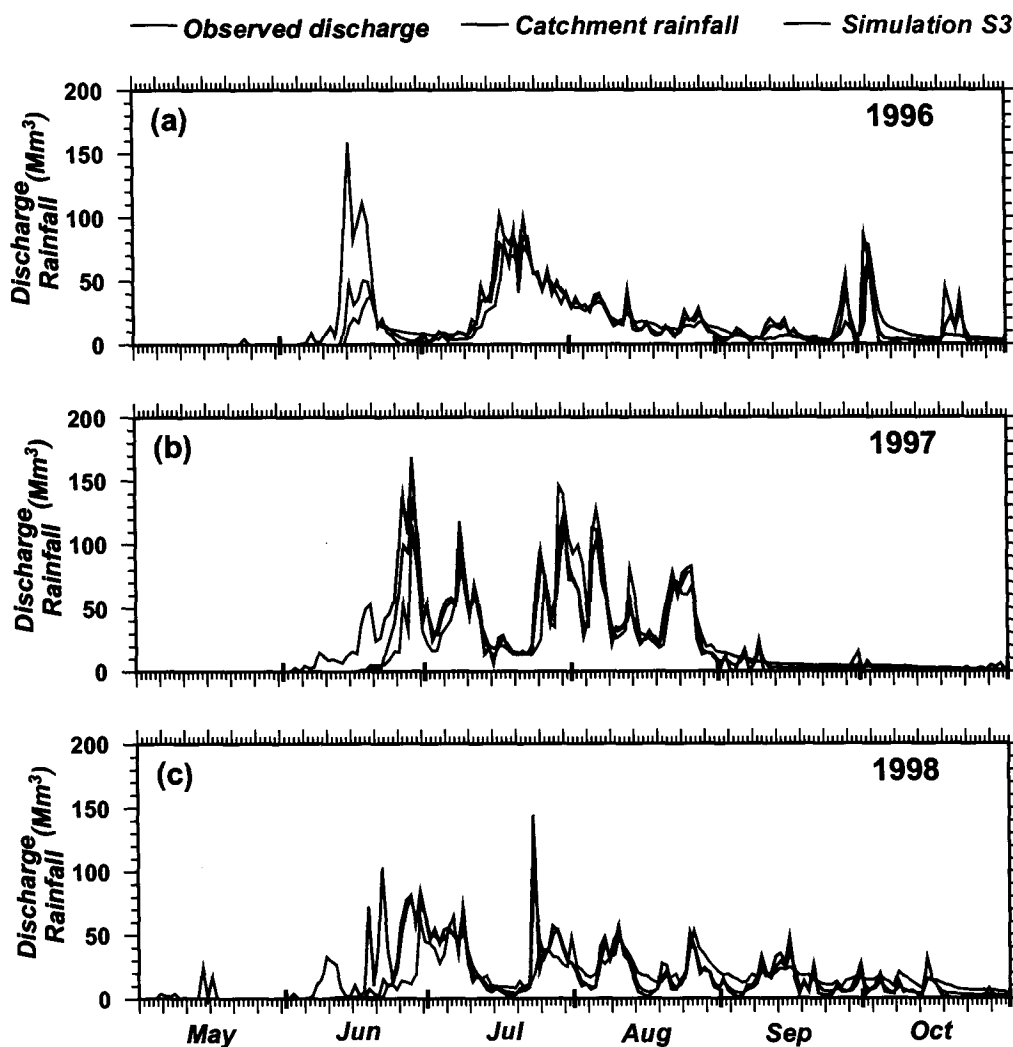
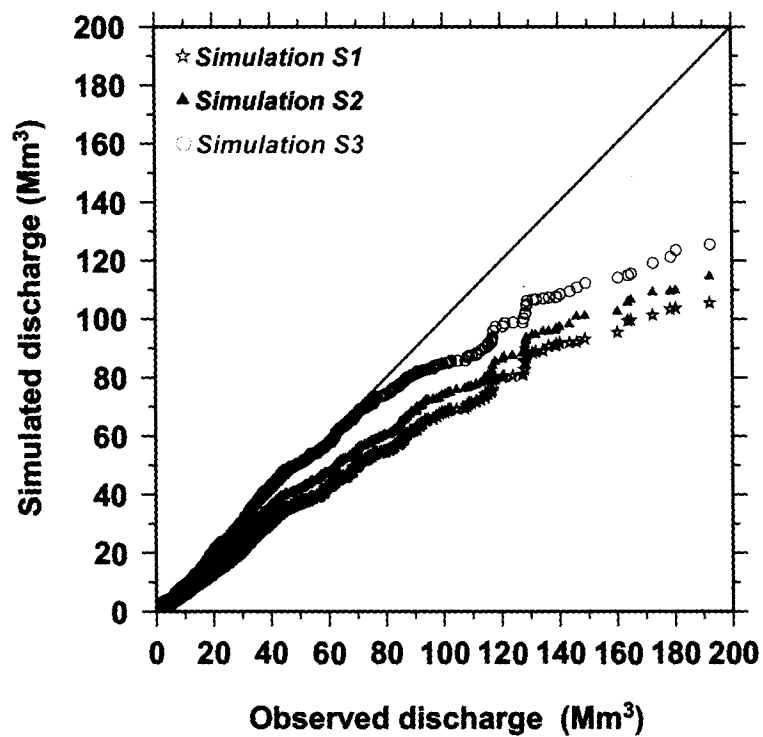


**Figure 5.13** Correspondence plot between the daily observed discharge (abscissa;  $\text{Mm}^3$ ) and simulated discharge (ordinate;  $\text{Mm}^3$ ) for June–September for the 15 validation years. Simulation *S3* (red hollow circles) performs much better than Simulations *S1* (hollow blue stars) and *S2* (filled black triangles). The maximum daily observed discharge is  $406.5 \text{ Mm}^3$ , but we have truncated the abscissa to  $200 \text{ Mm}^3$ . Only seven data points were discarded over the 15 years (1830 days): discharge is in the range  $200\text{--}250 \text{ Mm}^3$  on four days, in the range  $250\text{--}300 \text{ Mm}^3$  on two days, and is  $406.5 \text{ Mm}^3$  on one day. The underestimation seen in the simulations occurs mostly during July–August, and arises owing to the underestimation of peak rainfall events in the basin.



## Chapter 6

# Implications of the modelling framework

### 6.1 Introduction

The modelling framework developed in the preceding chapters has major implications for the hydrology of the Indian subcontinent. There is a dearth of information on the hydrological variables in the country [Shankar et al., 2004]. Apart from a fairly consistent and long-term data set on rainfall, data on other hydrological variables is non-existent: river discharge is another variable for which some data is available. Only a few of the rivers have sufficient data length; data for the rest of the rivers is available only for the short term. Most of this data is scanty and not easily available. The number of stream gauges is declining world over [Radhakrishna, 2003]. The situation is worse for other hydrological variables like evapotranspiration [Rao et al., 1971; Rao, 2001; Narasimhan, 2008; Maréchal et al., 2009], soil moisture, infiltration rate, for which data on the catchment scale is non-existent. A much bigger problem, though, is the dearth of modelling studies or quantitative frameworks. The focus of modelling studies in the country is limited to small catchment scales for managing hydrological projects, or to solve very specific problems using complex hydrologi-

cal models. There is also a spate of work on climate-change scenarios and their related feedback systems on the hydrology of the country. Hydrological simulation studies on the catchment (or larger) scale are not readily available: discharge simulations on daily scale are much rarer. Most of the information on hydrology in the country is available on either very small scale or based on some gross statistics over a region (state level) [Shankar et al., 2004; Rao, 1975; Jain et al., 2007]. This is despite the fact that freshwater (river discharge) is crucial for climate and water resources.

Shankar et al. [2004] realised and addressed this problem: they initiated the building of a hydrological framework consistent with the realities of the data availability of the country. They proposed that any framework should follow these four basic guiding principles.

1. The framework should include a simple hydrological model that can provide a reliable water balance of a river system.
2. Demands on the database required by the model should be consistent with the realities of the country.
3. The packages that incorporate the model should be able to handle a range of spatial scales, from small rivers to continental scales, to enable many groups working independently on different river basins, to dovetail their analyses into a coherent picture on the larger scale.
4. The models and their ancillary software should be freely accessible.

Hence, while developing our modelling framework, we have kept these guidelines in mind. Instead of going for a complex procedure with a very specific application, we have opted for a more simple approach, with a view to make it applicable in the general scenario.

## 6.2 Generality of framework: West-coast rivers

The modelling framework was tested for the Mandovi river. Simulations showed that the framework was able to simulate daily discharges for the Mandovi river basin remarkably well. There



were three reasons for choosing the Mandovi river for model-building. First, the Mandovi is typical of the westward flowing west-coast rivers; if the framework works here, it is expected to work elsewhere on the west coast also. Second, both the rainfall and discharge data were available for it, allowing us to build the parameterisation by validating discharge simulations with the observation. Third, it is the largest and the most important river of Goa (flowing near the National Institute of Oceanography in Panaji).

The most critical assumption is that the Mandovi is a river typical of the west coast. Successful application of our method to other west-coast rivers is contingent on the validity of this statement. We have selected two more rivers for which we had observed discharge data: Ulhas river to the north of Mandovi and Aghanashini river to the south (Figure 6.1). Combined with Mandovi, the three rivers cover a considerable fraction of the west coast, enabling us to examine the variability along the coast. A plot of the observed discharge (normalised for comparison) of these three rivers suggests (Figure 6.2) that the discharge patterns are comparable across most of the coast: the inter-river variability is no more than the interannual variability for any river. A similar result is obtained by performing a Kolmogorov-Smirnov test on the discharge data: the inter-river spread in the curves is comparable to the interannual spread for a river (Figure 6.3), suggesting that this method should work for the other rivers.

### 6.2.1 Annual variability and spatial variability

The rivers (on the west coast) for which the parameterisation is likely to require modification are the ones in Kerala because it experiences rain during the winter monsoon too, the longer west-coast rivers like the Narmada and the Tapti because their basins encompass a wider spectrum of hydrological regions, and the dry-region rivers like the Mahi ([Ramakrishnan et al., 2009]) and the Sabarmati.

**Figure 6.1** The location of discharge gauges for the Ulhas (blue, discharge gauge at Badlapur) Mandovi (black, Ganjem), and Aghanashini (red, Santeguli). The three rivers cover a large fraction of the Indian west coast. The catchment area of the Mandovi, Aghanashini and Ulhas are 872 km<sup>2</sup>, 1070 km<sup>2</sup>, and 785 km<sup>2</sup> respectively, at the location of the discharge gauge.

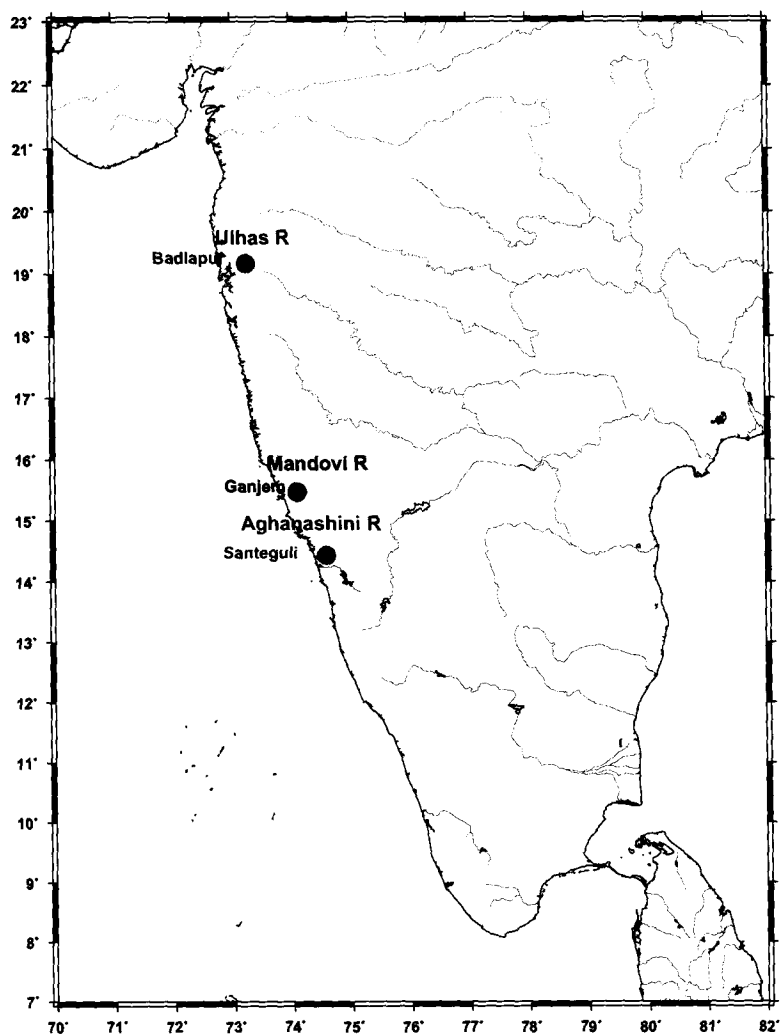
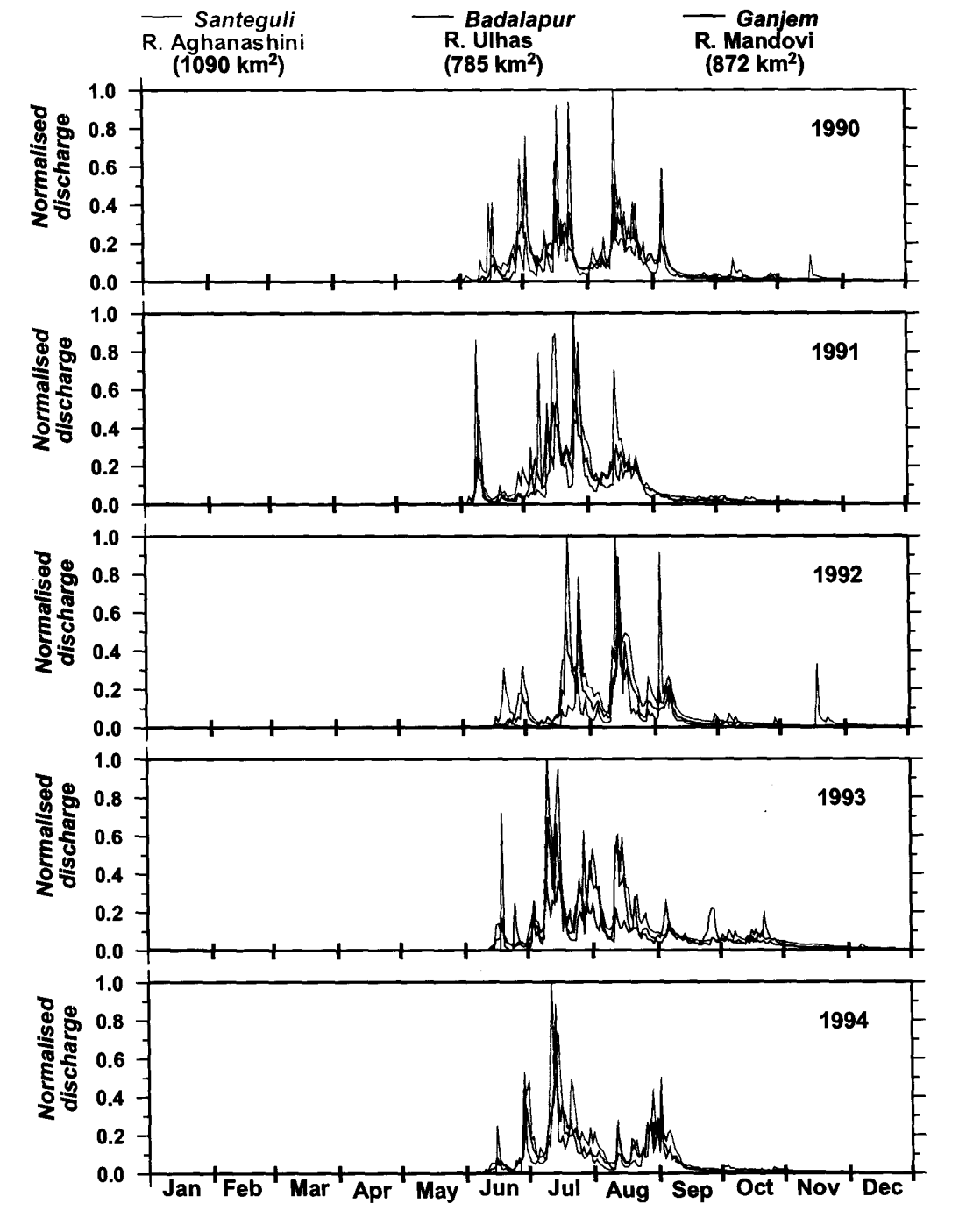
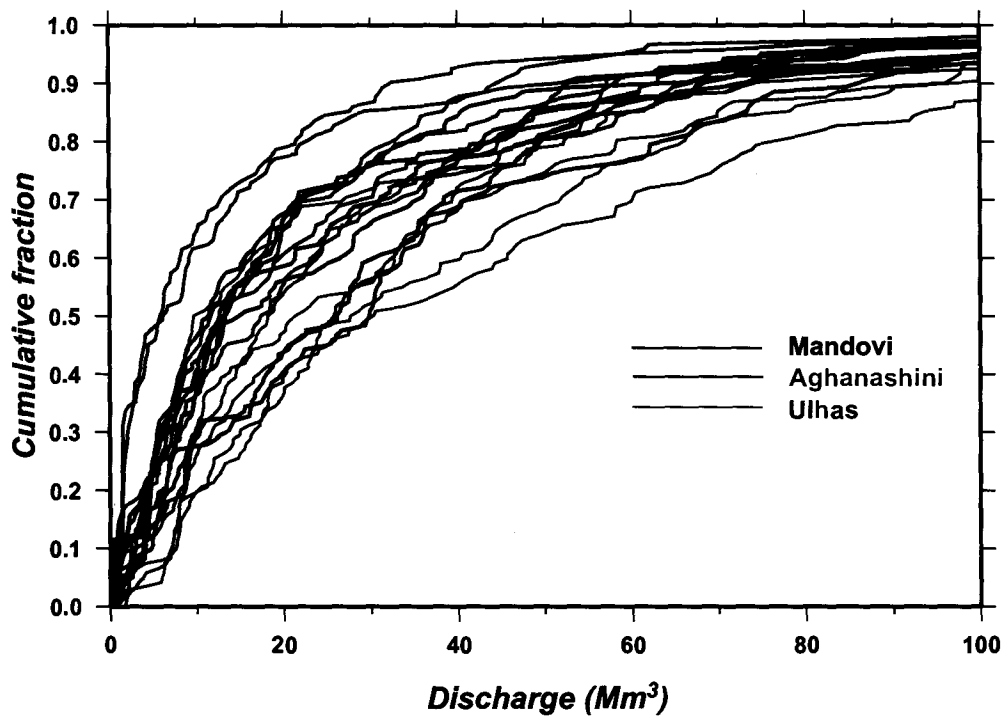


Figure 6.2 Daily normalised discharge for 1990–1994 for three west-coast rivers (Figure 6.1). The discharges are normalised by the highest daily discharge among any of the rivers occurring in the particular year. The rivers are Ulhas (blue), Mandovi (black), and Aghanashini (red).



**Figure 6.3** Kolmogorov-Smirnov diagram showing the cumulative distribution plot for daily discharge during June–September for 1990–1995 for the Ulhas (blue), Mandovi (black), and Aghanashini (red) rivers.



### 6.3 Assessment of the framework and future directions

#### 6.3.1 Caveats of the modelling framework

The modelling framework simulates the daily discharges for Mandovi river across the whole range of seasonal variability. This was achieved by improving the SCS parameterisation. Obtained using limited data, this parameterisation needs further improvement. One notable drawback is the need to specify a minimum duration ( $MD$ ) of 60 days for the peak-monsoon regime. This specification was necessitated by the need to preclude a prolonged weak spell or break, triggering a transition to the post-monsoon regime. Would such a constraint be valid in a year as exceptional as 2002, which saw one of the worst droughts on record, with the July rainfall deficit across India being almost 50% [Gadgil et al., 2002]? If such a break dries out the soil, a tendency for which was noted even in the simulations for 1992 and 1998, it is likely that the AMC thresholds and the  $CN(II)$  values would be different. A more elaborate parameterisation scheme is needed to handle such singular cases.

Another caveat is the specification of absolute rainfall thresholds as one of the criteria for Transition  $BC$ . Absolute thresholds are prone to giving erroneous results when the rainfall is “not normal”.

A more serious caveat is the averaging of AMC thresholds across a region. There is considerable variation in rainfall even within a region, with the rainfall changing by a factor of over two in the Ridge and Foothills regions (Figure 2.4). The thresholds should therefore be allowed to vary across the region. Likewise, the absolute rainfall thresholds used to determine the Transitions  $EA$  and  $AB$  should also be allowed to vary within a region.

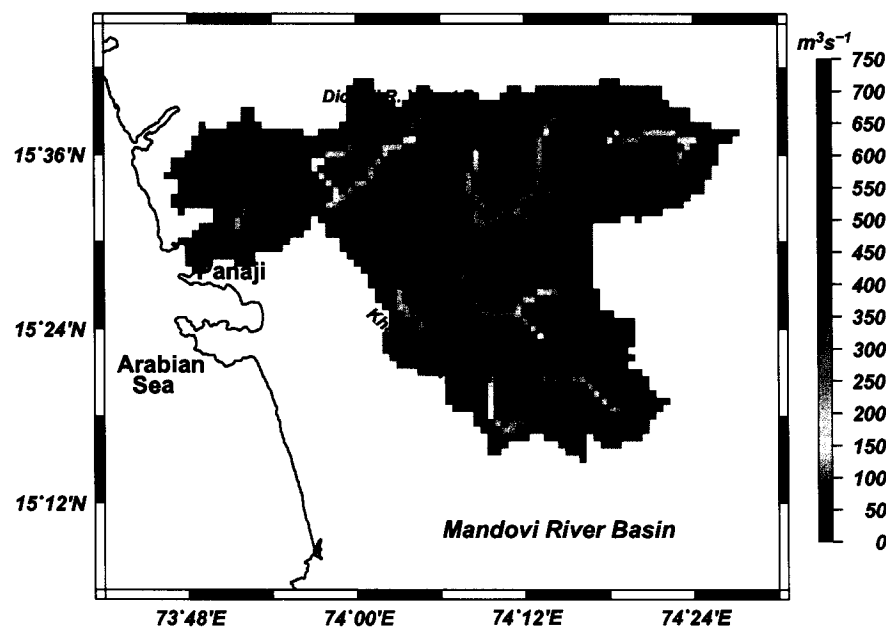
Hydrologically, monsoon onset, as defined here, is a process, not an event. This phase begins with sustained, continual rainfall with its occasional showers marking the end of the dry season. This phase ends when the discharge starts mirroring the rainfall. Since discharge gauges are not available in most basins, it is not convenient to use the discharge as a parameter to define Transition

BC, making it the most difficult transition to capture. Improvements in this part of the algorithm are needed to preclude the overestimation of discharge just before the transition occurs.

### 6.3.2 Strengths of the modelling framework

The framework simulates the hydrology of integrated terrestrial freshwater systems. It has the capability of resolving linked terrestrial hydrological systems, which include lakes and wetlands. Although lakes and wetlands are not important for the Mandovi basin, it is still advantageous to have such capabilities. The framework is also highly scalable and can be used to simulate river basins ranging from a very small scale to the continental scale.

**Figure 6.4** Simulated runoff for July 1992 (in  $\text{m}^3 \text{s}^{-1}$ ) in the Mandovi river basin. The catchment area is shown in colour along with the position of two discharge gauges: Ganjem and Kulem (black circles). The spatial variability in runoff is captured well. Some of the major tributaries (Rivers Khandepar, Mhapsa, Dicholi, Valvat) are identified on the map. The modelling framework allows one to calculate the freshwater discharge at any point along the river including the total river discharge into the Mandovi estuary at its mouth at Panaji (red circle) for which there is no information available. From Ganjem to Panaji, discharge doubles approximately, with major contribution from tributaries in between.

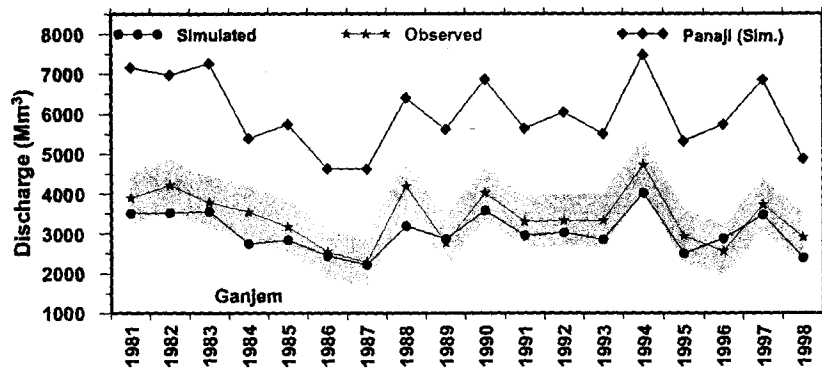


Apart from temporal variability in discharge, a major feature of this modelling framework is that it resolves spatial variability in discharge also (Figure 6.4). In addition to its obvious implications on water resources, spatial variability of discharge has crucial implications in many applications. For example, ocean models require discharge at the mouth of the river and also as a function of the coast line. Even to study the estuarine systems, discharge all along the estuarine network is a necessary requirement. For Mandovi, the discharge gauge at Ganjem, located at the upstream end of the estuary, is  $\sim 50$  km upstream of the mouth of the river. This is typical of the river discharge measurements; gauges were put beyond the influence of tidal action. There are no observations for events that happen from the gauging locations to the mouth of the rivers. For estimating river discharge at its mouth, the normal practice is to use the discharge observation as it is, or in some cases by some means of extrapolation; this is an unsuitable measure of the discharge at the mouth.

For example, an estimate of the Mandovi's discharge was reported by Rao [1975]. The Ganjem gauge did not exist then and Rao [1975] used a classification and extrapolation scheme to estimate the discharge. Based on the data for gauged rivers in India, Rao [1975] estimated that the discharge for river basins with 'high' rainfall was of the order of  $65 \text{ Mm}^3$  per  $100 \text{ km}^2$  of basin area. This method yielded a value of  $\sim 1320 \text{ Mm}^3$  for the Mandovi, which is almost a third of the discharge measured at Ganjem. This result is not surprising because the data used by Rao was from rivers spread across India, and rainfall varies from over 600 cm to less than 20 cm across the country. Our estimate of the discharge at Panaji was over  $6004 \text{ Mm}^3$ , with a standard deviation of  $890 \text{ Mm}^3$ . The ratio of the simulated discharge at Panaji to that at Ganjem varied between 1.8–2.1. Thus, discharge in the Mandovi increases almost two-fold from Ganjem to Panaji (Figures 6.5 and 6.6). A large fraction of this increase comes from the tributaries Khandepar ( $\sim 45\%$ ), Valvat ( $\sim 25\%$ ; includes Dicholi and Kudnem rivers), and the Mhapsa ( $\sim 14\%$ ; includes Moide and Asnoda rivers); the balance ( $\sim 16\%$ ) directly flows into the estuary from the land adjoining it (Figures 6.4 and 6.6). The model river channel terminates at the point where the height falls

below mean sea level in the GLOBE DEM. For the Mandovi, this point (where the river ends) is in the vicinity of Panaji. The rest of the Mandovi basin, which consists of the Aguada Bay, does not form a part of the river-runoff computations in THMB because the bottom of the bay is below mean sea level and therefore forms a part of the sea.

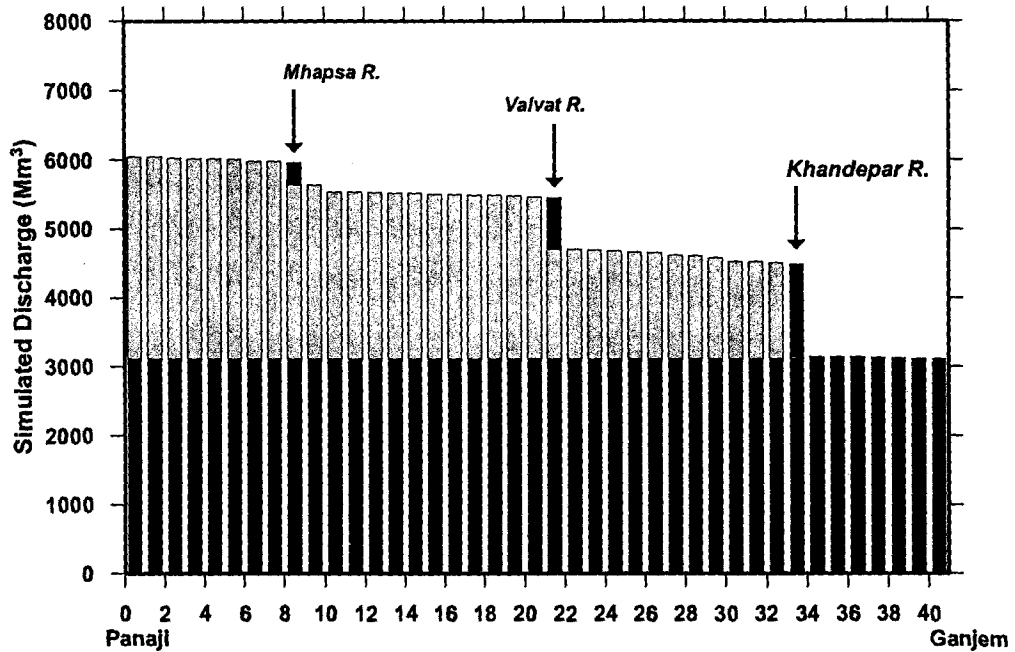
**Figure 6.5** Similar to Figure 3.5 with simulated discharges at Panaji included. The observed and simulated discharge at Ganjem are plotted for comparison with Panaji simulation.



This modelling framework makes very low demands on hydrological data. Apart from some information on the soil type in the basin, the entire model parameterisation is built using only the rainfall forcing. All model parameters are derived on the basis of the rainfall, which is a basic requirement for any hydrological model. In this low demand on input data lies the strength of the modelling framework. Furthermore, the results (Figures 6.2 and 6.3) suggest that the model should work for other basins on the Indian west coast too. That the model does not need to be calibrated separately for each river is an important point because most of these basins are ungauged. Hence, though the model has been validated only for the Mandovi, its potential region of application is considerable and spans most of the Indian west coast. In the context of Prediction in Ungauged Basins (PUB) [Sivapalan et al., 2003], this potential of the model is significant because, although most of these basins are ungauged, the discharge of these rivers into the eastern Arabian Sea is not small [Fekete et al., 2002], making them an important element of the local climate system.



**Figure 6.6** Bar chart showing the spatial variation of annual simulated discharge on the model grid. The height of the bar represents annual discharge (in  $\text{Mm}^3$ ) from Ganjem (on the right) to Panaji (on the left) for 1992 as a function of distance (abscissa is the number of grid cells from Panaji to Ganjem) along the main channel of river. Discharge in the channel increases almost two-fold from Ganjem to Panaji, most of this increase coming from the runoff from the Khandepar, Valvat (including Dicholi), and Mhapsa rivers (Figure 6.4). The contributions of these tributaries are shown in black.



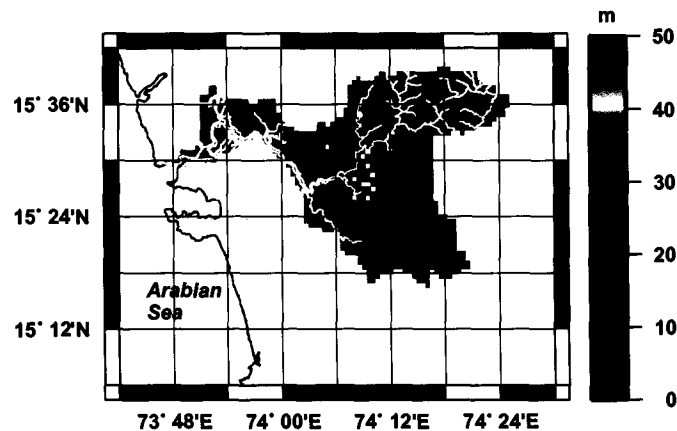
### 6.3.3 Future directions

Our modelling framework provides a tested tool to simulate the hydrology of the west coast of India. The next logical step is to apply it to the remaining west-coast rivers. In the course of this study, we have already collected an exhaustive data set of daily river discharge (from CWC) and daily rain-gauge data (from IMD). Daily-discharge data were available for 47 stations in 34 river basins. Rain-gauge data were collected from 589 stations covering the whole of the west coast, from Gujarat in the north to Kerala in the south. Availability of this crucial data implies that the framework can be extended to the whole of the west coast. Nevertheless, we did not

implement this framework for the other west-coast rivers. One of the reasons for not doing so was the inability of GLOBE DEM to resolve the west-coast river basins accurately: as discussed in chapter 2, considerable editing of GLOBE DEM is required to resolve the narrow channel. Like any other DEM, GLOBE gives average elevation for a grid cell. Also, like most of the other west-coast rivers, the Mandovi river is much narrower ( $\sim 100$  m) than the resolution of the GLOBE DEM, especially in its upstream reaches [Shankar et al., 2004]. Thus, GLOBE DEM topography and river directions derived from the topography required editing to represent the basin geometry accurately in the modelling framework. The DEM editing tool developed by Shankar et al. [2004] and Kotamraju and Shankar [2004] requires visual editing. High resolution of the GLOBE DEM (large number of grid cells) and the presence of a complex topography of the coast along with narrower streams, implies investment of large amount of time. So, instead of extending the framework to other rivers, we chose the more important task of building the model parameterisations. It is worth noting that this issue is not only related to the coarser resolution of GLOBE DEM with respect to west-coast rivers. Even a high-resolution DEM like SRTM [Farr et al., 2007] was unable to resolve the Mandovi channel. We tested the SRTM data (original resolution 3 arc seconds) by averaging the 3-arc-seconds elevation to the 30-arc-seconds GLOBE grid. The resulting DEM was used for a simulation. The results show that there are far fewer pits in the coarsened SRTM than were seen in the GLOBE DEM (Figure 6.7 (Figure 5 of Shankar et al. [2004])), implying that the elevations are reasonably good. The river does not, however, flow to the sea, the map of river flux showing instead a large number of short, unconnected channels (Figure 6.8). This lack of a well-defined river implies the need for manual, subjective editing. Hence, at least at coarsened resolutions like 30 arc seconds, the SRTM DEM is also unable to capture the river valleys sufficiently well (Figure 6.8). Using a higher-resolution DEM increases the computational expense considerably. Since a major potential application of this study is to estimate the river discharge into the Indian seas, even the 30 arc seconds resolution is sufficient for most of the oceanographic applications. Extension of this modelling framework to the rest

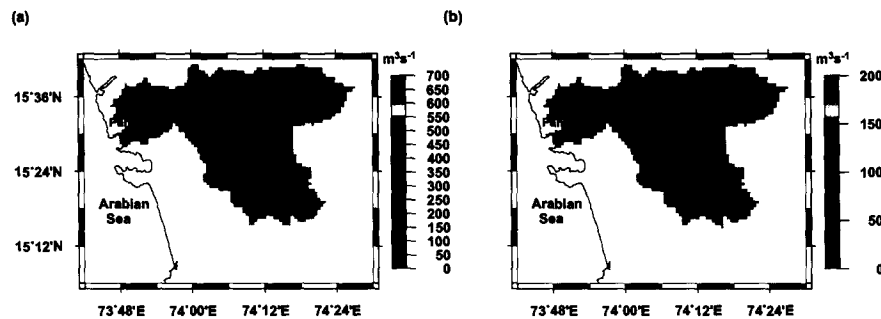
of the west coast is, however, a logical course for future studies. We envisage achieving this goal in two steps. First, as discussed earlier, application of the framework requires editing of the DEM, an exhaustive task in terms of the available resources. What is required is an automated editing algorithm to make the DEM hydrologically correct and resolve the river basin geometry. In GRASS GIS, watershed analysis tools like `r.watershed` and `TerraFlow` are available and they can be used to obtain a hydrologically correct DEM.

**Figure 6.7** Figure 5 in Shankar et al. [2004]. The stream network is not resolved, most of the local runoff piles up in 30–50 m deep pools, none of which exist in reality. The water level (in metres) is also shown. This was owing to the inability of the DEM to resolve the Mandovi river valley, which is much less than 1 km wide over much of its length. The large ‘lake’ seen in the centre of the basin is just upstream of the stream-low gauging station at Ganjem. Compare with the runoff map with the edited GLOBE DEM, where the stream network is resolved quite well (Figure 6.4).



Module `r.watershed` uses a least-cost search algorithm designed to minimize the impact of DEM data errors [Ehlschlaeger, 2001]. Module `TerraFlow`, a part of a software project called computations on massive grids [Toma et al., 2001, 2003] derives a hydrologically correct version of high resolution DEMs such as SRTM [Arge et al., 2000]. The project is designed using efficient algorithms for flow computation on massive numbers of grid cells containing terrain, such as SRTM DEM. `TerraFlow` computes the flow routing (path when a volume of water is poured on the terrain) and flow accumulation (amount of water flowing through the terrain) from

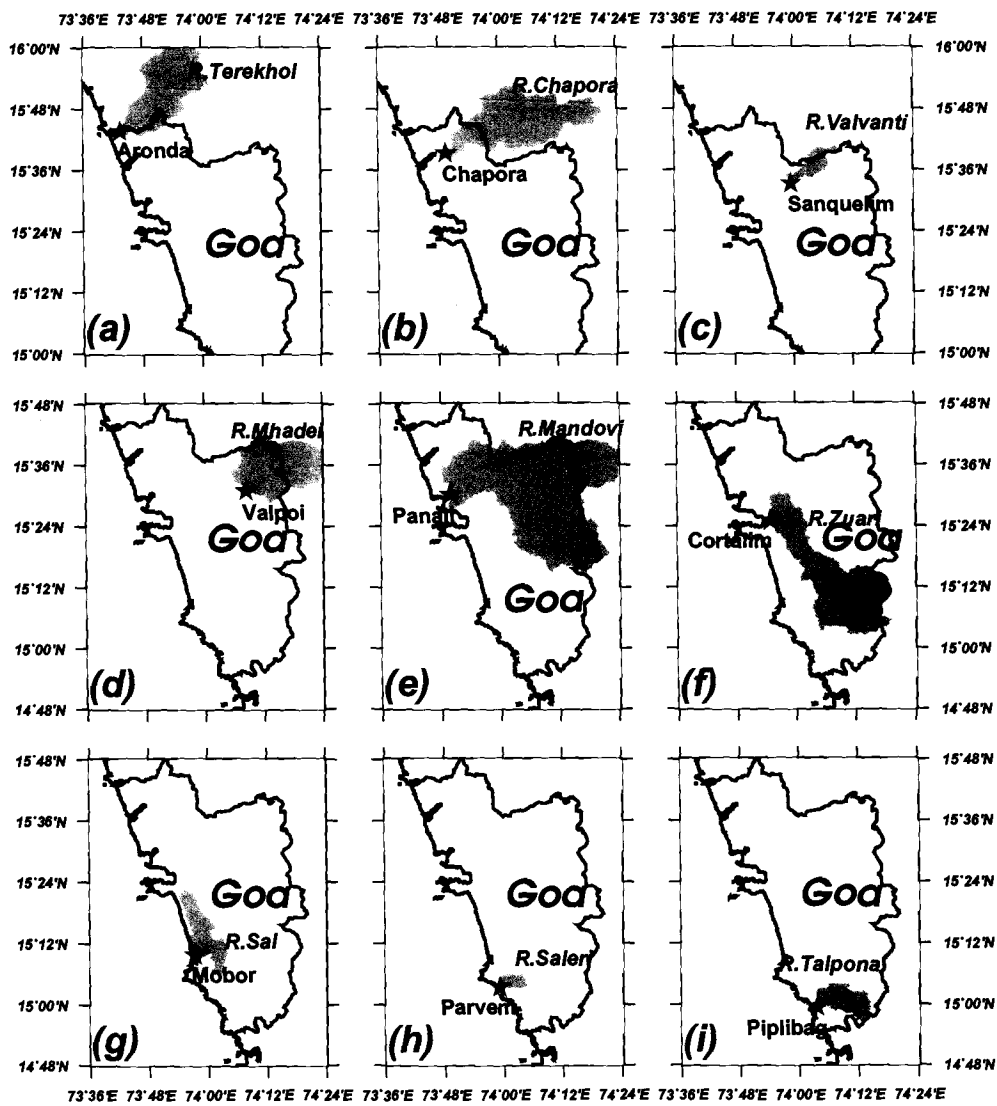
**Figure 6.8** Runoff ( $\text{m}^3 \text{s}^{-1}$ ) simulated for July using (a) GLOBE DEM (edited) and (b) the 3 arc seconds SRTM downsampled to 30 arc seconds (unedited). As with the unedited GLOBE DEM, the river does not flow in a continuous stream to the sea.



a given DEM. It is much faster (2 to 1000 times) than the other algorithms and has been used on massive datasets, up to  $10^9$  (1 billion) in size [Toma et al., 2003]. It uses a flooding algorithm to fill the sinks in a DEM [Arge et al., 2001]. Module `r.watershed` is more accurate than module `r.terraflow`, but this accuracy comes with the drawback of large computer time. A more careful approach (using case studies) is required to ascertain the relative accuracy of these two algorithms, which will require stream-network data (rivers digitized from toposheets). For a recent work on flood-assessment methodology in Goa [CFSC, 2009], we used both the algorithms to resolve the river basin geometry. We filled the SRTM DEM with the `r.terraflow` algorithm and then used `r.watershed` for watershed analysis. This combination of modules resolved the basin geometry of the rivers of Goa (Figure 6.9).

This result is significant, because once the need for manual editing is eliminated, hydrologically corrected DEMs can be used in the framework for the whole of the west coast. Implementation of format conversion between these two geometries and incorporation of the algorithms to the modelling framework is not expected to be as big an issue as managing the much greater computer time required when using the higher resolution SRTM DEM: running THMB with SRTM requires 1000 times more grid cells than the GLOBE DEM, implying much higher computational cost per simulation. Possible solutions to this problem are to use an averaged SRTM DEM, i. e., a coarser

**Figure 6.9** GRASS GIS modules are used to generate the hydrologically corrected and filled SRTM DEM for Goa. Again the GRASS module *r.watershed* can be used to derive the basin geometry. The areas plotted in grey are the watershed area over the location (red star) mentioned for the rivers of Goa. The place names mentioned on the map are the nearest town. Inclusion of these modules in the modelling framework is the next step.



resolution, or even parallelising THMB to run on a cluster computer.

Second, since rainfall is the main forcing field, we plan to prepare a high-resolution spatial rainfall data set for the west coast of India using the available rain gauge data and the method described in Chapter 3.

Thus, our work can be interpreted as a move in the right direction to address the problem of developing a modelling framework to quantify the hydrological variables, an important but often neglected issue. We hope that this thesis will provide a much needed impetus and a modest beginning in the direction of preparing a quantitative water budget for the whole country and an estimate of the discharge into the Indian seas. Simulated river discharge on the subcontinent scale can then be used for a variety of studies, including ocean and estuarine modelling, terrestrial ecosystem modelling, GCM studies, and water-resource studies.

## Chapter 7

### Summary

We have described a hydrological modelling framework to simulate the discharge of the west-coast rivers. The framework was tested for simulating the daily discharge of the Mandovi, a typical west-coast river. Discharge simulations compared well with the observations, capturing the spatio-temporal variability in the hydrological variables. This large spatio-temporal variability is a major feature of the west-coast rivers, which are fed by the summer monsoon rainfall. It is a direct consequence of the large spatial and temporal variability in the rainfall and its interaction with the other basin properties such as complex topography and characteristics of the soil.

The components of the modelling framework were described in Chapter 2. The framework was applied to the Mandovi basin. The framework consists of a hydrological routing algorithm (THMB), GLOBE DEM and GRASS-GIS. The framework is highly scalable and can be applied to both, the small river basins of the west coast and the big basins like the Ganga and Brahmaputra. It also requires little input data: for the rain-fed west-coast rivers, rainfall was the main input.

There is a large variability in rainfall on both spatial and temporal scales. Most of the west coast rainfall (~ 90%) occurs during the summer monsoon (June–September), with considerable inter-annual and intra-annual variability. Rainfall on the west coast, due to its orographic nature, also shows large spatial variability. Resolving this spatial variability was important as THMB

requires rainfall mapped on the model grid. Rainfall increases from west to east in the basin and owing to the barrier-like effect of the Sahyadri mountains, heavy rainfall occurs on the hills and slopes of the mountain range. Rainfall then collapses as we move further eastward to the leeward side of the Sahyadris. The annual rainfall varies from an average of 286 cm at Panaji on the coast to an average of 661 cm at Gavali on the windward slope of the Sahyadris. At Valpoi, which lies at the foothills of the Sahyadris, the average annual rainfall is 413 cm. On the leeward side, at Asoga, the average rainfall declines to 161 cm. The distance between Valpoi and Gavali and that between Gavali and Asoga is about 10 km. Capturing this sharp variability was a challenge because of the sparsity of the rain gauges. In the Mandovi (basin area 2032 km<sup>2</sup>) only five rain gauges are available.

In Chapter 3, we have presented a method to resolve the orographic rainfall. The method was incorporated into the modelling framework to map the rainfall on the model grid. A multivariate interpolation method (RST), using elevation as the third variable, was used for interpolating the rainfall. The method requires locations and heights of the rain gauges, along with a DEM, to obtain the rainfall maps. The key feature of the interpolation was to specify a ridge line to separate the windward and leeward sides of the Sahaydris in order to reduce the underestimation of the heavy rainfall on the hills and slopes. The interpolation was done separately for the leeward and windward sides by specifying the ridge line *a priori*. The resulting spatial fields were merged together to get the rainfall forcing.

In Chapter 4, we introduced a rainfall-runoff model, called the SCS method, into THMB. On the daily time scale, the complex relationship between rainfall and runoff implied that the simple parameterisation of THMB could not work. The SCS method, which was empirically derived, converts rainfall into runoff based on the basin properties and antecedent conditions. The SCS method was incorporated into THMB: the parameter  $\alpha$  was replaced by the parameters of the SCS method ( $CN$ ,  $\lambda$ , and AMC thresholds). This new parameterisation improved the daily simulations of discharge.



Initially, the SCS parameters were kept constant for the Mandovi basin, but the large variability of rainfall, and hence runoff in the basin, demanded a spatio-temporal variability in the SCS parameters also. There was still scope for improving the discharge simulations by including this variability.  $CN$  and  $\lambda$  depend on the physical characteristics of the basin and antecedent conditions (soil moisture condition). The physical characteristics of the basin vary in space and the soil moisture conditions (or AMC) vary with season. Although the short-term variations in SCS parameters were taken care of by the 5-day AMC conditions, the variability due to the seasonal cycle was not considered. Hence, the model parameters had to be a function of both space and long-term variations or season. The strong seasonality of rainfall, and hence the soil-moisture conditions, makes it important to resolve this variability.

In Chapter 5, incorporation of this spatio-temporal variability in model parameters was discussed. A major contribution was to develop an objective method to distinguish the long-term moisture regimes. This method uses only the rainfall data to define the different states of prevailing moisture conditions. According to the different regimes, model parameters are determined and used in the simulations. Incorporation of this spatio-temporal variation in model parameters improved the overall discharge simulations. The strength of the parameterisation lies in the limited demand it makes on the input data: apart from some information on the average soil type in the basin, the parameterisation is built solely on the basis of the rainfall that is used to force the model.

In summary, we have developed a modelling framework to simulate river discharges of the west coast of India. The modelling framework is highly scalable, it simulates river discharge considerably well, and its demand on input data is minimal. The salient points of the thesis are presented below.

1. The modelling framework is applied and tested for the Mandovi river. The discharge simulations compare well with the observations on annual to daily timescales.
2. Rainfall is the most important variable in the modelling framework owing to its availability

and relative accuracy. The complex mountainous terrain of the west coast, the large gradients of rainfall, and the small geographical area of the west-coast basins lead to a large underestimation of rainfall in existing global and regional rainfall datasets. To resolve this orographic rainfall on the west coast and obtain the rainfall forcing field, a rainfall-mapping algorithm was incorporated into THMB.

3. Resolving spatial and temporal variability in the runoff-generation process, which is parameterised by the SCS-CN method, requires exhaustive data on the physical, geographical, and biological characteristics, which are not easily available. The strength of our method is that these processes, especially long-term seasonal variations, are parameterised using only rainfall as input data. For most of the west-coast river basins, rainfall is the only available data owing to the sparse distribution of rain gauges. That the model does not need to be calibrated separately for each river is important because most of these basins are ungauged. Hence, though the model has been validated only for the Mandovi, its potential region of application is considerable for prediction in the several ungauged basins on the Indian west coast.

The implications of this modelling framework for the hydrology of the west coast are immense. The framework can be used to study the water budget of the region, providing valuable information in diverse fields for potential users. The two communities expected to benefit from this work are the oceanographic modelling community and water-resource planners.

## Appendix A

### Basic hydrological variables

#### A.1 Precipitation

Precipitation denotes the quantity of water falling on the land surface from the atmosphere. The liquid form of the precipitation is called rainfall, which is different from solid forms such as snowfall and hailstorm. It is common to use rainfall and precipitation interchangeably unless specified otherwise. The rainfall is caused by the adiabatic cooling and subsequent condensation of water vapour in a rising parcel of air. Based on the lifting mechanism of the air parcel, rainfall is classified into the three categories: frontal rainfall, convective rainfall, and orographic rainfall.

Rainfall is measured by rain gauges, which give the rainfall amount in depth units over a certain accumulation period. The period of accumulation is generally 24 hours. Another interesting variable is rain intensity or rain rate, but its measurements are done only for important meteorological stations, and they are not common. In India, rainfall measurements are made by the India Meteorological Department (IMD; URL <http://www.imd.gov.in>). It provides quality-controlled rain-gauge data to researchers. During the course of this work, rain-gauge data from 589 west-coast stations for the period 1975–2000 were collected from IMD.

## A.2 Evapotranspiration

Evapotranspiration denotes the amount of water transferred from the land surface to the atmosphere through its conversion from liquid to gaseous state. Conceptually, evapotranspiration is similar to precipitation, but reverse in direction of transfer. Evapotranspiration is also represented in depth units. Evapotranspiration consists of two processes, evaporation and transpiration. The term evaporation refers to the loss of water from the land surface through surface water bodies, soil moisture and vegetation surfaces. Transpiration refers to the process by which plants transfer water from the soil through their roots to the small openings in the leaves (stomata), from where water escapes to the atmosphere.

Evapotranspiration is a complex process depending upon the energy balance, prevailing wind, and relative humidity; availability of moisture is the limiting factor. A major concept to understand evapotranspiration is potential evapotranspiration. Potential evapotranspiration denotes the amount of water evapotranspired when the moisture supply is not limited. Measurement of actual evapotranspiration is very difficult. Except in short-term field experiments for land-atmosphere interaction studies, direct observations are not used in hydrological studies. In hydrology, evapotranspiration is generally estimated indirectly [Beven, 2001]. Evapotranspiration studies and estimates for India are still rare [Rao et al., 1971; Narasimhan, 2008; Krishna Kumar et al., 1987; Maréchal et al., 2009]. It is estimated only in full observatories of IMD.

## A.3 Subsurface water

The most complex hydrological process takes place under the land surface [Beven, 2001]. A large part of the rainfall that reaches the land surface is infiltrated into the surface soil layer to become subsurface water. The water that infiltrates the soil either becomes soil moisture (to evaporate later) or flows close to the surface as *throughflow* (unsaturated flow) or it percolates under gravity to become groundwater flow (saturated flow) through the soil or rock strata. Flow is saturated when

the porous medium (soil) has voids and these are completely filled with water and is unsaturated when some of the voids are still filled by air. Rainfall enters the soil zone and moves downwards into the water table. Water table is the surface where water in the pores is still at atmospheric pressure; it marks the upper layer of the saturation zone. Above the water table is the capillary fringe in which, owing to capillary action, pores are under saturation. Below the soil and capillary fringe is the intermediate zone where the movement of water is mainly downward. These zones are highly dynamic and show high variation in both temporal and spatial domain [Ward and Robinson, 2000]. Both saturated and unsaturated flow processes are important for surface-water hydrology as subsurface and groundwater outflow occur when the subsurface water emerges to become surface flow in a stream or spring [Chow et al., 1988]. Apart from these outflows, the groundwater is of no interest for surface hydrology as average residence time for groundwater is around 300 years [Ward and Robinson, 2000].

### A.3.1 Infiltration

Infiltration is the process by which water from rainfall is absorbed into the soil. The infiltration rate is the rate at which water enters into the soil at the surface. It is measured in cm/s. The maximum rate at which a given soil can absorb water is its *infiltration capacity*. When rainfall intensity exceeds the infiltration capacity, surface ponding occurs and overland flow results. Infiltration rate depends upon the state of soil surface, vegetation cover, property of the soil (hydraulic conductivity and porosity), and antecedent moisture condition.

### A.3.2 Soil water

Soil water is the water contained in the soil profile and the subsurface water in the unsaturated layers above the water table. This definition includes region of soil upto the subsoil layers, which can be from tens to even hundreds of meters below the surface. The ability to absorb and retain moisture is a very important control of the surface hydrological processes. Over thin and/or imper-

meable soils, rainfall runs off quickly, while deep and permeable soils can store moisture longer to contribute to river flow in even dry conditions. The soil-moisture capacity of a soil depends on its texture and structure.

### A.3.3 Groundwater

A part of the infiltrated water goes into the ground to be stored as groundwater. The groundwater is stored in saturated layers of the soil column. The top layer of this deep saturated zone of soil is called the water table. Although sitting deep, the groundwater also interacts with the surface water based on topography.

## A.4 Surface water

Surface water is water stored or flowing on the earth's surface. Rivers or streamflow form the most important component of surface-water hydrology.

A hydrologist quantifies the amount of water flowing in a river by a quantity called river discharge. At any point along the channel of a river, river discharge is defined as a volumetric flux of water through that location. Integration of this volume flow rate over a period of time gives the volume of water brought by the river at that point. Being a very important parameter in many fields, river discharge is known by a variety of names such as streamflow, inflow, river runoff, or freshwater influx. All these quantities denote river flow and the only difference is in describing flow in terms of volumetric rate or absolute volume.

An important concept to understand river flow is hydrograph or stream hydrograph. It is a plot of river discharge (both volume or volumetric flow) versus time at a location on a river. Surface runoff is defined as an *overland* flow that contributes to the stream hydrograph or flow in the river at any point. The surface runoff or overland flow is generated mainly by two basic processes. The first process is *infiltration excess runoff*, where runoff is generated when rainfall

intensity exceeds the infiltration capacity of the soil surface. This is also known as *Hortonian runoff* based on the name of Robert E. Horton. The second process is *saturation excess runoff*, where runoff is generated by rainfall on the saturated soil surface. In this case, rainfall intensity may not exceed the infiltration capacity of the soil. Surface runoff can be used to represent the point-scale processes (or grid scale) in the catchment or can be used at the catchment scale to represent a part of discharge (hydrograph) due to overland flow.

Different from the surface flow is the subsurface flow. This is the flow contributed to the river flow purely by subsurface processes. The major component of the subsurface flow is the *baseflow*. Baseflow was classically defined as the contributing part of the river flow which occurs even after the rainfall event has stopped, but, this usage is not strictly true. There is always some contribution of subsurface flow during a rain event.

#### A.4.1 River discharge measurements

The river discharge at a location is estimated by measuring the velocity of the stream and the cross-sectional area of channel at that point. Whenever measurement of velocity is not possible owing to operational reasons, river discharge is estimated by measuring the stage (water level in the stream) and using a stage-discharge rating curve to obtain the river discharge. The location where these measurements are obtained is called the stream gauging station and the measurements are called stream gauging. In India, the main agency involved in stream gauging is the Central Water Commission (CWC), from where discharge data was obtained for this thesis. Apart from CWC, many states have their own agencies involved in gauging operations.

#### A.5 Basin geometry

Watershed is the basic hydrological unit for surface water flow. It represents a geographical region contributing to the flow in the river at any point. The runoff (surface and subsurface) generated

over this area only is translated to the flow at the given point on the stream. The point for which this area is defined is known as *catchment outlet* and the area is known as the *catchment area* over this point. The entire area drained by a river along with its tributaries is known as *basin*, and the outlet is a sea, an inland lake, or wetlands.



## Appendix B

# Rainfall-mapping algorithm

### B.1 General problem of mapping

In general, what are available are point measurements of rainfall. A general formulation of interpolation can be defined as follows (following Mitas and Mitasova [1999]): Given the  $N$  values of rainfall  $P_n$ , where  $n = 1, 2, \dots, N$ , measured at  $n$  distinct points  $x_n$  within a defined region in a  $d$ -dimensional space ( $d = 1, 2, 3, \dots$ ),

$$x_n = [x_n^1, x_n^2, \dots, x_n^d], \quad (\text{B.1})$$

find the  $d$ -variate function  $F(x_n)$ , that passes through all the given rainfall points  $P_n$ , i. e.,

$$F(x_n) = P_n, \quad (\text{B.2})$$

where  $n = 1, 2, \dots, N$ . As there are an infinite number of functions satisfying the above criterion, additional conditions are required to arrive at a particular solution. A whole suite of different interpolation techniques are designed by choosing different additional conditions. The choices depend on the problem in hand, and are usually based on the different requirements of the applications. The most common interpolation techniques are usually based on geometrical surface interpolation, where each point influences the resulting surface at a certain finite distance (such as

Inverse-Distance Weighted (IDW)), or based on variational techniques like interpolation based on mathematical surface that have certain property (such as splines), or on the geo-statistical concept of random variation (such as kriging).

## B.2 Multivariate interpolation by regularised spline with tension (RST)

The general mathematical description of regularised spline method is given by Mitasova and Mitas [1993] and Mitasova et al. [1995]. The RST method (both its 2-*d* and 3-*d* formulation) was used by Hofierka et al. [2002] for interpolation of rainfall. The mathematical derivation given below follow from Hofierka et al. [2002].

The RST interpolation is a type of variational interpolation. Variational interpolation is based on the assumption that the interpolation should pass through (or as close as possible) to the data points and, at the same time, should be as smooth as possible. The spline function  $S(x)$  used for interpolation fulfills the above two requirements simultaneously, reducing the two requirements into a single condition:

1. it minimises the deviations from the measured points, and
2. at the same time, it is as smooth as possible, where the smoothness seminorm,  $I(S)$  (also known as smooth seminorm or roughness penalty) is the measure of smoothness.

Hence, the interpolation problem reduces to minimising  $\sum_{n=1}^N |p_n - S(x_n)|^2 w_n + w_o I(S)$ , where  $w_n$  and  $w_o$  are positive weighting factors ( $w_o/w_n$  is the smoothing parameter  $w$ ), and  $p_n$  is measured value at discrete points  $x_n$  (see Equation (B.1)), where  $n = 1, 2, \dots, N$  within a region of a  $d$ -dimensional space. For  $w_o/w_n = 0$  the function  $S(x)$  passes exactly through the data. The general solution of above minimisation can be represented as a sum of two components ([Talmi and Gilat, 1977])

$$S(x) = T(x) + \sum_{n=1}^N \lambda_n R(x, x_n), \quad (\text{B.3})$$

where  $T(x)$  is a ‘trend’ function and  $R(x, x_n)$  is a radial basis function. The explicit form of  $R(x, x_n)$  depends upon the choice of  $I(S)$ . In the literature, there exist numerous choices of splines [see Mitas and Mitasova, 1999, for previously known splines]. For the RST method,  $I(S)$  is chosen such that it can synthesise properties of previously known splines into a single function and have desired properties like an explicit form, multi-variate formulation, smooth derivatives of higher orders and variational freedom through tension and smoothing [Hofierka et al., 2002]. The explicit forms (for 2, 3, and  $d$  dimensions) of  $I(S)$  for RST are given in [Mitas and Mitasova, 1999; Hofierka et al., 2002]. The RST method is related to ANUSPLIN [Hutchinson, 1998a,b], a rainfall interpolation software, but uses a different form of  $I(S)$ , leading to different properties of the interpolated function. With a particular choice of coefficients, as mentioned in Hofierka et al. [2002], an explicit form of the RST function in 3- $d$  ( $d = 3$ ) is

$$S(x) = a_1 + \sum_{n=1}^N \lambda_n \left[ \sqrt{\frac{\pi}{\rho}} \operatorname{erf}(\sqrt{\rho}) - 2 \right], \quad (\text{B.4})$$

where  $\rho = (\varphi r/2)^2$ ,  $r^2 = \sum_{i=1}^d (x_i - x_{i,n})^2$  is the squared distance,  $\operatorname{erf}$  is the error function, and  $\varphi$  is the generalised tension parameter. The interpolation function given by Equation (B.3) is obtained by solving a system of  $N$  linear equations for the coefficients  $a_1$  and  $\lambda_n$ .

To resolve the effect of topography on precipitation, RST interpolation can be formulated with elevation as the third dimension (based on approach similar to Hutchinson and Bischof [1983]). Given the  $N$  values of rainfall  $P_n$ , where  $n = 1, 2, \dots, N$ , measured at  $n$  distinct points  $x_n$  within a defined region in a 3- $d$  space (following Hofierka et al. [2002]),

$$x_n = [x_n^1, x_n^2, x_n^3], \quad (\text{B.5})$$

we can compute a function  $p = F(x_1, x_2)$  representing the spatial distribution of precipitation over the terrain surface  $x_3 = G(x_1, x_2)$  as

$$p = F(x_1, x_2) = S(x_1, x_2, cG(x_1, x_2)), \quad (\text{B.6})$$

where  $c$  is the vertical rescaling parameter and  $S$  is the trivariate RST function.

The main advantage of the RST method is its flexibility, which is the result of a set of internal tuning parameters within a single basis radial function. This is in contrast with user-supplied variogram (subjective based on observed co-variances) used in geo-statistical method like kriging. The RST parameters like tension, smoothing and vertical scaling control the character of the resulting interpolated surface or volume. The resolution and smoothing of the DEM influences the spatial variability of the resulting precipitation map (Equation (B.6)). These parameters can be selected empirically or may be based on a cross-validation procedure.

### B.2.1 Implementation of RST in modelling framework

The spline methods are used for interpolation of various spatial variables like terrain and bathymetry [Mitasova and Mitas, 1993], climatic variables like rainfall [Hutchinson and Bischof, 1983; Hutchinson, 1995, 1998a; Hofierka et al., 2002], chemical concentrations and soil properties, and image rectification [see Mitas and Mitasova, 1999].

An advanced interpolation method like RST, with its flexibility and potential application in wide-ranging applications, becomes a desirable choice for incorporating in a GIS. A potential drawback of RST is the computational expense required to solve the system of linear equations for large datasets. As computer time scales as  $N^3$ , processing of large datasets makes a heavy demand on computer time. This problem was solved by implementing a segmentation process in the GRASS-GIS [Neteler and Mitasova, 2002]. The segmentation procedure is based on the fact that splines have a local behaviour and the impact of data points decreases rapidly with increasing distance from the given location. A detailed discussion of the RST method as implemented in GRASS-GIS as module `v.vol.rst` is given in chapter 3.

Though, the RST method is computationally intensive, the GRASS-GIS implementation was fast enough to be used for interpolating monthly rainfall for a small domain like the Mandovi basin. For extension of the modelling framework to daily simulations and its use in bigger domain, the extra computational overheads required to work in a GIS environment are avoidable.

---

Hence, source code (in *C*) of RST implementation in GRASS (`v.vol.rst`) was extracted to be a stand-alone program. The extracted RST module was incorporated into the modelling framework. The stand-alone RST interpolation function is called from within THMB code. Since THMB is in FORTRAN, mixed programming paradigms (C-FORTRAN inter-operability techniques) were used to achieve this task. This stand-alone program was parallelised using MPI (Message Passing Interface) to be used exclusively for rainfall mapping for much larger-scale applications, such as mapping rainfall for the entire west coast.

# Bibliography

- K. Aagaard and E. Carmack. The role of sea ice and other freshwater in the Arctic circulation. *Journal of Geophysical Research*, 94:14,485–14,498, 1989. 2
- R. B. Alley, J. Marotzke, W. D. Nordhaus, J. T. Overpeck, D. M. Peteet, R. A. Pielke, R. T. Pierrehumbert, P. B. Rhines, T. F. Stocker, L. D. Talley, and J. M. Wallace. Abrupt climate change. *Science*, 299(5615):2005–2010, 2003. doi: 10.1126/science.1081056. 2
- R. Ananthakrishnan, V. Srinivasan, A. R. Ramakrishnan, and R. Jambunathan. Synoptic features associated with onset of southwest monsoon over Kerala, forecasting manual, FMU report IV-18. 2, *India Meteorological Department, Pune*, 1968. 91
- J. T. Andrews. Millennial-scale climate variability. In J. H. Steele, K. K. Turekian, and S. A. Thorpe, editors, *Encyclopedia of Ocean Sciences*, pages 881–889. Academic Press, Oxford, 2009. 2
- L. Arge, L. Toma, and J. S. Vitter. I/O-Efficient algorithms for problems on grid-based terrains. In *Proc. Workshop on Algorithm Engineering and Experimentation*, 2000. URL <http://www.cs.duke.edu/>. 124
- L. Arge, J. Chase, L. Toma, J. S. Vitter, R. Wickremesinghe, P. Halpin, and D. Urban. Digital Terrain Analysis for Massive Grids. In *Proc. Symposium of the U.S. Chapter of International Association of Landscape Ecology*, 2001. 125

- J. G. Arnold, P. M. Allen, and G. Bernhardt. A comprehensive surface-groundwater flow model. *Journal of Hydrology*, pages 47–69, 1993. 61
- E. A. Baltas, N. A. Dervos, and M. A. Mimikou. Technical note: Determination of the SCS initial abstraction ratio in an experimental watershed in Greece. *Hydrology and Earth System Sciences*, 11(6):1825–1829, 2007. doi: 10.5194/hess-11-1825-2007. URL <http://www.hydrol-earth-syst-sci.net/11/1825/2007/>. 68
- V. Basappa and M. K. Jose. Identification of homogeneous rainfall regimes in parts of Western Ghats region of Karnataka. *Journal of Earth System Science*, 116, 2008. 48
- A. Baumgartner and E. Reichel. *The World Water Balance*. Elsevier, 1975. 3, 10
- K. J. Beven. *Rainfall-runoff modelling: The primer*. John Wiley and Sons Ltd, The Atrium, Southern Gate, Chichester, West Sussex, PQ19 8SQ, England, 2001 edition, 2001. 22, 59, 133
- M. Bosznay. Generalisation of SCS curve number method. *Journal of Irrigation and Drainage Engineering*, 115(1), 139–144 1989. 68
- M. L. Bouwer, T. Biggs, and J. Aerts. Estimates of spatial variation in evaporation using satellite-derived surface temperature and a Water Balance Model. *Hydrological Processes*, 22:670–682, 2008. 103
- D. J. Cazier and R. H. Hawkins. Regional application of the curve number method. *Water today and tomorrow*, Proc. A.S.C.E, 1984. 68
- CFFSC. Report of the Canacona Flash Floods Study Committee constituted by the Government of Goa. Technical report, National Institute of Oceanography (CSIR), 2009. URL <http://www.nio.org/>. 125
- J.-Y. Choi, B. A. Engel, and H. W. Chung. Daily streamflow modelling and assessment based on the Curve-Number technique. *Hydrological Processes*, 16:3131–3150, August 2002. 61

- V. T. Chow, D. R. Maidment, and L. W. Mays. *Applied Hydrology*. Water Resources and Environmental Engineering. McGraw-Hill Book Company, Singapore, 1988. 22, 59, 68, 69, 134
- M. T. Coe. Modeling terrestrial hydrological systems at the continent scale: Testing the accuracy of an atmospheric GCM. *Journal of Climate*, 13:686–704, 2000. 3, 13, 19, 22, 23, 24, 25, 27, 45, 52, 84
- M. T. Coe. A linked global model of terrestrial hydrologic processes: Simulation of modern rivers, lakes, and wetlands. *Journal of Geophysical Research*, 103:8885–8899, 1998. 1, 3, 19, 22, 25
- J. G. Cogley. Run-off from the world's landmasses: Amounts and uncertainties at 2-degree resolution. *Trent Climate journal*, 3(25):89, 1989. 3, 45
- M. H. Costa and J. A. Foley. Water balance of the Amazon Basin: Dependence on vegetation cover and canopy conductance. *Journal of Geophysical Research*, 102:23973–23989, 1997. 22
- N. A. C. Cressie. *Statistics for spatial data*. John Wiley & Sons Inc, New York, 1993. 35
- A. Dai and K. E. Trenberth. Estimates of freshwater discharge from continents: Latitudinal and seasonal variations. *Journal of Hydrometeorology*, 3:660–687, 2002. 1, 3, 10
- C. Daly. Guidelines for assessing the suitability of spatial climate data sets. *International Journal of Climatology*, 26:707–721, 2006. 37, 48
- G. Di Baldassarre and A. Montanari. Uncertainty in river discharge observations: A quantitative analysis. *Hydrology and Earth System Sciences*, 13(6):913–921, 2009. ISSN 1027-5606. URL <http://www.hydrol-earth-syst-sci.net/13/913/2009/>. 45
- W. T. Dickinson. Accuracy of discharge determinations. Technical report, Colorado State University, Fort Collins, USA, 1967. 45



- R. R. Dickson, J. Meincke, S.-A. Malmberg, and A. J. Lee. The “great salinity anomaly” in the northern North Atlantic 1968–1982. *Progress In Oceanography*, 20(2):103–151, 1988. 2
- P. Döll, F. Kaspar, and B. Lehner. A global hydrological model for deriving water availability indicators: Model tuning and validation. *Journal of Hydrology*, 270:105–134, 2003. 1, 3
- C. W. Downer, F. L. Ogden, W. D. Martin, and R. S. Harmon. Theory, development, and applicability of the Surface Water Hydrologic Model CASC2D. *Hydrological Processes*, 16:255–275, 2002. 22
- C. Ehlschlaeger. Using the  $A^T$  search algorithm to develop hydrologic models from digital elevation data. In *Proceedings of International Geographic Information Systems (IGIS) Symposium’89*, pages 275–281, Baltimore, MD, 2001. 124
- ETOPO, 2006. ETOPO2v2 2-Minute gridded global relief data, 2006. URL [www.ngdc.noaa.gov/mgg/fliers/06mgg01.html](http://www.ngdc.noaa.gov/mgg/fliers/06mgg01.html). 4
- T. G. Farr, P. A. Rosen, E. Caro, R. Crippen, R. Duren, S. Hensley, M. Kobrick, M. Paller, E. Rodriguez, L. Roth, D. Seal, S. Shaffer, J. Shimada, and J. Umland. The Shuttle Radar Topography Mission. *Reviews of Geophysics*, 45, 2007. 123
- B. M. Fekete and C. J. Vörösmarty. The current status of global river discharge monitoring and potential new technologies complementing traditional discharge measurements. In *Predictions in Ungauged Basins: PUB Kick-off*, 309. IAHS, 2007. 2
- B. M. Fekete, C. J. Vörösmarty, and W. Grabs. Global composite runoff fields based on observed river discharge and simulated water balances, 2000. URL <http://www.bafg.de/grdc.htm>. Rep. No. 22. 10
- B. M. Fekete, C. J. Vörösmarty, and W. Grabs. High resolution fields of global runoff combining

observed river discharge and simulated water balances. *Global Biogeochemical Cycles*, 16, 2002.

doi: 10.1029/1999GB001254. 3, 121

S. Gadgil, J. Srinivasan, R. S. Nanjundiah, K. Krishna Kumar, A. A. Munot, and K. Rupa Kumar.

On forecasting the Indian Summer Monsoon: The intriguing season of 2002. *Current Science*, 83:394–403, 2002. 118

K. Geetha, S. K. Mishra, T. I. Eldho, A. K. Rastogi, and R. P. Pandey. Modifications to SCS-CN

method for long-term hydrologic simulation. *Journal of Irrigation and Drainage Engineering*, 133:475–486, 2007. 61, 62

GLOBE. The Global Land One kilometer Base Elevation (GLOBE) Digital Elevation Model, Version 1.0. Online documentation, National Oceanic and Atmospheric Administration, National Geophysical Data Center, 2004. URL

<http://www.ngdc.noaa.gov/mgg/topo/globe.html>. 26

A. R. Gokul, M. D. Srinivasan, K. Gopalkrishnan, and L. S. Vishwanathan. Stratigraphy and

structure of Goa. Technical report, Geological Society of India, 1985. In, Earth resources for Goa's development. 79

P. Goovaerts. Geostatistical approaches for incorporating elevation into the spatial interpolation of rainfall. *Journal of Hydrology*, 228:113–129, 2000. 36

S. T. Graham, J. S. Famiglietti, and D. R. Maidment. 5–Minute, 0.5–degree, and 1–degree data

sets of continental watersheds and river networks for use in regional and global hydrologic and climate system modeling studies. *Water Resources Research*, 35:583–587, 1999. 3

GRASS Development Team, 2008. Geographic Resources Analysis Support System (GRASS)

software. Online, 2008. URL <http://grass.itc.it>. GRASS Development Team. 36, 37

- S. Hagemann and L. Dumenil. A parameterization of the lateral water flow of global scale. *Climate Dynamics*, 14:17–31, 1998. 2, 22
- W. Han and P. J. Webster. Forcing mechanism of sea level interannual variability in the Bay of Bengal. *Journal of Physical Oceanography*, 32:216–239, 2002. 10
- W. Han, J. P. McCreary, and K. E. Kohler. Influence of precipitation minus evaporation and Bay of Bengal rivers on dynamics, thermodynamics, and mixed layer physics in the upper Indian Ocean. *Journal of Geophysical Research*, 106:6895–6916, 2001. 10
- H. Hatun, A. B. Sando, H. Drange, B. Hansen, and H. Valdimarsson. Influence of the Atlantic subpolar gyre on the thermohaline circulation. *Science*, 309(5742):1841–1844, 2005. doi: 10.1126/science.1114777. 2
- R. H. Hawkins, B. Yu, S. K. Mishra, and V. P. Singh. Another Look at SCS-CN Method. *Journal of Hydrologic Engineering*, 6:451–452, 2001. 61, 68
- J. Hofierka, J. Parajka, H. Mitasova, and L. Mitas. Multivariate interpolation of precipitation using Regularized Spline with Tension. *Transactions in GIS*, 6:135–150, 2002. 35, 36, 48, 139, 140, 141
- J. Hofierka, T. Cebecauer, and M. Šúri. Optimisation of interpolation parameters using a Cross-validation. In R. Peckham and G. Jordan, editors, *Best Practice in Digital Terrain Modelling: Development and Applications in a Policy Support Environment*, European Commission Joint Research Centre, Ispra (VA), 2005. 45
- S. Howden and R. Murtugudde. Effect of river inputs into the Bay of Bengal. *Journal of Geophysical Research*, 106:19825–19843, 2001. 10
- M. F. Hutchinson. Interpolation of mean rainfall using thin plate smoothing splines. *International Journal of Geographical Information Systems*, 9:385–403, 1995. 35, 36, 141

M. F. Hutchinson. Interpolation of rainfall data with thin plate smoothing splines - Part I: Two dimensional smoothing of data with short range correlation. *Journal of Geographic Information and Decision Analysis*, 2:139–151, 1998a. 35, 140, 141

M. F. Hutchinson. Interpolation of rainfall data with thin plate smoothing splines - Part II: Analysis of topographic dependence. *Journal of Geographic Information and Decision Analysis*, 2: 152–168, 1998b. 35, 140

M. F. Hutchinson and R. J. Bischof. A new method for estimating the spatial distribution of mean seasonal and annual rainfall applied to Hunter Valley, New South Wales. *Australian Meteorological Magazine*, 1983. 140, 141

M. K. Jain, S. K. Mishra, P. S. Babu, K. Venugopal, and V. P. Singh. Enhanced runoff curve number model incorporating storm duration and a nonlinear  $I_a - S$  relation. *Journal of Hydrologic Engineering*, 11:631–635, 2006. 12

S. K. Jain, P. K. Agarwal, and V. P. Singh. *Hydrology and water resources of India*, volume 57 of *Water Science and Technology Library*. Springer, Dordrecht, Netherlands, 2007. 103, 113

J. E. Janowiak, A. Gruber, C. R. Kondragunta, R. E. Livezey, and G. J. Huffman. A comparison of the NCEP/NCAR reanalysis precipitation and the GPCP rain-gaugesatellite combined data set with observational error considerations. *Journal of Climate*, 6:1009–1026, 1998. 27

J. S. Jeffrey, J. O. Carter, K. B. Moodie, and A. R. Beswick. Using spatial interpolation to construct a comprehensive archive of Australian climate data. *Environmental Modeling & Software*, 16:309–330, 2001. 35

A. G. Journel. Modelling uncertainty and spatial dependence: Stochastic imaging. *International Journal of Geographical Information Systems*, 10:517–522, 1996. 35

- P. Y. Julien, B. Saghaian, and F. L. Ogden. Raster-based hydrological modeling of spatially varied surface runoff. *Water Resources Bulletin*, 31:523–536, 1995. 22
- E. Kalnay, M. Kanamitsu, R. Kistler, W. Collins, D. Deaven, L. Gandin, M. Iredell, S. Saha, G. White, J. Woollen, Y. Zhu, M. Chelliah, W. Ebisuzaki, W. Higgins, J. Janowiak, K. C. Mo, C. Ropelewski, J. Wang, A. Leetmaa, R. Reynolds, R. Jenne, and D. Joseph. The NCEP/NCAR 40-year Reanalysis Project. *Bulletin of the American Meteorological Society*, 77:437–471, 1996. 27, 28, 103
- D. G. Kingston, D. M. Lawler, and G. R. McGregor. Linkages between atmospheric circulation, climate and streamflow in the northern North Atlantic: research prospects. *Progress in Physical Geography*, 30(2):143–174, 2006. doi: 10.1191/0309133306pp471ra. 2
- V. Kotamraju and D. Shankar. Using the GRASS GIS in a framework for quantifying water resources in India. In *Poster presented at MapIndia 2004*, New Delhi, India, 2004. 26, 123
- K. Krishna Kumar, K. Rupa Kumar, and R. K. Rakhecha. Comparison of Penman and Thornthwaite methods of estimating potential evapotranspiration for Indian conditions. *Theoretical and Applied Climatology*, 38:140–146, 1987. 103, 133
- A. Kulkarni, S. S. Sabade, and R. H. Kripalani. Intra-seasonal Vagaries of the Indian Summer Monsoon Rainfall. Technical report, Indian Institute of Tropical Meteorology, Pune, 2006. 91
- T. M. Lenton, H. Held, E. Kriegler, J. W. Hall, W. Lucht, S. Rahmstorf, and H. J. Schellnhuber. Tipping elements in the Earth's climate system. *Proceedings of the National Academy of Sciences*, 105(6):1786–1793, 2008. doi: 10.1073/pnas.0705414105. 2
- S. W. Lyon, M. T. Walter, P. Gerard-Marchant, and T. S. Steenhuis. Using a topographic index to distribute variable source area runoff predicted with the SCS Curve-Number equation. *Hydrological Processes*, 18(15):2757–2771, June 2004. 60

- J. C. Maréchal, M. R. R. Varma, J. Riotte, J. M. Vouillamoz, M. S. M. Kumar, L. Rui, M. Sekhar, and J. J. Braun. Indirect and direct recharges in a tropical forested watershed, Mule Hole, India. *Journal of Hydrology*, 364:272–284, 2009. 84, 112, 133
- J. Martin, J. D. Burton, and D. Eisma. *River Inputs to Ocean Systems*. United Nations Press, New York, 1981. 12
- C. Michél, A. Vazken, and C. Perrin. Soil Conservation Service curve number method: How to mend a wrong soil moisture accounting procedure. *Water Resources Research*, 41:1–6, 2005. 60
- J. Miller, G. Russell, and G. Caliri. Continental scale river flow in climate models. *Journal of Climate*, 7:914–928, 1994. 3, 22
- S. K. Mishra and V. P. Singh. *Soil Conservation Service Curve Number (SCS-CN) Methodology*, volume 42 of *Water Science and Technology Library*. Kluwer Academic Publishers, Dordrecht, Netherlands, 2003. 62, 65, 66, 67, 68, 69, 70, 94
- S. K. Mishra and V. P. Singh. Long-term hydrological simulation based on the Soil Conservation Service curve number. *Hydrological Processes*, 18:1291–1313, February 2004. 61
- S. K. Mishra and V. P. Singh. Another look at SCS-CN method. *Journal of Hydrologic Engineering*, 4(3):257–264, 1999. 61
- S. K. Mishra, V. P. Singh, J. J. Sansalone, and V. Aravamuthan. Modified SCS-CN method: characterization and testing. *Water Resources Management*, 17:37–68, April 2003. 61
- S. K. Mishra, M. K. Jain, P. K. Bhunya, and V. P. Singh. Field applicability of the SCS-CN-Based Mishra–Singh general model and its variants. *Water Resources Management*, 19:37–62, 2005. 10.1007/s11269-005-1076-3. 68
- S. K. Mishra, R. P. Pandey, M. K. Jain, and V. P. Singh. A rain duration and modified AMC-

- dependent SCS-CN procedure for long duration rainfall-runoff events. *Water Resources Management*, 22:861–876, 2008. 69, 70
- L. Mitas and H. Mitasova. *Geographical Information Systems: Principles and technical issues*, volume 1, chapter Spatial Interpolation, pages 481–492. John Wiley & Sons, 1999. 35, 36, 138, 140, 141
- H. Mitasova and L. Mitas. Interpolation by Regularized Spline with Tension: I. Theory and implementation. *Mathematical Geology*, 25:641–665, 1993. 35, 36, 139, 141
- H. Mitasova, L. Mitas, W. M. Brown, D. P. Gerdes, I. Kosinovsky, and T. Baker. Modelling spatially and temporally distributed phenomena: new methods and tools for GRASS GIS. *International Journal of Geographical Information Systems*, 9:443–446, 1995. special issue on integrating GIS and Environmental modelling. 139
- T. N. Narasimhan. A note on India's water budget and evapotranspiration. *Journal of Earth System Science*, 117(3):237–240, 2008. 12, 103, 112, 133
- T. N. Narasimhan. Water: Science and society. *Current Science*, 89(5):787–793, 2005. 12
- M. Neteler and H. Mitasova. *Open Source GIS: A GRASS GIS Approach*. Kluwer Academic Publishers, Dordrecht, Netherlands, 2002. 26, 35, 36, 37, 141
- M. G. New, M. Hulme, and P. D. Jones. Representing twentieth-century space–time climate variability. Part I: Development of a 1961–90 mean monthly terrestrial climatology. *Journal of Climate*, 12:829–856, 1999. 28, 35
- M. G. New, M. Hulme, and P. D. Jones. Representing twentieth-century space–time climate variability. Part II: Development of 1961–90 monthly grids of terrestrial surface climate. *Journal of Climate*, 13:2217–2238, 2000. 28

- D. S. Pai and M. R. Nair. Summer monsoon onset over Kerala: New definition and prediction. *Journal of Earth System Science*, 118:123–135, 2009. 91
- A. Papoulis and S. U. Pillai. *Probability, Random Variables and Stochastic Processes*. McGraw Hill Publication, 2002. 65
- M. C. Peel and T. A. McMahon. Continental runoff - A quality-controlled global runoff data set. *Nature*, 444:E14–E14, 2006. 3
- G. D. Perry, P. B. Duffy, and N. L. Miller. An extended data set of river discharges for validation of general circulation models. *Journal of Geophysical Research*, 101:21339–21349, 1996. 3
- B. J. Peterson, R. M. Holmes, J. W. McClelland, C. J. Vorosmarty, R. B. Lammers, A. I. Shiklomanov, I. A. Shiklomanov, and S. Rahmstorf. Increasing river discharge to the Arctic Ocean. *Science*, 298(5601):2171–2173, 2002. doi: 10.1126/science.1077445. 2
- V. M. Ponce and R. H. Hawkins. Runoff curve number: Has it reached maturity? *Journal of Hydrologic Engineering*, 1(1):11–19, 1996. 60, 61, 66, 70
- B. P. Radhakrishna. Linking of major rivers of India - bane or boon? *Current Science*, 84: 1390–1394, 2003. 112
- M. Rajeevan, J. Bhate, J. D. Kale, and B. Lal. Development of a high resolution daily gridded rainfall data set for the Indian region. Technical report, India Meteorological Department, Pune, 2006a. IMD Meteorological Monograph No. Climatology 22/2005. 49
- M. Rajeevan, J. Bhate, J. D. Kale, and B. Lal. High resolution daily gridded rainfall data for the Indian region: Analysis of break and active monsoon spells. *Journal of Climate*, 86(3):296–306, 2006b. 7, 29, 49, 50
- D. Ramakrishnan, A. Bandyopadhyay, and K. N. Kusuma. SCS-CN and GIS-based approach



- for identifying potential water harvesting sites in the Kali watershed, Mahi river basin, India. *Journal of Earth System Science*, 118:355–368, 2009. 114
- R. Ramesh and M. G. Yadava. Climate and water resources of India. *Current Science*, 89(5): 818–824, 2005. 12
- K. L. Rao. *India's Water Wealth: Its assessment, uses and projections*. Orient Longman, New Delhi, 1975. 12, 26, 113, 120
- K. N. Rao, C. R. V. Raman, C. E. J. Daniel, and S. Venkataraman. Evaporation over India. Technical Report PPSR No. 146, India Meteorological Department, Meteorological Office, Pune, 1971. 112, 133
- P. S. Rao. Large-scale field experiments and modelling land surface processes: A review. *Journal of Agrometeorology*, 3:1–21, 2001. 112
- R. P. Sarkar. A dynamical model of orographic rainfall. *Monthly Weather Review*, 94:555–572, 1966. 48
- R. P. Sarkar. Some modifications in a dynamical model of orographic rainfall. *Monthly Weather Review*, 95:673–684, 1967. 48
- R. Sausen, S. Schubert, and L. Dumenil. A model of river runoff for use in coupled atmosphere-ocean models. *Journal of Hydrology*, 155:337–352, 1994. 3, 22
- SCS. Hydrology, National Engineering Handbook. Technical report, Soil Conservation Service, United States Department of Agriculture, Washington, D.C, 1971. 69, 70
- SCS. Hydrology, National Engineering Handbook. Technical report, Soil Conservation Service, United States Department of Agriculture, Washington, D.C, 1985. 65
- D. Shankar. Seasonal cycle of sea level and currents along the coast of India. *Current Science*, 78:279–288, 2000. 10

- D. Shankar and S. R. Shetye. Why is mean sea level along the Indian coast higher in the Bay of Bengal than the Arabian Sea? *Geophysical Research Letters*, 28:563–565, 2001. 10
- D. Shankar and S. R. Shetye. Are interdecadal sea level changes along the Indian coast influenced by variability of monsoon rainfall? *Journal of Geophysical Research*, 104:26031–26042, 1999. 10
- D. Shankar, V. Kotamraju, and S. R. Shetye. A quantitative framework for estimating water resources in India. *Current Science*, 86(4):543–552, February 2004. 12, 23, 24, 26, 27, 28, 52, 94, 103, 112, 113, 123, 124
- S. S. C. Shenoi, D. Shankar, and S. R. Shetye. Differences in heat budgets of the near-surface Arabian Sea and Bay of Bengal: Implications for the summer monsoon. *Journal of Geophysical Research*, 107, 2002. doi: 10.1029/2000JC000679. 10
- Z.-H. Shi, L.-D. Chen, N.-F. Fang, D.-F. Qin, and C.-F. Cai. Research on the SCS-CN initial abstraction ratio using rainfall-runoff event analysis in the Three Gorges Area, China. *CATENA*, 77(1):1–7, 2009. 68
- M. Sivapalan, K. Takeuchi, S. W. Franks, V. K. Gupta, H. Karambiri, V. Lakshmi, X. Liang, J. J. McDonnell, E. M. Mendiondo, P. E. O’Connell, T. Oki, J. W. Pomeroy, D. Schertzer, S. Uhlhenbrook, and E. Zehe. IAHS decade on Predictions in Ungauged Basins (PUB), 2003–2012: Shaping an exciting future for the hydrological sciences. *Hydrological Sciences*, 48(6):857–880, December 2003. 121
- M. C. Smith and D. L. Thomas. *Encyclopedia of water science*, chapter Hydrological Process Modelling, pages 518–520. Taylor and Francis, 2008. 61
- E. P. Springer, B. J. McGurk, R. H. Hawkins, and G. B. Colthrap. Runoff curve numbers from watershed data. A.S.C.E. Watershed management Symposium Proceedings, 1980. 68

- T. S. Steenhuis, M. Winchell, J. Rossing, Z. A. Zollweg, and M. F. Walter. SCS runoff equation revisited for variable source runoff areas. *Journal of Irrigation and Drainage Engineering*, 121: 234–238, 1995. 61
- K. Suprit and D. Shankar. *Prediction in ungauged basins for sustainable water resources planning and management*, chapter Simulating the discharge of the Mandovi River, Goa, pages 175–186. Jain Brothers, New Delhi, 2006. 32, 35
- K. Suprit and D. Shankar. Resolving orographic rainfall on the Indian west coast. *International Journal of Climatology*, 28:643–657, 2008. 26, 35, 41, 52, 94, 103
- K. Suprit, D. Shankar, V. Venugopal, and N. V. Bhatkar. Simulating the daily discharge of the Mandovi river, west coast of India. *Hydrological Sciences Journal*, 2011. Accepted for publication. 77
- A. Talmi and G. Gilat. Method for smooth approximation of data. *Journal of Computational Physics*, 23:93–123, 1977. 139
- L. Toma, R. Wickremesinghe, L. Arge, J. S. Chase, J. S. Vitter, P. N. Halpin, and D. Urban. Flow computation on massive grids. In *Proc. ACM Symposium on Advances in Geographic Information Systems*, 2001. URL [http://www.cs.duke.edu/geo\\*](http://www.cs.duke.edu/geo*). 124
- L. Toma, R. Wickremesinghe, L. Arge, J. S. Chase, J. S. Vitter, P. N. Halpin, and D. Urban. Flow computation on massive grid terrains. *GeoInformatica, International Journal on Advances of Computer Science for Geographic Information Systems*, 7(4):283–313, December 2003. URL [http://www.cs.duke.edu/geo\\*](http://www.cs.duke.edu/geo*). 124, 125
- M. Tomczak. Spatial interpolation and its uncertainty using automated anisotropic inverse distance weighting (IDW): Cross-validation/jackknife approach. *Journal of Geographical Information and Decision Analysis*, 2:18–33, 1988. 37

- TRMM, 2006. TRMM on-line documentation, 2006. URL <http://trmm.gsfc.nasa.gov/3b43.html>. 30
- USDA, 1980. CREAMS - A field scale model for chemicals, runoff, and erosion from agricultural management systems. Congressional Research Report 26, 1980. 61
- USGS. Shuttle Radar Topography Mission (SRTM), 3 arc-second scene, unfilled unfinished 2.0. Online documentation, 2004. URL <http://glcf.umiacs.umd.edu/data/srtm/>. 26
- C. J. Vörösmarty, B. M. Fekete, and B. A. Tucker. *Global river discharge database (RivDis Version 1.0), Vol. 0: Introduction, overview, and technical notes*. International Hydrological Program Tech. Document in Hydrology SC. 96/WS/26. UNESCO, Division of Water Sciences, 1 rue Miollis, 75732 Paris, France, 1996. 3, 22
- M. Wanielista. *Hydrology and Water Quantity Control*. John Wiley and Sons, Singapore, 1990. 59
- R. C. Ward and M. Robinson. *Principles of Hydrology*. Alfred Waller, McGraw-Hill Publishing Company, Shoppenhangers Road, Maidenhead, Berkshire SL6 2QL, England, 2000. 134
- D. White. Grid-based application of runoff curve numbers. *Journal of water resources planning and management*, 114(6):601–612, 1988. doi: 10.1061/(asce)0733--9496(1988)114:6(601). 61
- M. Yaremchuk, Z. Yu, and J. P. McCreary. River discharge into the Bay of Bengal in an inverse ocean model. *Geophysical Research Letters*, 32:DOI: 10.1029/2005GL023750, 2005. 12
- D. N. Yates. Approaches to continental scale runoff for integrated assessment models. *Journal of Hydrology*, 201:289–310, 1997. 3
- R. A. Young, C. A. Onstad, D. D. Bosch, and W. P. Anderson. AGNPS — A Non-point source pollution model for evaluating agricultural watersheds. *Journal of Soil Water Conservation*, 44: 168–173, 1989. 61

---

B. Yu. Theoretical justification of SCS method for runoff estimation. *Journal of Irrigation and Drainage Engineering*, 124(6):306-310, 1998. doi: 10.1061/(ASCE)0733-9437(1998)124:6(306). URL <http://link.aip.org/link/?QIR/124/306/1>. 61